

COMPARATIVE DAMAGE OF DIFFERENT TRUCK CONFIGURATIONS ON JOINTED
PLAIN CONCRETE PAVEMENT

by

TITO P. NYAMUHOKYA

Presented to the Faculty of the Graduate School of
The University of Texas at Arlington in Partial Fulfillment
of the Requirements
for the Degree of

MASTER OF SCIENCE IN CIVIL ENGINEERING

THE UNIVERSITY OF TEXAS AT ARLINGTON

August 2009

ACKNOWLEDGEMENTS

The author would like to offer deepest thanks to his supervising professor, Dr. Stefan A. Romanoschi for his guidance and unconditional support throughout the course of this research. None of the work herein would have been possible without his help and encouragement.

Thanks are also extended to the other members of his thesis committee Dr. Guillermo Ramirez and Dr. James C. Williams for their valuable advice and review of this manuscript. In addition, the author would like to thank the faculty and staff of the Department of Civil Engineering at the University of Texas-Arlington for their valuable assistance during his graduate studies.

The author would like to convey many thanks to the New York State Department of Transportation for sponsoring this research. Also, the author appreciates material and moral support from Dr. Mbaki Onyango, Dr. Sireesh Saride, Miguel Portillo, Said Selemani, and all friends and students in civil engineering at the University of Texas-Arlington and Kansas State.

Most of all, the author would like to give special thanks to his wife, Hilda, and daughter, Rose, for their uncountable love, encouragement, and great support. The author also delivers enormous thanks to his special mother, Maria, brothers, sisters and the whole family back in Africa and all over the world.

Lastly the author would like to thank families of Mr. Chacha, Dr. Otieno, Mr. Bascom, and others in America who helped him to go through hard times during his studies.

July 1, 2009

ABSTRACT

COMPARATIVE DAMAGE OF DIFFERENT TRUCK CONFIGURATIONS ON JOINTED PLAIN CONCRETE PAVEMENT

Tito P. Nyamuhokya, M.S

The University of Texas at Arlington, 2009

Supervising Professor: Stefan A. Romanoschi

This study estimated the damage done by trucks with 35 different configurations on a typical structure of a Jointed Plain Concrete Pavement. The configurations were proposed by New York Department of Transportation, the sponsor of this study. The generalized three dimensional finite element program Abaqus was used to calculate the response of linear elastic rigid pavement structure under truck loading. The loads for each truck case were placed at critical locations on the surface of the pavement to obtain the maximum tensile stresses at the bottom of concrete slab. The computed tensile stresses were used in Darter fatigue model (1977) to calculate for each truck case the allowable number of axles that causes fatigue failure of the concrete pavement.

Base on the combination of allowable number of axles for each truck case, relative truck damages were developed and used to compare the damage effects of the 35 truck case configurations on the Jointed Plain Concrete Pavement. The results indicate that the most critical damages to the rigid pavement were caused by truck cases with high and unevenly load distribution and spacing between axles. Other results included are: (1) increase in damage when loads were shifted between same size axles, (2) decrease in truck damage when loads were shifted from tandem axle to quad axle, (3) decrease in truck damage when spaces were increased between axles of a quad axle, and (4) increase in truck damage when, within a group of axles, the axles were moved from equally to unequally spaced.

Another analysis tool which was used in this research to compare trucks base on the performance of rigid pavement was the Mechanistic Empirical Design Guide (MEPDG). The guide has software which was used to calculate bottom up transverse cracks on the pavement caused by 10 out of the 35 truck cases proposed by NYSDOT. Other truck cases could not be analyzed by the software because the trucks axles were unequally loaded and spaced. The MEPDG analysis on the 10 truck cases indicates the same trend of truck damages as the Finite Element analysis on the same truck cases when truck axle types and/or loads positions were changed. However the effect of changing the truck configuration and axle loads on the damage ratios computed by the MEPDG software was higher than on the ratio predicted from the finite element method.

TABLE OF CONTENTS

ACKNOWLEDGEMENTS	ii
ABSTRACT	iii
LIST OF FIGURES	ix
LIST OF TABLES	xii
Chapter	Page
1. INTRODUCTION	1
1.1 Introduction	1
1.2 Research Objectives	3
2. BACKGROUND	5
2.1 Rigid Pavement	5
2.2 Basic Structural Components of Rigid Pavement	8
2.3 Distresses on Rigid Pavement	12
2.3.1 Transverse fatigue cracks	12
2.3.2 Faulting	14
2.4 Damage equivalency for various vehicle/wheel configurations	15
2.5 Mechanistic-Empirical Pavement Design Guide (MEPDG)	23
2.5.1 Introduction	23

2.5.2	Advantages of new Mechanistic Empirical Pavement Design Guide over the empirical AASHTO design guides (1986, 1993).....	23
2.5.3	Design approach.....	24
2.5.4	Design inputs	25
2.5.5	JPCP distress prediction models	31
3.	FINITE ELEMENT MODELING AND DAMAGE ANALYSIS OF JOINTED PLAIN CONCRETE PAVEMENT (JPCP)	37
3.1	Introduction.....	37
3.2	Overview - Finite Element Program	38
3.2.1	Elements.....	39
3.2.2	Material Module.....	41
3.3	Finite Element Model Development.....	45
3.3.2	General Assembly	45
3.3.3	Finite Element Mesh	46
3.3.4	Boundary conditions	49
3.3.5	Contacts.....	50
3.3.6	Materials	51
3.3.7	Loading	51
4.	MECHANISTIC-EMPIRICAL DAMAGE ANALYSIS OF JOINTED PLAIN CONCRETE PAVEMENT (JPCP).....	55
4.1	Analysis and Design Inputs	55
4.2	Sequence of MEPDG software inputs as used in this study	56
4.2.1	General.....	56

4.2.2	Traffic inputs.....	59
4.2.3	Climate.....	69
4.2.4	Structure.....	70
5.	DAMAGE ANALYSIS AND RESULTS	74
5.1	Truck configuration	74
5.2	Finite element results and analysis	77
5.3	Discussion of the results of the FE	83
5.3.1	Effect of changing the loads and position of axles in a group.....	84
5.3.2	Effect of increasing the number of axles in a group while maintaining the axle load distribution.....	85
5.3.3	Effect of shifting loads from one axle to another axle of the same size.	87
5.3.4	Effect of load shifting for axles of unequal sizes (from a tandem to quadem axle)	90
5.3.5	Effect of increasing spacing in an axle group of a truck.....	91
5.3.6	Truck damage comparison under undesirable axles loading configuration.....	92
5.4	Analysis and Results of MEPDG.....	92
5.5	MEPDG - Discussion of the results	94
5.5.1	General	94
5.5.2	Effect of load shifting (equal sized axles).....	94
5.5.3	Effect of load shifting (unequal sized axles).....	96
5.5.4	Effect of increase spaces between axles of an axle group	96
5.6	Comparison between MEPDG and FE truck damages	97
6.	SUMMARY, CONCLUSION AND RECOMMENDATIONS.....	101

6.1 Summary and conclusion	101
6.2 Recommendations	104
Appendix	Page
A. TRUCKS/AXLES CONFIGURATIONS AND LOADING	105
B. MEPDG – PERFORMANCE OUTPUT FOR JOINTED PLAIN CONCRETE PAVEMENT	112
REFERENCES	149
BIOGRAPHICAL INFORMATION	151

LIST OF FIGURES

Figure	Page
2.1: Typical rigid pavement sections (WSDOT, 2009)	6
2.2: Jointed Plain Concrete Pavements (ACPA 2009).....	6
2.3: Jointed Reinforced Concrete Pavements (ACPA 2009)	7
2.4: Continuously Reinforced Concrete Pavement (ACPA 2009).....	8
2.5: Aggregate Interlock	11
2.6: Dowel bar in place	12
2.7: Transverse cracks development: (a) bottom up cracks, (b) top down cracks (c) photo of a complete transverse crack.....	13
2.8: Joint faulting development: (a) cross-section view (b) top view	14
2.9: Effect of tire inflation pressure (Darestani et al, 2006)	15
2.10: Purdue LEF's for rigid pavements (Zaghloul, 1994).....	22
2.11: MEPDG flow diagrams (NCHRP, 2004)	25
2.12: Trucks classification (khanum, 2005).....	30
3.1: Degrees of freedom on coordinate system.....	44
3.2: Assembled JPCP model	46

3.3: Partitions for slab with dowel holes.....	47
3.4: Dowel bar Mesh.....	47
3.5: Solid to solid embedded elements	488
3.6: 3D brick element (C3D8R).....	48
3.7: Jointed Plain Concrete Pavement Mesh.....	49
3.8: Boundary conditions	50
3.9: Tire imprints size (all dimensions in inches)	52
3.10: Model surface partitions	53
3.11: Axle positioning.....	54
5.1: Types of axles	75
5.2: Maximum Tensile Stresses at the bottom of a Slab caused by axle A3 of Truck L32.	77
5.3: Effect of changing axle position in a group of axles (FEM)	85
5.4: Set a-Effect of increasing axle and loads to axle groups of a truck (FEM).....	86
5.5: Set b-Effect of increasing axle and loads to axle groups of a truck (FEM).....	86
5.6: Set c-Effect of increasing axle and loads to axle groups of a truck (FEM).....	87
5.7: Truck L6 – Effect of shifting loads between equal axles (FEM).....	88
5.8: Truck L7 – Effect of shifting loads between equal axles (FEM).....	89
5.9: Truck case L8 – Effect of shifting loads between equal axles (FEM).....	89

5.10: Rate of change of damage due to trucks L6, L7 and L8.....	90
5.11: Effect of load shifting from tandem to quadem axles (FEM).....	91
5.12: Effect of increasing spacing of a tandem axle (FEM)	92
5.13: Truck case L6– Effect of shifting loads between equal axles (MEPDG).....	95
5.14: Truck case L7– Effect of shifting loads between equal axles (MEPDG).....	95
5.15: Effect of load shifting from tandem to quadem (MEPDG)	96
5.16: Effect of changing axle spacing for truck L15 (MEPDG).....	97
5.17: MEPDG – FE comparison: Effect of load shifting (Tandem to tandem)	98
5.18: MEPDG – FE comparison: Effect of load shifting (Tridem to tridem).....	99
5.19: MEPDG – FE comparison: Effect of load shifting (tandem to quad)	99
5.20: MEPDG – FE comparison: Effect of changing axle spacing	100

LIST OF TABLES

Table	Page
3.1: Material Properties.....	51
4.1: Jointed Plain Concrete Pavement performance criteria.....	58
4.2: Vehicle class distributions used.....	61
4.3: Hourly Truck Traffic Distributions.....	62
4.4: Traffic growth models	62
4.5: One month tandem-axle load distribution-default values (in %).....	64
4.6: Monthly axle load distribution values (in %) for truck cases analyzed by MEPDG	65
4.7: MEPDG default average number of axles per truck.....	67
4.8: MEPDG-Truck class average number of axles used	67
4.9: Pavement design layers and properties used in MEPDG	73
5.1: Modified axle loads	76
5.2: Calculated damage relative to axle L1 (FEM).....	78
5.3: Calculated damage relative to truck L6a (FEM)	78
5.4: Summary of MEPDG performance output	93

CHAPTER 1

INTRODUCTION

1.1 Introduction

Pavements are engineering structures placed on natural soils and designed to withstand the traffic loading and the action of the climate with minimal deterioration and in the most economical way (Hudson et al, 2003). The majority of modern pavement structures may be classified as flexible or rigid pavement structures. A *flexible pavement* consists of a surface layer constructed of flexible materials (typically asphalt concrete) over granular base and sub base layers placed on the existing, natural soil. A *rigid pavement* consists of a Portland cement concrete surface layer supported by a subbase or subgrade. The rigid pavements can further be categorized depending on the types of joints constructed and use of steel reinforcement (Gillespie, 1993). Each of these pavement types has specific failure mechanisms, each failure mechanism being caused by specific factors. Example of such failure mechanisms include: fatigue damage of rigid pavements, fatigue damage of flexible pavements, faulting of rigid pavements, rutting of flexible pavements, and roughness of rigid and flexible pavements. These failure mechanisms are caused by the following factors: heavy vehicle loadings, climate, drainage, materials properties, and inadequate layer thicknesses (Hudson et al, 2003). Out of these factors, heavy vehicle loads are the major source for pavement damage.

Magnitude and configuration of vehicular loads together with the environment have a significant effect on induced tensile stresses within concrete pavement (Yu et al, 1998). Heavy

vehicles loads subject the pavements to high stresses causing damage. However not all trucks have the same damaging effects; their damage depends on speed, wheel loads, number and location of axles, load distributions, type of suspension, number of wheels, tire types, inflation pressure and other factors (Gillespie et al, 1993). The proper estimation of truck damage is important to truck permit regulators since the fees and penalties applied to truck operators for using the roads are related to the distresses induced to the road network. Regulators must permit trucks and allocate costs to vehicle operators in accordance with truck damage induced to pavements. The proper evaluation of truck damage also helps the highway engineers in the optimization of pavement design and maintenance activities (Zaghloul et al, 1994).

In recent years, several studies have estimated the truck damage by computing the responses (stresses, strains and deflections) of pavements under heavy vehicles loadings using mechanistic approaches (Chen et al, 2002). Therefore in response to the need for mechanistic pavement design and analysis procedures, researchers are increasingly using three dimensional finite element analysis techniques to quantify the response of the pavement system to applied axle and temperature loading (Davids, 2000). Another tool that would allow estimation of truck damages is the new Mechanistic Empirical Design Guide for pavements (NCHRP, 2004). Due to its advanced modeling capabilities, it is expected that federal and state transportation agencies will phase out the old empirical AASHTO Pavement Design Guide (1986,1993) to let the new Mechanistic Empirical Design Guide handle nowadays pavement design challenges such as increased number and weight of heavy vehicles (FHWA, 2005).

1.2 Research Objectives

The primary objective of this study is to calculate the response of jointed plain concrete pavement (JPCP) structure to passes of trucks of several configurations and, to compare the truck damage of each configuration based on the computed response. Specifically the research aimed at evaluating the truck damage when:

- Truck axles (i.e. tandems, quadems etc.) are loaded unequally,
- Number of axles in a group of axles are increased or decreased (change of axle type),
- Axle spacing are varied,
- Individual axles of the same group (i.e. axles in a tandem group) share load unequally.

Thirty-five truck configurations were studied based on the configurations proposed by the New York State Department of Transportation (NYSDOT), the sponsor of this research work.

In order to accomplish the research goal, a generalized three-dimensional finite element program (ABAQUS/CAE) was used in assessing the relationship of concrete pavement and effect of truck axles. The 3D-FEM is capable of simulating stationary or moving truck loads on a pavement. In this research, axle loads in the form of pressure at the pavement surface were applied on FE model of a rigid pavement and the maximum tensile stresses and strains due to individual axle groups were calculated. The stresses were then used in fatigue models to calculate the number of allowable passes of each truck that would induce fatigue cracking. The allowable truck passes were used to calculate relative truck damages in reference to one truck.

The Mechanistic-Empirical Design software was also used to estimate truck damage, but only for particular cases. The Mechanistic Empirical Design software is calculating and plotting fatigue cracking, faulting and IRI (International Roughness Index) against the number of load

repetitions. In this study the MEPDG software was used to analyze only ten truck configurations because it cannot model trucks with complex axle configurations and loadings such as unequal load distribution or unequally spaced axles in a group of axles. The analysis data used in the MEPDG software include: input traffic volumes, vehicle characteristic, environmental data (i.e. local climatic conditions) and pavement layers material properties and sizes. After each analysis run of the ten trucks cases, plots of fatigue cracks (bottom up and top down cracks), faulting and IRI were automatically drawn in spreadsheet. Thereafter predicted bottom up cracks at the end of year 40 were used to determine relative truck damage.

CHAPTER 2

BACKGROUND

This chapter presents a summary of background information related to damage on rigid pavements caused by heavy vehicles. Trucks are the major contributor toward pavement failure; therefore it is important to know how and to what extent they affect pavements. This review begins with describing the rigid pavement and associated distresses followed by description of various work on truck damage equivalency evaluation and findings. Also, an overview of the new Mechanist Empirical Design Guide is provided in this chapter.

2.1 Rigid Pavement

Rigid pavements are a pavement structures that deflect very little under loading because of the high stiffness of the Portland cement concrete used in the construction of surface layer. The pavement structural layers are composed of stiff Portland cement concrete surface layer on top of a base or sub base layer (when used) as shown in Figure 2.1. When viewed from top, the pavement is divided into two major parts; the traveling lanes for carrying desired traffic loads, and shoulders that act as support to the edges of the pavement and provide space for disabled vehicles to stop or drive slowly. Typical rigid pavements may be constructed with joints only, joints and steel reinforcement or steel reinforcement only. Depending on the type of construction, rigid pavements are named either Jointed Plain Concrete Pavement (JPCP), or Jointed Reinforced Concrete Pavement (JRCP) or Continuously Reinforced Concrete Pavement (CRCP).

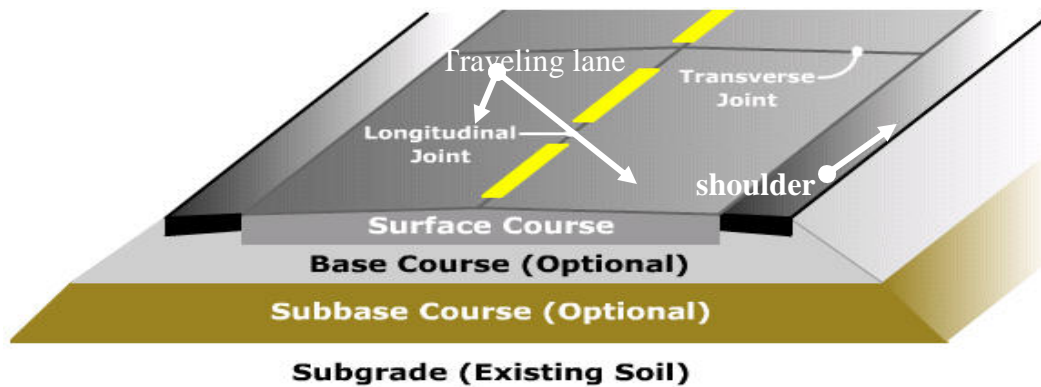


Figure 2.1: Typical rigid pavement sections (WSDOT, 2009)

Jointed Plain Concrete Pavement (JPCP): Jointed Plain Concrete Pavement is the most widely used type of rigid concrete pavement (ACPA, 2009). Its construction costs are lower than those of the other two types of rigid pavements. JPCP is designed with short joint spacing that eliminates the development of transverse cracks (Figure 2.2). In fact, joints relieve stresses in the concrete pavement and act as predetermined paths for development of transverse shrinkage cracks. In most cases the joints are provided with dowel bars spaced at 12 inch intervals. The typical size of slabs for Jointed Plane Concrete Pavement is 12 to 15 ft wide by 15 to 20 ft long (WSDOT, 2009).

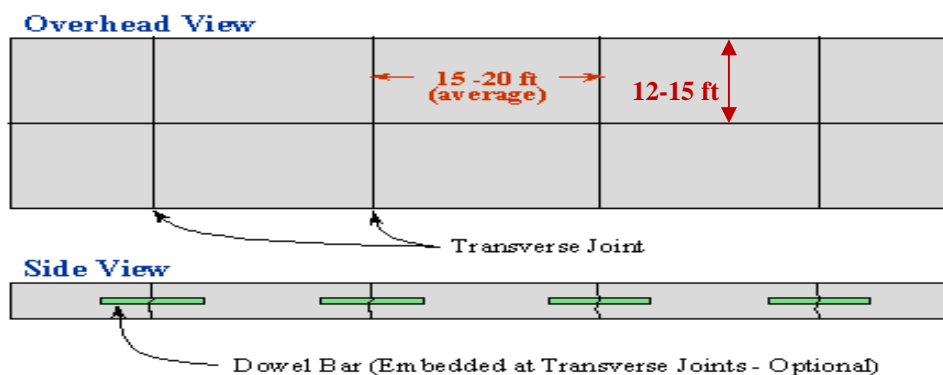


Figure 2.2: Jointed Plain Concrete Pavements (ACPA 2009)

Jointed Reinforced Concrete Pavement (JRCP): JRCP comprised of concrete surface layer with steel reinforcement and transverse joints to control cracks (Figure 2.3). The steel reinforcement in JRCP is in the form of wire mesh or deformed bars and does not increase the strength of the pavement but allow the use of longer joint spacing (Huang, 2004). The meshes enhance use of longer joints because they hold tightly together the transverse cracks that would develop within the concrete slab (NCHRP 2003). The typical JRCP joint spacing varies from 25 to 50 ft (WSDOT 2009). Because of longer joint spacing, dowels are always provided for joint load transfer purposes. The JRCP pavements are rarely used in the US for highway pavements because of long term performance problems (WSDOT 2009).

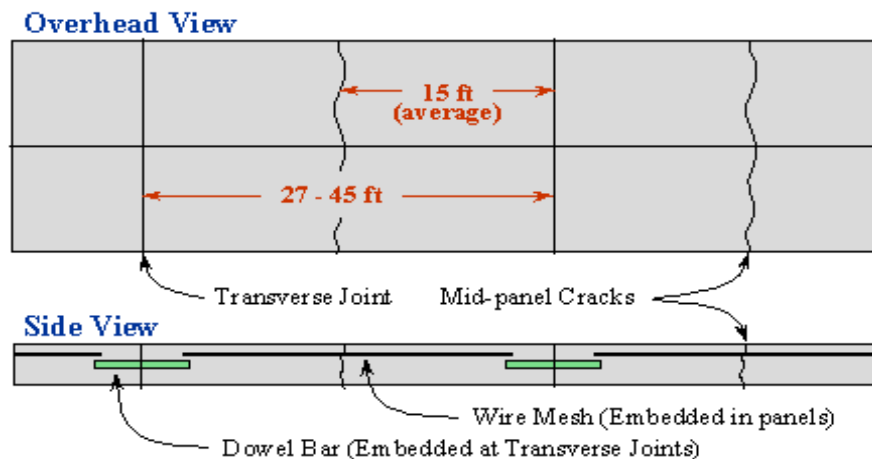


Figure 2.3: Jointed Reinforced Concrete Pavements (ACPA 2009)

Continuously Reinforced Concrete Pavement (CRCP): Continuously Reinforced Concrete Pavements are constructed free of contraction joints (Figure 2.4). CRCP allows transverse cracks to occur but holds them tightly with steel reinforcement (NCHRP, 2003). The transverse cracking behavior in CRCP depends on concrete properties (drying shrinkage, thermal properties, tensile strength, creep, and elastic modulus), reinforcing steel properties (bar diameter

and coefficient of thermal expansion), and environmental conditions (AASHTO, 1993). Typically the reinforcement steels make up 0.6-0.7 percent of the concrete cross section area (WSDOT, 2009). Because of the joint-free design and reinforcements, the CRCP pavement thickness can be reduced. However its construction costs are higher than the other two types of rigid pavements.

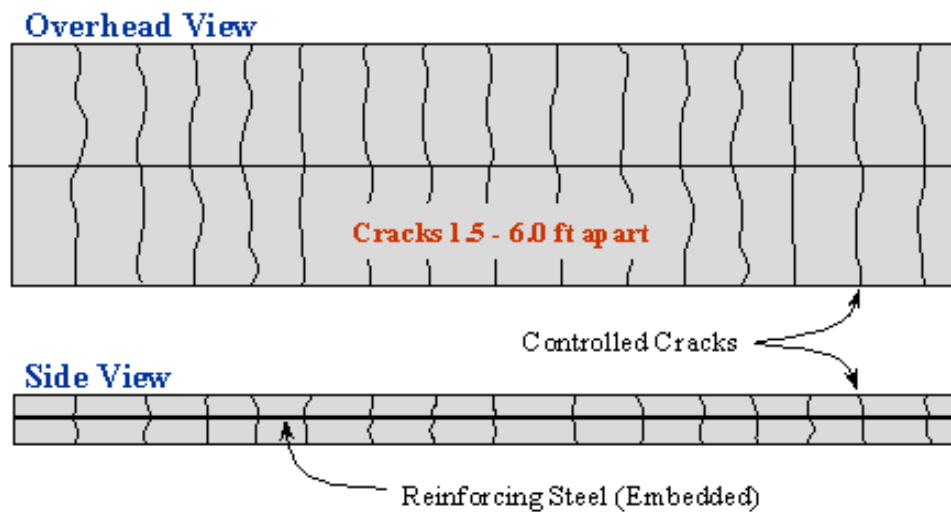


Figure 2.4: Continuously Reinforced Concrete Pavement (ACPA 2009)

2.2 Basic Structural Components of Rigid Pavement

A typical rigid pavement structure includes the following components: concrete surface course, base course, sub base course, joints and load transfer mechanisms. All of these components must be well designed and coordinated to develop a fully functional rigid pavement.

Concrete surface course: This is a layer in contact with traffic loads. It is designed to resist the wear caused by traffic and the environment. Also the surface offers a smooth ride to drivers, friction for braking, noise control and good drainage. The surface course is made up Portland cement concrete. The concrete material mixture is normally comprised of cement (binder), coarse aggregates, fine aggregates, water and admixtures if necessary.

Base course: This is the layer right below the surface course. The basic functions of the base course are to distribute the loads over a wider area, provide additional drainage and frost resistance, provide uniform support to the concrete slab and a stable platform for construction equipments and minimize movement due to slab pumping. According to WSDOT, 2009, the base course may be constructed of:

- Crushed aggregate
- Stabilized aggregates or soils
- Dense-graded hot mix asphalt
- Permeable hot mix asphalt
- Lean concrete

Subbase course: This is a layer between the base course and the subgrade. Its major function is to add support to the pavement structure, but it can also:

- Minimize the movement of fine soils from the subgrade into the pavement structure,
- Improve drainage,
- Restrict frost action damage, and
- Provide a working platform for the construction of the base course.

In most cases the materials for the subbase are weaker than those of the base course but better than the subgrade soils. The commonly used materials for subbase are aggregates and high quality structural fill.

Joints and load transfer mechanisms: Joints are purposeful discontinuities placed in rigid pavement concrete slabs. According to ACPA, 2009, joints are provided for the following reasons:

- To control contraction and expansion within concrete slabs,
- To separate concrete cast at different times, and
- To reduce compressive stresses that develop at T and unsymmetrical intersections, ramps, bridges and anywhere differential movement between the pavement and a structure may take place.

When the joints are provided in the pavement concrete slabs, the traffic load distribution from one slab to the neighboring slab is done through a load transfer mechanism.

If the load transfer mechanism is secured properly, both the loaded and unloaded slabs deflect equally, that means the load transfer efficiency is 100%. The load transfer efficiency is defined by the following equation.

$$\text{Load transfer efficiency} = \frac{\Delta a}{\Delta l} \times 100\% \quad [2.1]$$

Where: Δa = loaded slab deflection

Δl = unloaded slab deflection

Normally load transfer mechanism in concrete pavements can be provided in two ways, aggregate interlock and dowel bars.

- Aggregate interlock

Aggregate interlock is the mechanical locking which forms between the fractured surfaces along the crack below the joint saw cut (see Figure 2.5) (ACPA, 2001). This type of

interlock is good for low-volume roads. The aggregate interlock method is good for joints widths less than 0.9 mm (0.035 inches)



Figure 2.5: Aggregate Interlock

- Dowel Bars

Dowel bars are short steel bars that provide a means of load transfer between slabs without restricting horizontal movement of the concrete. They provide a load transfer efficiency of about 70 to 100 percent. The dowel bars are typically 1.25 to 1.5 inches in diameter, 18 inches long and spaced 12 inches apart. In order to prevent corrosion, dowel bars are either coated with stainless steel or epoxy. Dowel bars are usually inserted at mid-depth of the slab and coated with a bond-breaking substance or sleeved with a plastic cover on one half to prevent bonding to the PCC (Figure 2.6) (WSDOT, 2009). This half of the dowel bars is made to be loose in the concrete in order to allow the concrete to move freely as it expands and contract. Thus no cracks will occur due to limits in concrete movement.



Figure 2.6: Dowel bar in place

2.3 Distresses on Rigid Pavement

Distresses on pavements refer to damage that hinders pavement performance. The extent and severity of the distresses are mainly due to the variation of subgrade soil strength, pavement materials characteristics, traffic loading, environmental effects, construction quality and age. Common rigid pavement distresses include: spalling, faulting, cracking, joint seal damage, longitudinal cracks, transverse fatigue cracks, D-cracking, popouts, pumping, settlement, etc. In this research, only damage due to transverse fatigue cracks and faulting were needed to compare relative damage of trucks. Therefore the two distresses are further explained in the next two sections.

2.3.1 Transverse fatigue cracks

Transverse cracks develop on all concrete types, usually perpendicular to the pavement centerline. The width of the cracks developed may go up to 6mm (FHWA, 2003). The means by which the cracks develop differ from one type of rigid pavement to another. In Jointed Plain Concrete Pavement (JPCP), transverse cracks are caused by repeated traffic loading, drying shrinkage of the concrete, temperature variations, curling/warping, existence of transverse

cracking in the underlying layers and late or inadequate transverse joint sawing. The transverse cracks may either start at the bottom or the top of the concrete slab depending upon the temperature and/or moisture gradients. When temperature and moisture gradients are negative (i.e. low temperature and less moisture at top of concrete surface), the cracks initiate from top of concrete slab, while bottom-up cracks develop when temperature and moisture gradient are positive (i.e. low temperature and less moisture at bottom of concrete slab) (Figure 2.7).

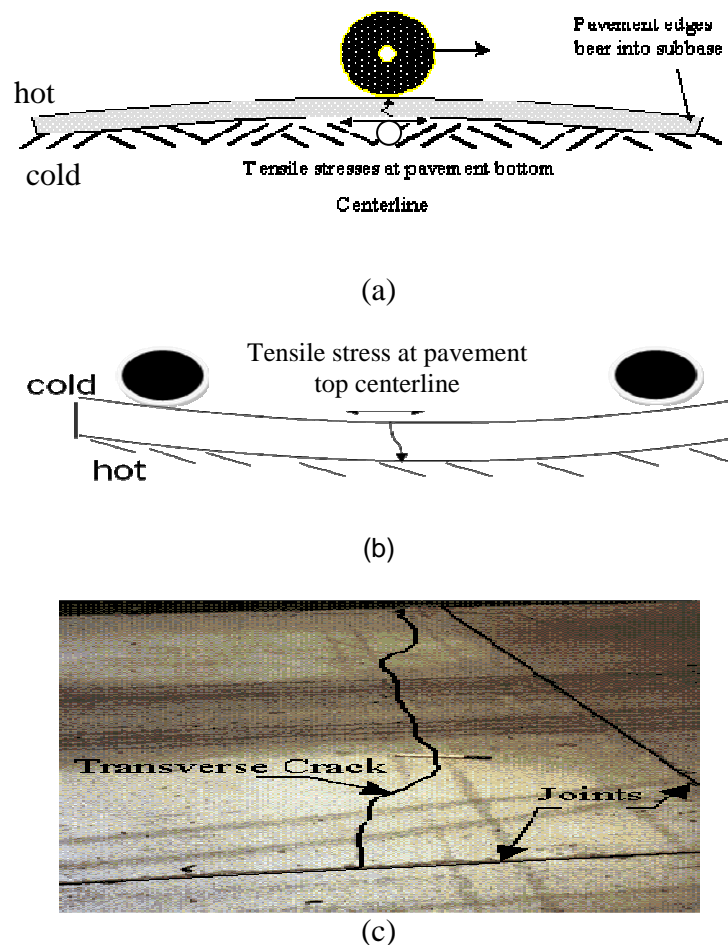


Figure 2.7: Transverse cracks development: (a) bottom up cracks, (b) top down cracks (c) photo of a complete transverse crack.

2.3.2 Faulting

Faulting is recorded when a difference in elevation of concrete slab(s) across joints or cracks is observed (Figure 2.8). The major cause for faulting is heavy traffic loading and climatic loading. If dowels are used, dowel loosening and enlargement of dowel sockets also play a part in faulting. Pavements with poor drainage are more likely to develop faulting than those with good drainage. Also, erosion under joints due to poor subbase materials contributes in faulting. In fact, the progression of faulting is a function subbase/base material; the poorer the subbase/base is, the higher is the faulting.

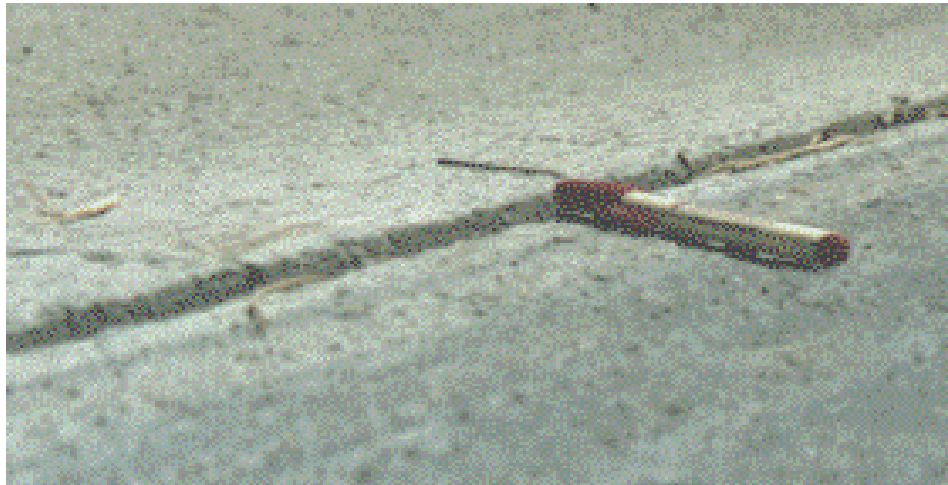
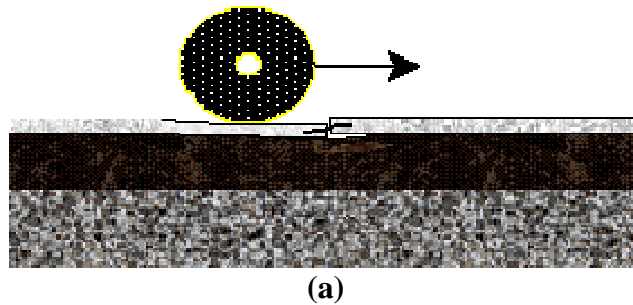


Figure 2.8: Joint faulting development: (a) cross-section view (b) top view

2.4 Damage equivalency for various vehicle/wheel configurations

Darestani et al (2006) used a finite element program, everFE2.23, to determine the critical configuration and position of axle groups on jointed plain concrete pavement. This was part of a review work for a 2004 Australia Design Guide which is based on PCA pavement design methods (Darestani et al, 2006). At first a single axle single tire (SAST) of 53kN was placed at the centre, then at the middle of the longitudinal edge, and finally at the corner of the concrete base to determine the effect of tire pressure on pavement response. At each location the tire inflation pressure was varied from 500 kPa to 1400 kPa. The results obtained showed that the variation of tire inflation pressure has no significant effect to the pavement when the wheel is placed at the centre of the slab or middle of the longitudinal edge of the slab. However, when the wheel is placed at the corner of the pavement; an increase in inflation pressure produces greater concrete tensile stress (Figure 2.9).

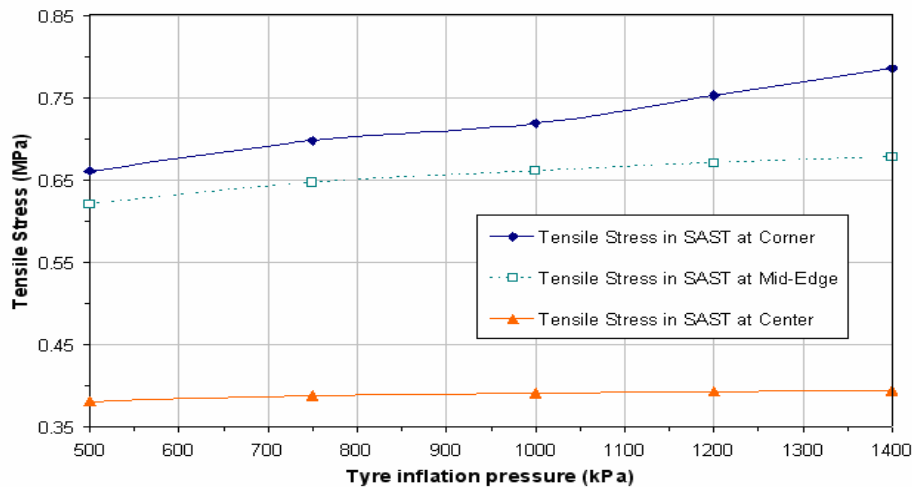


Figure 2.9: Effect of tire inflation pressure (Darestani et al, 2006)

Also, Darestani et al (2006) studied the effect of the spacing between axles in a given axle groups. Three types of axle group base on Austroads (2004) were used to investigate the

effects of varying the spacing between axles in a given axle group on the response of rigid pavement. The axles considered were Tandem Axle Single Tire (TAST), Tandem Axle Dual Tire (TADT) and Tridem Axle Dual Tire (TRADT). Each axle load was individually placed at the centre of the longitudinal edge of the pavement. The axles spacing was varied between 1,000 mm to 1,600 mm at an interval of 100 mm. The study showed that the increase in axle spacing linearly decreases the base deflection and nonlinearly reduces tensile stress in concrete. According to Darestani et al (2006) all of the analyses were performed on a single slab; thus more studies are needed to see the effects of interconnected slabs.

Gillespie et al (1993) studied the effect of heavy vehicles, tire (type, inflation pressure etc.), pavement, and environmental factors as determinants of pavement damage. The study examined the characteristics of trucks and their effect on fatigue damage of pavements. The ILLI-SLAB finite element model was used to model rigid pavements and vehicle loading characteristics. The study found that damage to rigid pavement were dominated by fatigue caused by longitudinal tensile stresses near the centre bottom edge of a slab. Out of all factors assessed, the static axle load was found to have the greatest effect on fatigue damage, with a variation factor of 20:1 over a range of axle loads from 10 to 22 kips. The assessed axle damage are represented based on equivalency damage caused by an 18 kips standard axle.

The study adopted the Vesic fatigue model to analyze the axle fatigue damage. The model was first introduced by Vesic and Saxena in 1969. Vesic combined Westergaard plate theory and AASHO Road Test data to develop the following relationship:

$$N_{2.5} = 225000 \times \left(\frac{MR}{\sigma} \right)^4 \quad [2.2]$$

Where

$N_{2.5}$ = Number of axle passes to failure

σ = Maximum tensile stress of concrete slab

MR = Modulus of rupture of concrete slab

Damage per axle or Load Equivalent Factor (LEF) for any axle can be derived from equation (2.2) base on the allowable passes of the axle and allowable passes of 18ks standard axle.

$$LEF = \frac{\frac{1}{N_x}}{\frac{1}{N_{18}}} = \left(\frac{\sigma_x}{\sigma_{18}} \right)^C \quad [2.3]$$

Where

$C = 4$ for Vesic and Saxena analysis.

Subscript x refers to stresses from axle type x

Subscript 18 refers to stresses from standard single axle dual tire of 18lb

Kuo et al. (2001) revisited Vesic and Saxena LEF eq. 2.3 to establish the constant power C . The study used the Abaqus finite element analysis package to model a 3D AASHTO rigid pavement. In this model, unlike the AASHTO test, a temperature difference was considered and estimated as follows;

$$TD = 13.5786 - \frac{52.181}{D} \quad [2.4]$$

Where

TD = Temperature difference

D = Slab thickness ranging from 6 to 14 inches.

By substituting into eq. 2.3 the values of LEF from AASHTO design guide (1993) and on the right hand side replace the stresses with the values obtained from the analyzed rigid pavement model, the power C was estimated to range from 5 to 6, depending on the base thickness.

Apart from revisiting eqn. 2.3, Kuo et al. developed a new model for the estimation of LEF. The equation is a result of the analysis of rigid pavements in Taiwan, modeled in 3D FEM. It accommodates the effects of base strength, thickness and joint load transfer design. It is a regression equation with constants $C1$, $C2$, $C3$ and $C4$ as shown below;

$$LEF = \left(\frac{Q_t}{Q_{18}} \right)^{C1} \times \left(\frac{V_t}{V_{18}} \right)^{C2} \times 10^{C3(R_t - R_{18}) + C4} \quad [2.5]$$

Where

$$Q_t = 1.1 \times L_t + 0.8 \times B_{st}$$

$$Q_{18} = 1.1 \times 18 + 0.8 \times B_{st}$$

$$V_t = 1.2 \times D + 0.3 \times L_t$$

$$V_{18} = 1.2 \times D + 0.3 \times L_t$$

$$L_t = \text{Axle load (kips)}$$

$$B_{st} = 10^{-6} \times E_b \times D_b$$

$$R_t = \frac{L_t}{D + 0.9 \times B_{st}}$$

$$R_{18} = \frac{18}{D + 0.9 \times B_{st}}$$

$$E_b = \text{Young Modulus of base material (psi)}$$

D_b = Thickness of base (in)

D = Thickness of Slab (in)

C_1 , C_2 , C_3 and C_4 are regression constants provided by Kuo et al (2000).

Hiller et al. (2005) adopted the influence line approach to determine the magnitude and location of critical stresses in concrete pavement. Multiple analyses of ISLAB finite element model were used to calculate stresses after every 0.3m axle loading position. This study found that when the steer and drive axles of a truck are spaced between 2.8m and 6.4m apart, they cause top down fatigue cracks given the condition that concrete slab surface temperature is higher than that at bottom. The maximum stress that caused the top down cracks was found to be located near the center of the slab. Also, the study found that maximum bottom up stresses occurs near or at the mid slab under the applied loaded axle. When using the influence line approach it was also possible to determine stress ranges for each passing of set of axles. The study refers to stress range as the difference between the maximum flexural stress applied during cyclic loading of a slab (i.e. axle wheels passes) and the minimum flexural stress existing within the concrete before applying cyclic loading (this is a minimum stress resulted from temperature).

Hiller et al (2005) used the following fatigue stress model by Tepfers (1979) to determine the allowable number of loads for a given axle load and climate combination.

$$\frac{\sigma_{\max}}{MOR} = 1 - \beta(1 - R) \log N \quad [2.6]$$

Where

N = Number of axle repetition to failure (reliability = 50%)

MOR = Concrete Modulus of Rupture

σ_{\max} = Maximum flexural stress applied during cyclic loading

σ_{\min} = Minimum flexural stress before loading (Taken from temperature effects)

$$R = \frac{\sigma_{\min}}{\sigma_{\max}}$$

β = Calibration coefficient (0.0685 for concrete)

Also, the study suggests that equation 2.6 can be modified to equation 2.7 when a minimum flexural stress is taken to be zero (i.e. maximum stresses only). This new model gives a smaller number of axle repetitions to failure.

$$\frac{\sigma_{\max}}{MOR} = 1 - \beta \log N \quad [2.7]$$

Zaghloul et al. (1994) studied the effect of overloaded vehicles on Indiana Highways. They used Finite element analysis (Abaqus, 1989) and field performance data to develop Purdue load equivalent factors. The Purdue Load Equivalent Factor (Purdue LEF) for rigid pavement was developed based on two statistical models for the maximum surface deflection (MSD). One model predicts MSD from one pass of any axle configuration in consideration. The other model predicts MSD from repetitions of an 18-kip standard axle. From the two models, the LEF is determined as the number of repetitions from an 18-kip standard axle load that causes the same MSD as one pass of any axle in consideration (Figure 2.10). Also, the study found that speed is a significant factor in determining maximum surface deflection of a rigid pavement. Therefore the two MSD models are presented mathematically into two sets depending on vehicle speed.

Low Speeds Model (<20mph):

For one pass of any axle,

$$MSD = a * D^4 + b * N + c * T + d * N^2 \quad [2.8]$$

For repeated passes of 18-kip standard axle load,

$$MSD = (a + b * T) * C. \quad [2.9]$$

High Speeds Model (>20mph):

For one pass of any axle,

$$MSD = a * D^4 + b * N + c * T + d * S * N + e * S * D^4 + f * S \quad [2.10]$$

For repeated passes of 18-kip standard axle load,

$$MSD = (a + b * T) * C. \quad [2.11]$$

Where,

D = load per axle

T = Slab thickness (inch)

N = Number per axles

S = Speed (mph)

C= Number of 18 kip SAL

a to f = Regression coefficients as determined by Zaghoul et al. (1994) depending on speed and other factors.

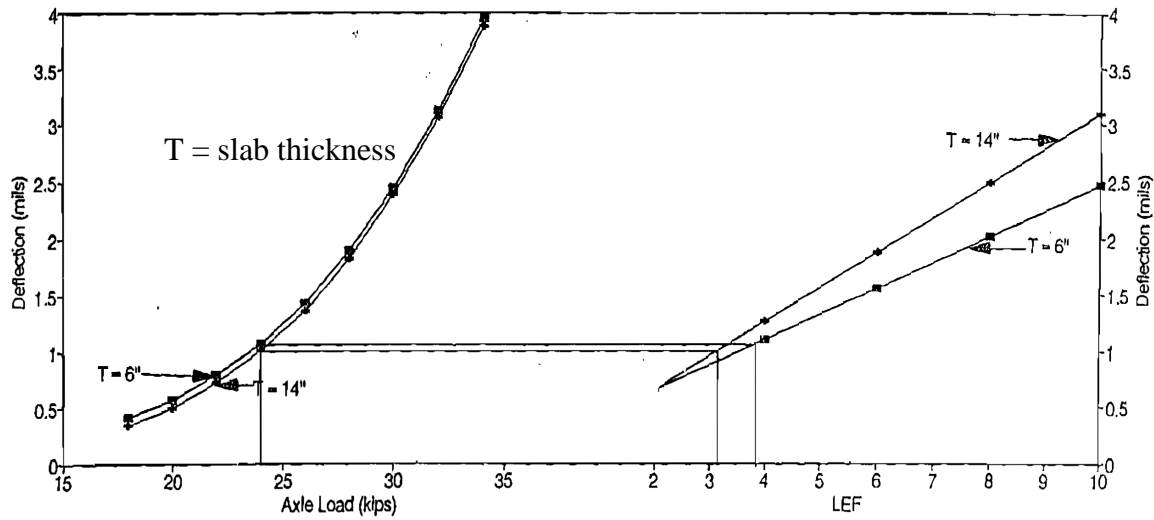


Figure 2.10: Purdue LEF's for rigid pavements (Zaghloul, 1994)

Huang, (2004) used Darter fatigue model, 1977 and Portland Cement Association (PCA) fatigue models to illustrate pavement damage calculations. Darter fatigue analysis uses the following expression for allowable number of axle repetitions.

$$\log(N_f) = f_1 - f_2 \left(\frac{\sigma}{MR} \right) \quad [2.12]$$

Where,

N_f = Allowable load repetitions at conditions

MR = Concrete modulus of rupture

σ = Applied maximum tensile/flexural stress

f_1 = 16.61 (Darter and Barenberg, 1977)

f_2 = 17.61 (Darter and Barenberg, 1977)

Portland Cement Association (PCA) suggests a more conservative approach to calculate the allowable repetitions, recommending the use of Packard and Tayabji, 1985 expressions (Yang H. Huang, 2004).

$$\text{For } \frac{\sigma}{MR} \geq 0.55 : \quad \log(N_f) = 11.737 - 12.077 \left(\frac{\sigma}{MR} \right) \quad [2.13a]$$

$$\text{For } 0.45 < \frac{\sigma}{MR} < 0.55 : \quad N_f = \left(\frac{4.2577}{\frac{\sigma}{MR} - 0.325} \right)^{3.268} \quad [2.13b]$$

$$\text{For } \frac{\sigma}{MR} \leq 0.45 : \quad N_f = \text{unlimited} \quad [2.13c]$$

2.5 Mechanistic-Empirical Pavement Design Guide (MEPDG)

2.5.1 Introduction

The Mechanistic Empirical Pavement Design Guide for analysis and design of pavements is a product of project 1-37A initiated in 1996; sponsored by National Cooperative Highway Research Program (NCHRP, 2004). The guide combines empirical relationship obtained from field data with theoretical predictions based on the mechanics of materials to efficiently analyze both flexible and rigid pavements. AASHTO expressed the need of this guide to replace the AASHTO empirical design guides in 1986, but implementation was difficult. Thanks to the introduction of high-speed computers, the new Mechanistic Empirical Pavement Design Guide is now practical (Khanum, 2005).

2.5.2 Advantages of new Mechanistic Empirical Pavement Design Guide over the empirical AASHTO design guides (1986, 1993).

According to FHWA (2008), the advantages of the mechanistic-empirical approach over the traditional empirical approach are:

- It incorporates a wide range of materials properties,
- It increases pavement longevity,

- It handles higher traffic levels, higher tires pressures and increased loads,
- It handles different climatic conditions,
- It includes aging and seasonal effects in estimating pavement performance (i.e. asphalt harden with time), and
- It can evaluate the effects of base erosion under rigid pavement.

2.5.3 Design approach

Yoder and Witczak (1975) noted that for any pavement design procedure to be completely rational, three components must be considered fully:

- The theory used must predict the assumed distress parameters,
- The material properties applicable to the theory selected must be evaluated and
- The relationship between magnitude and parameters in question to the performance level desired must be determined.

This design guide analyzes pavement problems following the approach summarized in figure 2.12. Firstly the design covers the development of input values for analysis. One of the important considerations at this stage is foundation analysis. The processes considered under foundation analysis include stiffness determination, evaluation of volume changes, frost heave, thaw weakening, subgrade improvement and drainage considerations. Other inputs considered at this stage are material characteristics where properties such as stiffness are changing with time. Also, traffic input and climatic changes are part of parameters considered at this stage.

A second stage of design process deals with structural/performance analysis. At this stage, the design guide analyses a trial design base on predetermined failure criteria. The process is cumulative, where damages calculated in the first month are used as initial damages for a

second month, the second month damages are used as initial damages for the third month and so on until the end of expected design life. If the trial design does not pass the performance criteria, modifications are done and the analysis re-run. This loop continues until all performance criteria are met (NCHRP 2004).

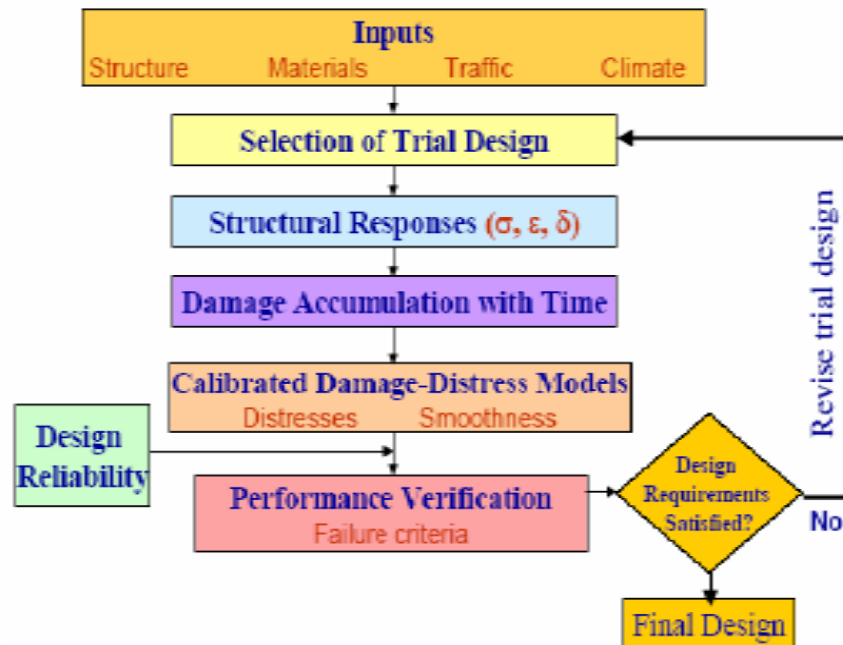


Figure 2.11: MEPDG flow diagrams (NCHRP, 2004)

2.5.4 Design inputs

The Mechanistic Empirical Design Guide allows the designer to use materials, traffic loads and environmental loads inputs depending on the importance of the project and availability of resources. The inputs in the guide are divided in three levels of applications:

Level-1 input is employed where high accuracy is needed especially for designing heavily trafficked pavements or wherever there is poor safety or economic consequence as a result of early failure. Level-1 input requires detailed data from field and or laboratory. This level needs more time and resources than the other two.

Level-2 inputs give a moderate level of accuracy. This level does not differ much from the earlier versions of the AASHTO guide. With limited resources and equipment, inputs can be obtained from an agency data base and limited testing programs, or derived from the available data.

Level-3 inputs provide the lowest level of accuracy. The design use of this level of inputs is preferred for lower volume roads. The inputs may be typical average values for the region.

The MEPDG does not restrict combination of level in one project. For instance, Level-1 concrete modulus of rupture, Level-2 traffic load spectra and Level-3 subgrade resilient modulus may be used in the same project.

2.5.4.1 Foundation design

The foundation soil/subgrade is the natural material underneath a constructed pavement. Also may be referred to as the bed for the pavement. The MEPDG provides a layout on how the foundation parameters for use in pavement are determined.

First the foundation soil properties are evaluated. The evaluation procedure includes:

- Laboratory testing of undisturbed or reformed field samples obtained from subsurface site exploration.
- Non destructive testing of the existing pavement foundation.
- Intrusive testing such as the Dynamic Cone Penotrometer (DCP).
- Using existing data from agencies' experience with subgrade at the region.

The properties obtained at this stage relate to stiffness of foundation soil (i.e. resilient modulus).

Secondly the subsurface soil profiles are determined in both vertical and horizontal directions. Subsurface investigations procedures and laboratory testing programs may be used to

obtain soil types, densities, moisture content, water table level, swelling and frost susceptible soils.

Finally troublesome foundation soils must be identified. Knowing the locations and the conditions such as highly compressible soils, expansive and swelling soils, etc, may allow specific treatment program to be put in place to bring the soil to the desired properties.

2.5.4.2 Materials

The MEPDG divides the materials properties into three categories:

In the first category, properties such as elastic modulus and Poisson's ratio are needed to predict the state of stress, strain and displacement within the structure when subjected to external loads.

The second category includes material properties that are related to distress or smoothness functions. Examples of the considered distresses are fatigue cracks of JPCP, faulting of JPCP and punchout. The materials parameters laid out by the Guide to enhance the functionality of smoothness and distress models include: modulus, Poisson's ratio, strength, expansion-contraction characteristics, friction between slab and base, erodibility of core layers, drainage characteristics, plasticity and other properties that affects given distress mechanism.

The third category deals with material parameters related to climatic effects such as plasticity index, gradation parameters, absorptivity, heat capacity, coefficient of thermal expansion, etc.

2.5.4.3 Environmental effects

The MEPDG can accommodate climatic conditions from any region. Climatic effects accelerate the severity of most pavement distresses. Factors such as precipitation, temperature, freeze-thaw cycle, depth to water table, drainability of pavement layers, infiltration potential of materials and many others affect significantly the performance of both flexible and rigid pavements.

Climatic conditions in the pavement structure and subgrade over several years are well analyzed in the guide using a climatic modeling tool known as Enhanced Integrated Climatic Model (EICM). The EIMC computes and predicts the following conditions to the entire pavement: temperature in pavement layers, resilient modulus adjustment factors, pore water pressure, water content, frost and thaw depths, frost heave, and drainage performance. The EICM is coupled as an integral part of the M-E pavement design guide software.

2.5.4.4 Traffic

Pavements are first and foremost designed to carry traffic without exhibiting failure during their design life. Therefore this design guide takes traffic data as one important element for structural analysis and design of pavements. ME-PDG requires the same traffic data for all types of pavements and designs (new or rehabilitated). Also the guide uses monthly cumulative number of vehicles to describe the traffic load. The previous AASHTO pavement design guide uses the equivalent single axle load (ESAL) approach.

Agencies responsible for traffic data collection use Weigh-In-Motion (WIM), Automatic vehicle classification and counting and traffic forecasting models to obtain the following information:

- Base year traffic volume
- Vehicle class distributions
- Axle load distribution factors
- Directional and lane distribution factors
- Axle and wheel base configuration
- Tire inflation pressure and tire characteristics
- Truck growth factors
- Truck lateral distribution factors
- Monthly distribution factors and
- Hourly distribution factors

In this Guide, traffic data for design of pavements are divided into three levels:

Level-1 – There is enough and firm knowledge regarding traffic characteristics. This is possible only when the data have been collected along or near the road to be designed.

Level-2 – There is a modest knowledge of traffic characteristics. This is true only when regional/statewide truck volumes are available.

Level-3 – There is poor knowledge of past and future traffic characteristics. This means that a designer has to rely on default values computed from national wide data base.

ME-PDG classifies truck traffic in accordance with FHWA classes. The classification summary is shown in Figure 2.12














SCHEMATIC DESCRIPTION		TRAFFIC CLASS DESCRIPTIONS	
1-2 axles		1	Motorcycles
		2	Passenger cars
		3	Two axles and tire single units
		4	Buses
3-5 axles		5	Two axles and tire single units
		6	Three axles single units
		7	Four or more axle single units
		8	Four or less axle single trailers
5 + axles		9	Five axle single trailers
		10	Six or more axle single trailers
		11	Five or less axle multi-trailers
		12	Six axle multi-trailers
		13	Seven or more axle multi-trailers

Figure 2.12: Trucks classification (khanum, 2005)

2.5.5 JPCP distress prediction models

The JPCP performance may be measured in terms of three distresses: Transverse cracking, faulting and smoothness. All of the distresses can be calculated at different levels of reliability. The MEPDG uses the following statistical models to calculate cracking, faulting and smoothness of the Jointed Plain Concrete Pavement.

2.5.5.1 Cracking Model

Transverse cracks in Jointed Plain Rigid Pavement may develop in two ways: Bottom-up and top-down cracking. The percentage of slabs with transverse cracks is calculated by equation 2.14. The model assumes the cracks will not happen all together on the same slab (NCHRP, 2004).

$$CRK = \frac{1}{1 + FD^{-1.68}} \quad [2.14]$$

Where,

CRK = predicted amount of bottom-up or top-down cracking

FD = Calculated fatigue damage.

The general expression for fatigue damage is:

$$FD = \sum \frac{n_{i,j,k,l,m,n}}{N_{i,j,k,l,m,n}} \quad [2.15]$$

Where,

FD = Fatigue damage;

$n_{i,j,k,l,m,n}$ = Applied number of load application at condition i, j, k, l, m, n .

$N_{i,j,k,l,m,n}$ = Allowable number of load applications at condition i, j, k, l, m, n .

i = age, j = month, k = axle type, l = load level, m = temperature difference, and n = traffic path.

The allowable number of load applications is determined using the following fatigue model:

$$\log(N_{i,j,k,l,m,n}) = C_1 \left(\frac{MRi}{\sigma_{i,j,k,l,m,n}} \right)^{C_2} + 0.4371 \quad [2.16]$$

Where,

$N_{i,j,k,l,m,n}$ = Allowable number of load applications at condition i, j, k, l, m, n

MRi = PCC modulus of rupture at age i, psi

$\sigma_{i,j,k,l,m,n}$ = Applied stress at condition i, j, k, l, m, n

C_1 = Calibration constant=2.0; and

C_2 = Calibration constant=1.22.

The sum of both types of transverse cracks is determined as follows:

$$TCRACK = (CRK_{Bottom-up} + CRK_{top-down} - CRK_{Bottom-up} * CRK_{top-down}) * 100\% \quad [2.17]$$

Where,

TCRK = total cracking (percent).

$CRK_{Bottom-up}$ = Predicted amount of bottom-up cracking (fraction)

$CRK_{Top-down}$ = Predicted amount of bottom-up cracking (fraction)

2.5.5.2 Faulting Model

Mean transverse joint faulting is predicted incrementally on every month. A faulting increment is determined each month, and the level of faulting that exists at any month affects the magnitude of increment. The following equation is used to determine faulting at each month as a sum of all previous months in the pavement life.

$$Fault_m = \sum_{i=1}^m \Delta Fault_i \quad [2.18]$$

$$\Delta Fault_i = C_{34} * (FAULTMAX_{i-1} - \Delta Fault_{i-1})^2 * DE_i$$

$$FAULTMAX_1 = FAULTMAX_0 + C_7 * \sum_{j=1}^m DE_j * \log(1 + C_5 * 5.0^{EROD})^{C_6}$$

$$FAULTMAX_0 = C_{12} \delta_{curling} * \left[l \log(1 + C_5 * 5.0^{EROD}) * \log\left(\frac{P_{200} * wetdays}{P_s}\right) \right]^{C_6}$$

Where,

$Fault_m$ = Mean joint faulting at the end of month m , in.

$\Delta Fault_i$ = Incremental change (monthly) in mean transverse joint faulting during month i , in.

$FAULTMAX_i$ = Maximum mean transverse joint faulting for month i , in.

$FAULTMAX_0$ = Initial maximum mean transverse joint faulting, in.

$EROD$ = Base/subbase erodibility factor.

DE_i = Differential deformation energy accumulated during month i ; this is the factor that takes into account the effect of traffic loading. The MEPDG mathematical model for DE is as follows:

$$DE = \frac{k}{2(\delta_{loaded}^2 - \delta_{unloaded}^2)} \quad (lb/in) \quad [2.19]$$

Where

k = modulus of subgrade reaction

δ_{loaded} = deflection of loaded slab

$\delta_{unloaded}$ = deflection of unloaded slab

$\delta_{curling}$ = Maximum mean monthly slab corner upward deflection PCC due to temperature curling and moisture warping.

P_S = Overburden on subgrade, lb.

P_{200} = Percent subgrade material passing #200 sieve.

$Wetdays$ = Average annual number of wet days (greater than 0.1 in rainfall).

C_1 to C_8 , C_{12} and C_{34} are national calibration constant, which are;

$$C_{12} = C_1 + C_2 * FR^{0.25}$$

$$C_{34} = C_3 + C_4 * FR^{0.25}$$

$C_1 = 1.29$; $C_2 = 1.1$; $C_3 = 0.001725$; $C_4 = 0.0008$; $C_6 = 0.4$; $C_7 = 1.2$

Where;

FR = Base freezing index defined as percentage of time the top base temperature is below freezing (32 °F) temperature.

The functional form of the model reflects the hypothesis that faulting potential depends of amount of the PCC slab curling, base erodibility, and the presence of fines and free water in the subgrade. Faulting potential decreases with an increase of overburden pressure on the subgrade. The rate of faulting increase depends on the faulting level; it decreases when faulting increases until it stabilizes at a certain level.

2.5.5.3 IRI Model

One of the important characteristics a pavement has to offer to its users is comfort. The comfortable condition is achieved when the longitudinal profile of the pavement surface is fairly smooth. The MEPDG defines smoothness in terms of International Roughness Index (IRI). In terms physical condition at a site, smoothness is defined as a life time change in shape of the

longitudinal profile of a pavement with reference to a perfectly flat profile. The IRI model of smoothness prediction (see equation 2.20) includes joint faulting, joint spalling and transverse cracking.

$$IRI = IRI_i + C_1 * CRK + C_2 * SPALL + C_3 * TFAULT + C_4 * SF \quad [2.20]$$

Where,

IRI = predicted IRI, in/mi.

IRI_i = initial IRI, in/mi.

CRK = percentage slabs with transverse cracks.

TFAULT = total joint faulting cumulated per mi, in.

$$C_1 = 0.8203$$

$$C_2 = 0.4417$$

$$C_3 = 1.4929$$

$$C_4 = 25.24$$

SF = site factor

$$= AGE (1+0.5556*FI) (1+P_{200})*10^{-6}$$

AGE = pavement age, years

FI = freezing index, °F-days

P_{200} = percentage foundation materials passing No. 200 sieve.

SPALL = percentage of joints with spalling (medium and high severity).

$$= \left[\frac{AGE}{AGE + 0.01} \right] \left[\frac{100}{1 + 1.005^{(-12*AGE+SCF)}} \right]$$

SCF = scaling factor base on site, design, and climate related variables

$$\begin{aligned} &= -1400 + 350 * \text{AIR\%} * (0.5 + \text{PREFORM}) + 3.4 * f'c * 0.4 - 0.2 * (\text{FTCYC} * \text{AGE}) + 43 * \text{hpcc} \\ &- 536 * \text{WC_Ratio} \end{aligned}$$

AIR% = percentage air content

PREFORM = 1 if perform sealant is present; 0 if not

f'c = compressive strength of concrete, psi

FTCYC = average annual number of freeze thaw cycles

hpcc = slab thickness, in

WC_Ratio = water-cement ratio of concrete for the slabs

2.6 Summary

This chapter has reviewed various studies that attempted to analyze the fatigue failure of concrete pavement due to truck passes. The chapter discussed data collection methods, statistical models and modeling software used by different researchers to achieve their goals. Also, the chapter discussed types of rigid pavement and different distresses that lead to the concrete pavement performance failure.

The next chapter and the following one describe in detail the approach and modeling software used in this research to calculate damage on jointed plain concrete pavement caused by different truck configurations.

CHAPTER 3

FINITE ELEMENT MODELING AND DAMAGE ANALYSIS OF JOINTED PLAIN CONCRETE PAVEMENT (JPCP)

3.1 Introduction

A comparison analysis of the predicted levels of fatigue stresses in a Jointed Plain Concrete Pavement (JPCP) caused by different traffic configurations was completed using the Abaqus/CAE 6.7.5 (2008) software. The software allows rigid pavements to be modeled in 3D as a stress-dependent multilayer system with truck loads applied on the surface to induce stresses, strains and deflections.

This study determined maximum load-induced tensile stresses at the bottom of the concrete slab of a finite element rigid pavement model. The model was created by Abaqus to analyze stresses and strains to the pavement caused by 35 different truck cases proposed by New York State Department of Transportation (Appendix A). The tensile stresses were used in Darter (1977) and Tepfer (1979) fatigue models to calculate the allowable number passes for different groups of axles. The inverted sum of ratios of one to allowable number of each axle group was taken as the estimate of the allowable number of passes for each truck case. The obtained allowable number of passes for each truck case was used as a basis for comparing different truck cases.

Another tool that could be used for analyzing trucks damage on rigid pavement is the Mechanistic Empirical Pavement Design Guide software. Unlike the Finite Element program,

MEPDG program has inbuilt distress models that allow it to directly calculate transverse cracks, faulting and roughness. Unfortunately, the MEPDG program cannot analyze groups of axles with unequally distributed loads and spacing. Therefore 25 cases out of the 35 NYSDOT proposed truck cases which had complicated axle groups could not be analyzed by the MEPDG program. However, the program analyzed the remaining 10 truck cases and the estimated truck damage was compared with truck damage calculated by the Finite Element program and the associated fatigue models.

3.2 Overview - Finite Element Program

Finite element methods originate from the need to solve complex elasticity and structural analysis problems in civil, aerospace and mechanical engineering. In the US, the early work can be traced back in mid 1950's (Clough, 1999). Currently there are many 2D and 3D finite element programs for design and analysis of complex engineering problems. Finite element programs such as 2D-ILLI-SLAB, 2D-JSLAB, ISLAB200, KENSLAB, 2D-WESLAYER, 2D-WESLIQUID, 3D-EverFE, 3D-DYNASLAB, ABAQUS, NIKE3D, ANSYS and others are available for pavements analysis. ABAQUS, NIKE3D and ANSYS are generalized finite element programs while the rest of the listed finite element programs are designed for analyzing rigid pavements.

As introduced in the previous section, the generalized finite element program Abaqus was used to analyze stresses and strains in a Jointed Plain Rigid Pavement due to a range of truck axle configurations. The Abaqus software is capable of analyzing and simulating static and/or dynamic stresses on structures such as engines, falling objects, buildings and soil masses. The early version of Abaqus was released about two decades ago while the current version,

Abaqus/CAE 6.7.5, released 2008 was used for this study. This current version works in the following sequence.

- Create parts geometry,
- Define Materials and sections,
- Properly Assigne sections and materials to the parts geometry,
- Mesh parts Geometry,
- Assemble parts to make the model,
- Define analysis steps and output request,
- Define contacts and other interactions,
- Apply loads and boundary conditions,
- Submit job for analysis,
- Examine the analysis results.

3.2.1 Elements

Abaqus comprises a range of different types of elements. These are small divisions of a geometric model provided for analysis purposes. The elements are well coordinated to allow load analysis depending upon material behavior of the model. The elements may be modeled as:

- Submit job for analysis,
- One-dimensional elements,
- One-dimensional elements,
- Two-dimensional elements,
- Three-dimensional elements,
- Cylindrical elements,

- Axisymmetric elements,
- Axisymmetric elements with nonlinear, asymmetric deformation.

The element library for Abaqus/CAE 6.7.5 includes the following types of elements.

- Stress/displacement elements
- Couple temperature displacement elements
- Pore pressure elements
- Piezometric elements
- Heat transfer or mass diffusion elements
- Forced convection heat transfer elements
- Acoustic elements
- Hydrostatic fluid elements and
- User-defined elements.

The Abaqus mesh built for this study required stress-strain analyses; hence solid continuum stress/displacement elements were predominately used. Stress/displacement elements have only displacement degree of freedom. The elements may exist in the following families.

- Hydrostatic fluid elements,
- Continuum (solid) elements,
- Connector elements,
- Structural elements,
- Rigid elements,
- Contact elements, and
- Special purpose elements.

The family of stress/displacement element used for this research was the continuum (solid) elements. The solid elements in Abaqus are available for linear analysis and complex non linear analysis. They may work as one, two and three linear (first order) and quadratic (second order) interpolation elements. Second order elements perform better than first order elements when problems that do not involve complex contact conditions, impact, or severe element distortions, are encountered. First order triangular and tetrahedral elements require a very fine mesh to achieve sufficiently accurate results.

Solid elements have an option of reduced integration. Reduced integration elements have less running time especially in three dimensions. When reduced integration conditions are accommodated in second order elements, more accurate results are obtained than with full integration elements.

3.2.2 Material Module

Material models are used to compute the response to any change of stresses and strains and depend upon the material type and behavior. Sufficient definitions of materials provide suitable properties for those elements with which the material is associated and for all analysis procedures through which the model will run.

Materials behavior in Abaqus may be used freely or with restriction. For example conductivity can be used in any material definition while metal plasticity requires other definitions like elastic material behavior. Sometimes materials may be defined as a function of temperature and/or independent field variables. Abaqus material behaviors fall into the following categories:

- General properties (material damping, density, thermal expansion),

- Thermal properties,
- Hydrostatic fluid properties,
- Acoustic properties,
- Elastic mechanical properties,
- Equation of state,
- Mass diffusion properties,
- Electrical properties, and
- Pore fluid flow properties.

The analysis of pavement structures in this study used linear elastic material behavior. Thus the discussion follows concentrate on elastic properties.

3.1.2.1 Linear elastic behavior

This is a simplest material behavior whereby the stress-strain relationship is defined by a straight line. The behavior follows Hooke's law, where the total stress is defined from the total elastic strain as

$$\sigma = D^{el} \varepsilon^{el}, \quad [3.1]$$

Where

σ = Total stress

D^{el} = Fourth-order elasticity tensor

ε^{el} = Total elastic strain.

The linear elastic model can be in the form of isotropic, orthotropic, or anisotropic material behavior and is valid for small strains (i.e. 5%). The simplest form of linear elastic is the isotropic case, where the stress-strain relationship is defined as follows.

$$\begin{Bmatrix} \varepsilon_{11} \\ \varepsilon_{22} \\ \varepsilon_{33} \\ \varepsilon_{12} \\ \varepsilon_{13} \\ \varepsilon_{23} \end{Bmatrix} = \begin{bmatrix} 1/E & -\nu/E & -\nu/E & 0 & 0 & 0 \\ -\nu/E & 1/E & -\nu/E & 0 & 0 & 0 \\ -\nu/E & -\nu/E & 1/E & 0 & 0 & 0 \\ 0 & 0 & 0 & \frac{2(1+\nu)}{E} & 0 & 0 \\ 0 & 0 & 0 & 0 & \frac{2(1+\nu)}{E} & 0 \\ 0 & 0 & 0 & 0 & 0 & \frac{2(1+\nu)}{E} \end{bmatrix} \times \begin{Bmatrix} \sigma_{11} \\ \sigma_{22} \\ \sigma_{33} \\ \sigma_{12} \\ \sigma_{13} \\ \sigma_{23} \end{Bmatrix} \quad [3.2]$$

The expression shows that elastic properties are fully defined by the modulus of elasticity, E , and Poisson's ratio, ν .

Linear elastic properties can be used with stress/displacement element or coupled temperature displacement elements. Abaqus recommends the use of a hyperelastic model when large elastic strains are expected.

3.1.2.2 Load Module

The Load component in Abaqus/CAE is designed to define and place boundary conditions and loads on the model to be analyzed. The two major parts of load module are explained as follows:

- Boundary Conditions

Boundary conditions define edges and ends of an object in regard to displacements and rotations in stress/displacement analysis, temperature in heat transfer or coupled thermal-stress analysis, electrical potential in coupled thermal-electrical analysis, pore pressure in soil analysis,

etc. Abaqus has the following boundary conditions types with degrees of freedom shown in figure 3.1.

- XSYMM Symmetry about X plane (degrees of freedom 1,5,6 = 0)
- YSYMM Symmetry about Y plane (degrees of freedom 2,4,6 = 0)
- ZSYMM Symmetry about Z plane (degrees of freedom 3,4,5 = 0)
- XASYMM Antisymmetry about X plane (degrees of freedom 2,3,4 = 0)
- YASYMM Antisymmetry about Y plane (degrees of freedom 1,3,5 = 0)
- ZASYMM Antisymmetry about Z plane (degrees of freedom 1,2,6 = 0)
- PINNED Pinned (degrees of freedom 1,2,3 = 0)
- ENCASTRE Fixed (degrees of freedom 1,2,3,4,5,6 = 0)

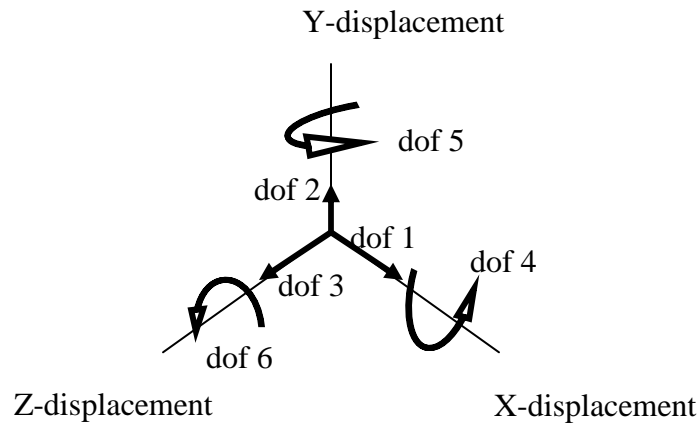


Figure 3.1: Degrees of freedom on coordinate system

- Loads

There are many types of loading procedure available with Abaqus. The loads which are generally used for analysis are:

- Concentrated loads,

- Distributed loads,
- Thermal loads,
- Acoustic and shock loads, and
- Pore fluid flow.

The next section will discuss the load type which was used in this study.

3.1.2.3 Distributed loads

Two ways of specifying distributed loads exist in Abaqus: loads on elements and loads on surfaces. Element-based distributed loads may be applied on element bodies, surfaces or edges. Surface-based loads may be applied on geometric surfaces or edges. With element-based loads, element number and distributed load type must be specified. With surface-based, surface or edge name and distributed load type (i.e. pressure) must be specified.

3.3 Finite Element Model Development

3.3.2 General Assembly

The modeled JPCP pavement consisted of three layers: the concrete slab surface, the base (subbase) and the subgrade soil. The surface slab was divided into travelling lanes and shoulders. Dowel and tie bars were provided at every transverse joint and longitudinal joint respectively.

Initially the model had 8 slabs and 8 shoulders, each 12 inch thick. The slabs and shoulders were 12ft x 15ft and 6ft x 15ft respectively. This model was prepared to fit a static truck of about 720 ft in length. The model required a large mesh size and long time to run. After a number of the model runs, it was obvious that stresses on one slab were negligibly reflected to a third slab from the loaded one. In order to have short time runs and reasonable mesh sizes, five shoulders and two slabs were removed. The number of dowels and ties included became 54 and

84 respectively. The dowel size was 18 inches long and 1.5 inches in diameter, while the ties were 30 inches long and 1 inch in diameter. The final JPCP assembled model is shown in figure 3.2.

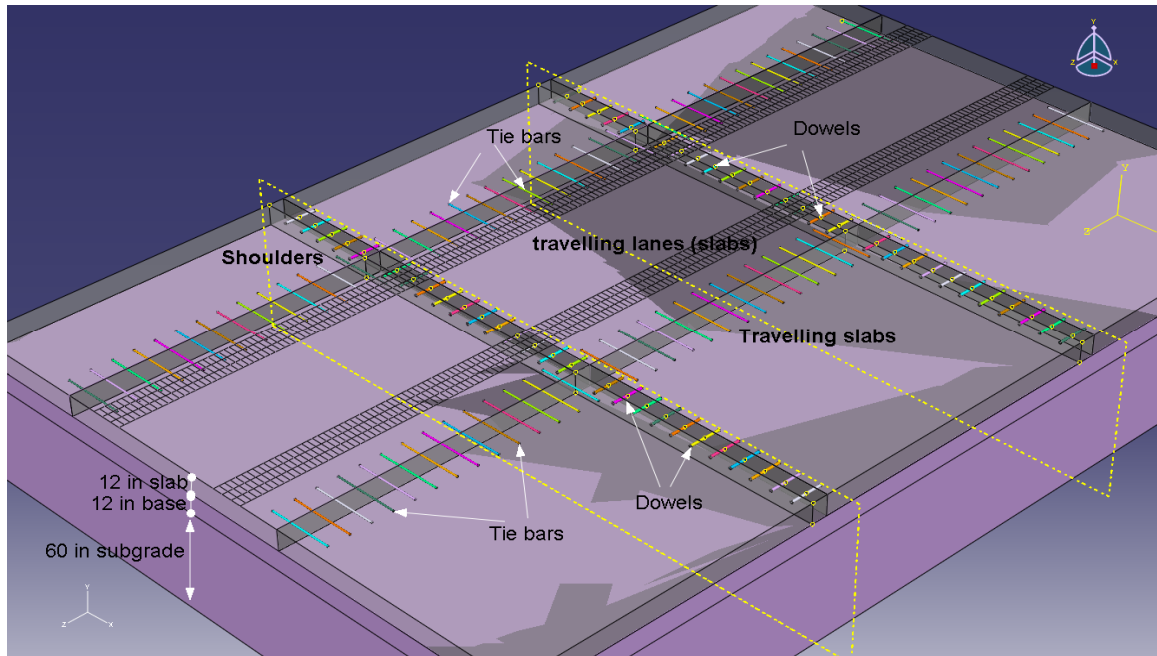


Figure 3.2: Assembled JPCP model

3.3.3 Finite Element Mesh

The analyzed JPCP model consists of 12 parts meshed independently. The base and subgrade block easily meshed with 3D brick element. Meshing of concrete slabs was not straight forward. This was because of dowel holes at one end of the slabs. The meshing was managed by partitioning each slab into two blocks. The first block was solid and the other consisted of through dowel holes (Figure 3.3).

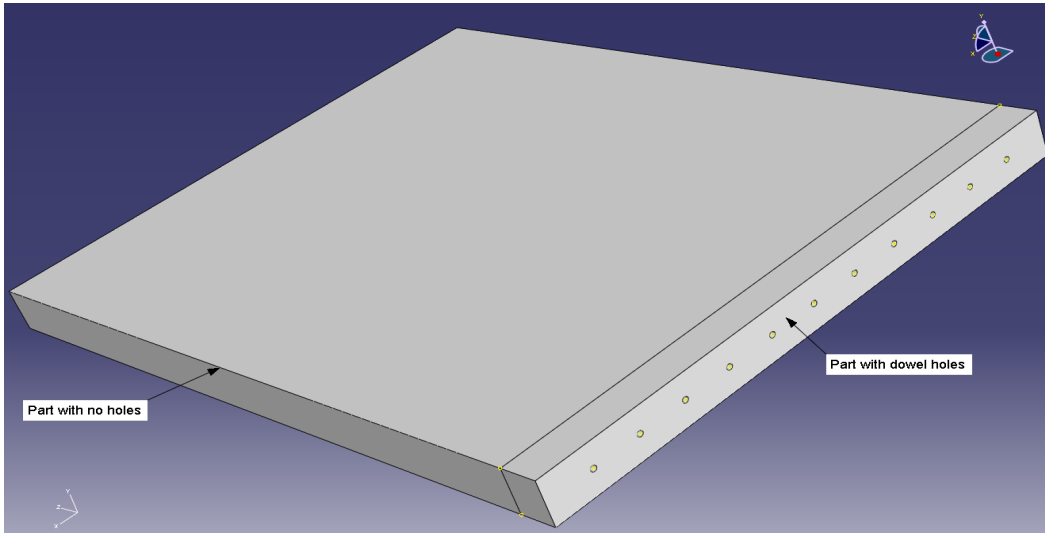


Figure 3.3: Partitions for slab with dowel holes

The other parts of the model were dowels and ties. While each tie was meshed as one part bonded in concrete, each dowel had to be divided into two sections before meshing. One section was bonded in concrete (embedded part) and another one was fitted into dowel holes (sliding part) (Figure 3.4). The elements for the embedded part of dowel, all ties bars and the host concrete formed a solid-to-solid type of embedded elements (Figure 3.5). The embedded elements allowed the solid rebar-reinforcements to be fully bonded in concrete slabs.

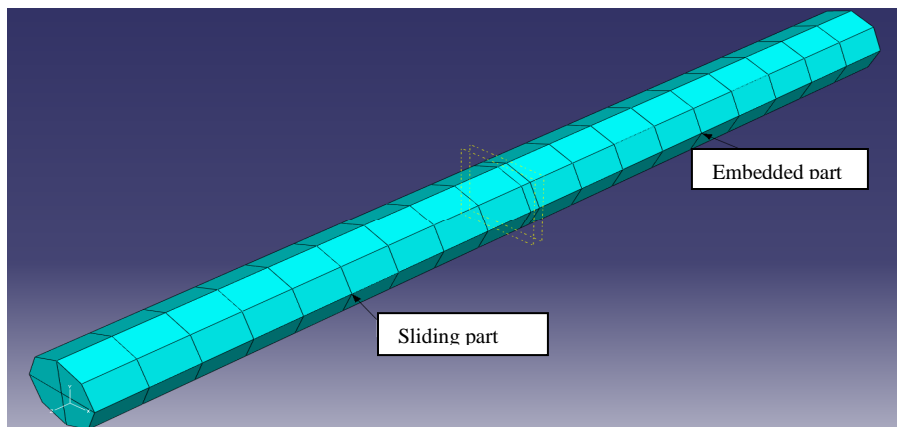


Figure 3.4: Dowel bar Mesh

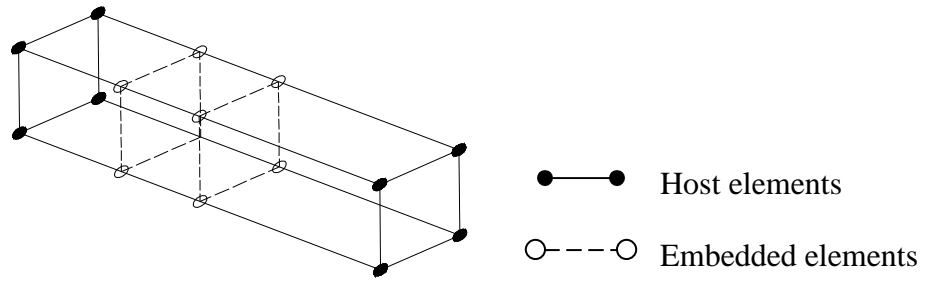


Figure 3.5: Solid to solid embedded elements

3D brick solid elements (hexagonal C3D8R 8-node) were used for the whole model (Figure 3.6). These elements are good for linear analysis which is the case for this model. The size of the elements varied depending upon the importance of the section. The sections sought to produce the needed stresses and strains (i.e. loaded sections), were meshed with small sized elements (fine mesh). The remaining sections had large sized elements (course mesh). The variation of elements sizes was because small dimensions allowed detailed analysis but on the expense of memory and computational time. On the other hand coarse mesh did not result in a detailed analysis but used little memory and shorter time. The element size adopted for the coarse mesh was 9×9 inches, while for the fine mesh 3×3 inches elements were used. However ties and dowels were assigned 1×1 inch elements sizes because they were relatively small. In total 198,619 nodes and 163,615 elements were used in the model, as shown in Figure 3.7.

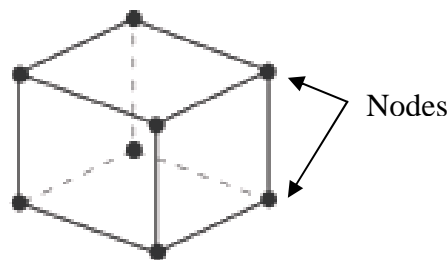


Figure 3.6: 3D brick element (C3D8R)

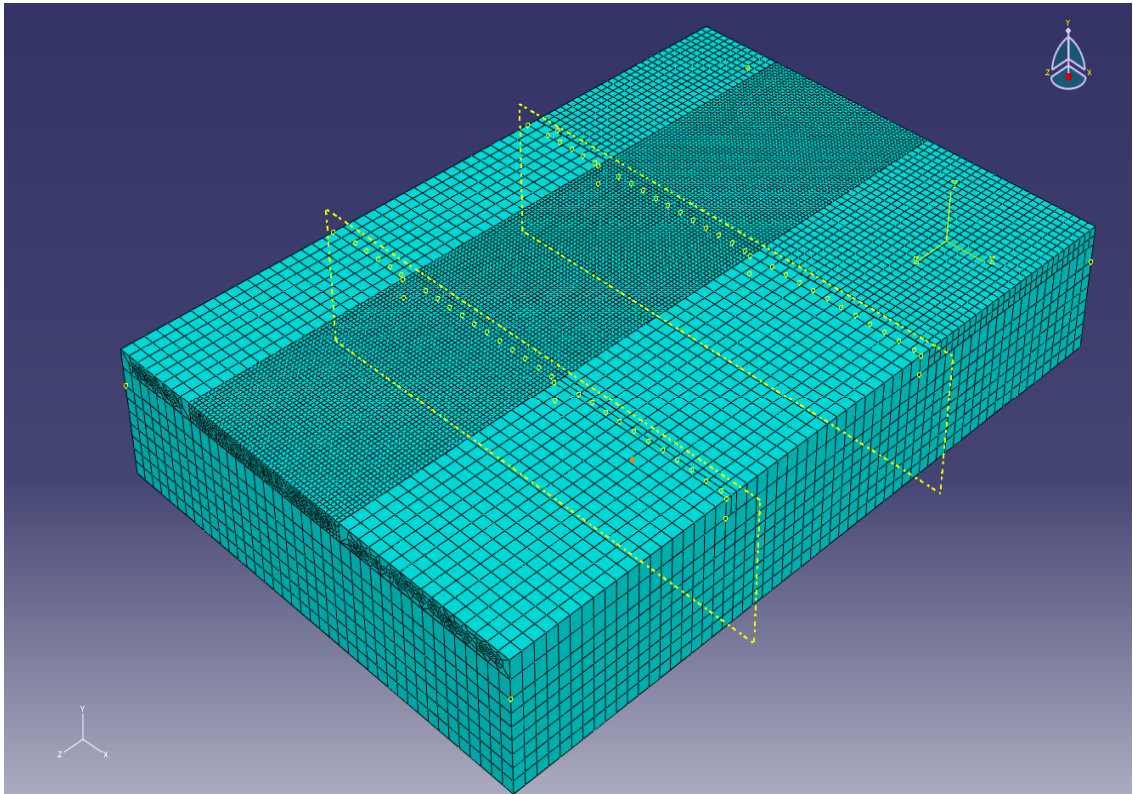


Figure 3.7: Jointed Plain Concrete Pavement Mesh

3.3.4 Boundary conditions

Boundary conditions were applied to the pavement mesh model to define circumferential and bottom constraints as expected in the field (Figure 3.8). The bottom of the pavement subgrade was at a depth of 72 inches from the bottom of the concrete slab and assumed to be resting on bedrock. Therefore in order to simulate this condition in Abaqus, the bottom of the pavement model was constrained against all directions. On the other hand, the sides of the pavement model were constrained against all horizontal movements (x-direction and y-direction) but allowed to move vertically. This was done because the loads were applied to an internal slab far away from the edges of the pavement.

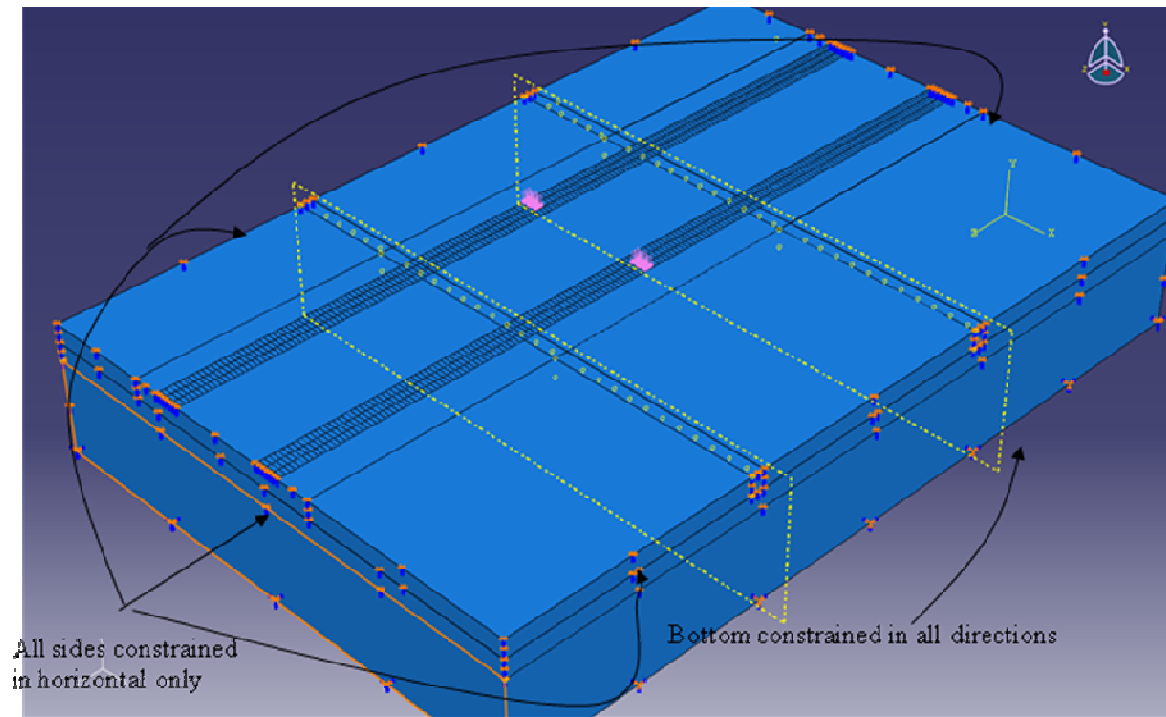


Figure 3.8: Boundary conditions

3.3.5 Contacts

The finite elements analysis defines pairs of contacts as either surface-to-surface or node-to-surface. Both methods were appropriately used in the pavement model depending on the shape of surfaces in contact. The surface-to-surface method was used to model base-slab contact; while node-to-surface method used to model dowel-slab contact. The contact normal behavior was used with “hard contact” option which minimized penetration of slave surface (a surface which is allowed to move) into master surface (a fixed surface) and did not allow transfer of tensile stresses across the interface (ABAQUS).

3.3.6 Materials

This analysis assumed the pavement materials are linear elastic (i.e. material behavior controlled by Young's modulus and Poisson's ratio) because very small strains (<5%) were expected. The materials used in the model are given in Table 3.1.

Table 3.1: Material Properties

Part	Materials	Young's modulus, E (psi)	Poisson's Ratio, ν	Density, γ (pci)	Modulus of rupture, (psi)
Slab/shoulders	Concrete	4,000,000	0.15	0.087	700
Base	Crushed stones	35,000	0.35	0.081	—
Subgrade	Medium clay	5000	0.45	0.06	—
Dowel/Ties	steel	29,000,000	0.2	—	—

3.3.7 Loading

3.3.7.1 Tire imprint model

A tire imprint refers to the contact area between the tire and pavement surface. According to PCA (1984), the tire imprint may be assumed to be rectangular or rectangular with two circles. The tire imprint size depends on contact pressure which is assumed to be equal to the tire pressure. The average tire pressure in a truck tire varies from model to model and it is governed by the speed at which a specific truck will travel, the load to be carried and the condition in which the truck will travel (Kanonik, 2003). Generally, the average pressure in truck tires can range from 70 to 140 psi. This study used 80 psi average tire pressure and 18 lb dual tire single

axle to design a rectangular tire-print of 9 x 6 inches (Figure 3.9). The length L of the tire-print was calculated using equation 3.3.

$$L = \sqrt{\frac{A_c}{0.5227}} \quad [3.3]$$

Where;

L = length of the tire print

A_c = Contact area (load on one tire/pressure of the tire)

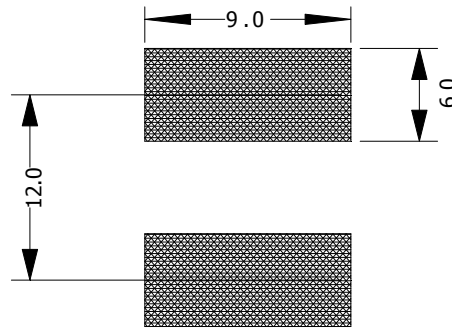


Figure 3.9: Tire imprints size (all dimensions in inches)

3.3.7.2 Surface partitions

There are two ways in which external loads may be applied to an Abaqus model: element loading or surface loading. This study used the surface loading procedure. The surfaces along which the truck tires passed were partitioned into small sections multiple of the designed tire prints. The sizes of the small sections and the tire prints were 3 x 6 inches (Figure 3.10).

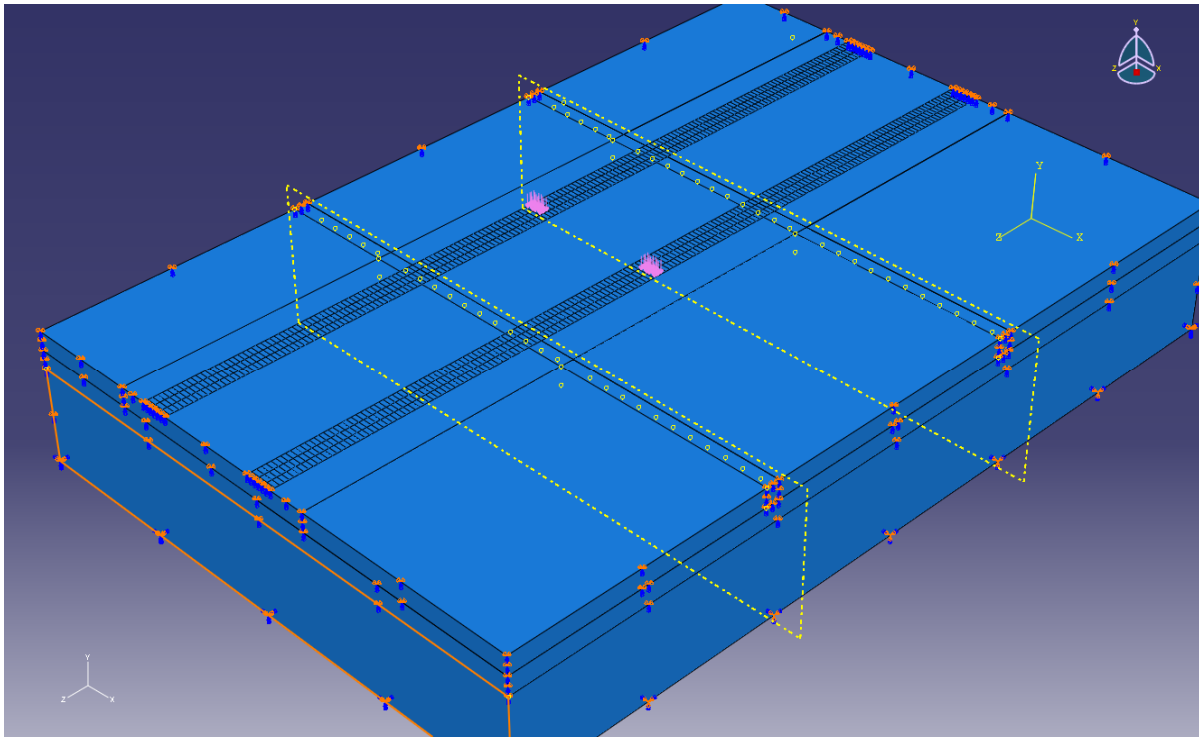


Figure 3.10: Model surface partitions

3.3.7.3 Axle positioning

In Abaqus finite element model, traffic loads may be applied statically or dynamically. In this research, each axle group of a truck case applied at a critical position was analyzed statically to obtain maximum stresses and strains. All axle loads were positioned 18 inches away from the slab edge to reflect an average tire position on the pavement. Along the edge line, axles were positioned in order that maximum tensile stresses/strains that cause bottom-up cracks may be achieved (see figure 3.11). Top-bottom stresses were not calculated because the model did not consider temperature and moisture gradient.

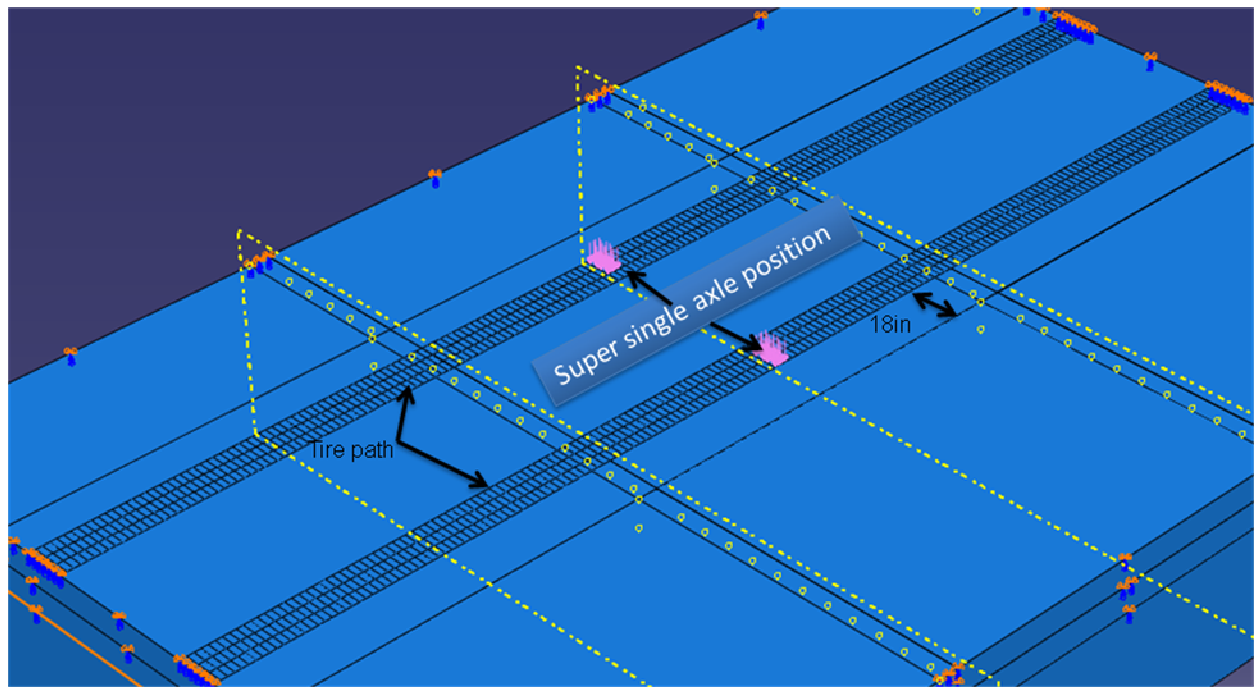


Figure 3.11: Axle positioning

CHAPTER 4

MECHANISTIC-EMPIRICAL DAMAGE ANALYSIS OF JOINTED PLAIN CONCRETE PAVEMENT (JPCP)

Until recently, the AASHTO design guide (1993) had been used for the design of flexible and rigid pavements in the US and some parts of the world. But because of its inability to meet new traffic and material challenges as discussed in chapter 2, a new Mechanistic Empirical Pavement Design guide (MEPDG) has now introduced (NCHRP, 2004). The computer software associated with the MEPDG guide was used in this study to analyze truck damage on Jointed Plain Concrete Pavements (JPCP). The damage types assessed were: fatigue cracking, faulting and roughness. The truck damage at the end of year 40 was recorded and compared in terms of fatigue cracking as in the finite element analysis.

This chapter presents MEPDG damage analysis and procedures for JPCP as a result of different trucks configurations. As explained in the previous chapter, the software is capable of only analyzing trucks with equally distributed loads and spacing between axles of the same group. Of the 35 truck cases proposed by NYSDOT only 10 met the criteria. The trucks are: L6, L7, L8, L9, L10, L11, L12, L13, L14, and L15 (Appendix A).

4.1 Analysis and Design Inputs

The inputs into the Mechanistic-Empirical Pavement Design Guide software define the conditions under which the pavement is expected to perform. The inputs of the MEPDG depend

on the level of accuracy needed (Chapter 2). Better results are expected when more data and high level of accuracy are used within the analysis.

Generally the inputs required for the MEPDG are:

- Inputs for pavement structure, such as thickness of layers, types of materials, joint spacing, etc.
- Inputs for existing conditions, such as traffic, subgrade, environment, etc.
- Input for materials, such as mix design properties of slab concrete and other layers

4.2 Sequence of MEPDG software inputs as used in this study

The following four categories of inputs were used in this study.

- General,
- Traffic,
- Climate and
- Pavement structure.

4.2.1 General

The MEPDG software requires general inputs to describe the type of project, the life limit of the project, design criteria and information that identify the project files. This part of MEPDG software is divided into three inputs screens: general information, project identification, and analysis parameters.

4.2.1.1 General information

This section gives a designer a wide range of options as outlined here below.

Type of design: This input allows the software to pick the appropriate method of design and performance model for the chosen type of design. The designer has the option of inserting the following design types: new flexible pavement, new Jointed Plain Concrete Pavement, new continuously Reinforced Concrete Pavement, Restoration of Jointed Plain Concrete Pavement, and Concrete (PCC) and Asphalts overlays. For this study, Jointed Plain Concrete Pavement was chosen to be the type of design.

Design life: This is the total number of years the designed pavement is expected to be in service. The expected life is counted from the day the pavement is open to traffic to the end of the assumed design life. This study used a design life of 40 years and recorded analysis data at the end of year 40.

Pavement construction month: This is the month when the surface (PCC) layer is placed. The month set a reference for environmental conditions (i.e., temperature variation) and changes to surface layer materials properties. The input estimates the “zero stress” temperature in the PCC slab during construction. The “zero stress” temperature affects the faulting properties of Jointed Plain Concrete Pavement. In this study, July 2009 was chosen as the construction month.

Traffic opening month: This input set a time when the damage effects of traffic start to be evaluated. Other parameters that vary with traffic and time (i.e., moduli of layers) are also evaluated. In this study, August 2009, was chosen as the traffic opening month.

4.2.1.2 Site Identification

In the MEPDG software the user has to input information regarding identification and documentation purpose. The input required includes: section ID, project ID, beginning and end mile posts, and traffic direction. The information provided at this screen does not affect the analysis and design process.

The location identification for this project was New York. However other identifications required were chosen to suit this study only. For example, the project ID was “thesis” because the research was part of the author’s master’s degree while the section IDs carried names of truck types because each truck type was analyzed individually. Also, the study identified the begin mile post and end mile post to be 00+00 and 05+00 respectively.

4.2.1.3 Analysis Parameters

This screen allows the user to insert criteria for performance prediction of either rigid pavements or flexible pavements. The parameters required for this study was; International Roughness Index (IRI), mean joint faulting and transverse cracking. Table 4.1 shows the range and default criteria. This study used the default criteria

Table 4.1: Jointed Plain Concrete Pavement performance criteria

Parameter	Criteria Range	Default Criteria	Assumed reliability ⁽¹⁾
Initial IRI (in/mi)	0-200	63	-
Terminal IRI (in/mi)	0-300	172	90
Mean Joint faulting (in)	0-0.25	0.12	90
Transverse cracking (% slabs cracked)	0-50	15	90

(1) The assumed reliabilities are within the range of reliabilities values used for interstate highways (NCHRP, 2004).

4.2.2 Traffic inputs

The traffic volumes and axle loads are important in design and analysis of pavements. While the 1993 AASHTO Pavement Design Guide expresses traffic in terms of equivalent single axle loads (ESALs), the new MEPDG pavement design and analysis method requires a better estimate of all heavy vehicles axles that will travel on the pavement.

The object of this study was to assess and compare damages due to different truck configurations. Therefore each truck was analyzed separately, but the traffic volume was kept constant for all case studied.

The MEPDG traffic inputs are divided into the following sections:

4.2.2.1 General traffic information

The information required at this section are: Initial two way Annual Average Daily Truck Traffic (AADTT), number of lanes in the design direction, percentage of trucks in design direction, percentage of trucks in design lane, and operational speed.

- Initial two way AADTT

The initial Annual Average Daily Truck Traffic (AADTT) form a traffic volume base where the MEPDG software use for calculating future AADTT. MEPDG software allows the user to insert initial AADTT ranging from 100 to 25,000. This study assumed an AADTT of 24,000 throughout.

- Number of lanes in design direction

This study assumed two lanes were in the design direction.

- Percentage of trucks in design direction

MEPDG software allows percentage of trucks in design direction to range from 50 to 60.

This study assigned 55% trucks in the design direction.

- Percentage of trucks in design lane

MEPDG recommends 50% to 100% of trucks to be assigned in the design lane. This study assumed 90% trucks used the design lane.

- Operational speed

This study assumed a speed of 40 mph throughout.

4.2.2.2 Traffic monthly adjustment factors

Truck traffic monthly adjustment factors (MAF) refers to the proportion of annual trucks of a given class that occurred in a certain month. Mathematically, the Traffic Adjustment factor is represented by equation 4.1.

$$MAF_i = \frac{AMDTT_i}{\sum_{i=1}^{12} AMDTT_i} \times 12 \quad [4.1]$$

Where;

MAF_i = Monthly adjustment factor for month i

$AMDTT_i$ = Average monthly daily traffic for month i .

MEPDG uses monthly adjustment factors to determine the monthly variation of trucks within the initial year. This study adopted the default values provided with the design guide software. The MEPDG default values are 1.0 for all months.

4.2.2.3 Vehicle class distribution

Vehicle class distribution screen allows the user to insert the percentage of the base year Annual Average Daily Truck traffic (AADTT) for truck class 4 through 13. The MEPDG design guide requires the sum of all AADTT to be 100%. The design guide software is provided with default values base on the US average data. In this study each truck case was analyzed individually. Therefore, each vehicle class was assigned 100 % of the traffic available (Table 4.2).

Table 4.2: Vehicle class distributions used

Vehicle Class	MEPDG Default	Vehicle distribution (%) for each truck case									
		L6	L7	L8	L9	L10	L11	L12	L13	L14	L15
4	1.8	0	0	0	0	0	0	0	0	0	0
5	24.6	0	0	0	0	0	0	0	0	0	0
6	7.6	0	0	0	0	0	0	0	0	0	0
7	0.5	0	0	0	0	0	0	0	0	0	0
8	5.0	0	0	0	0	0	0	0	0	0	0
9	31.3	100	0	0	100	0	0	0	0	0	0
10	9.8	0	100	100	0	100	100	100	100	100	100
11	0.8	0	0	0	0	0	0	0	0	0	0
12	3.3	0	0	0	0	0	0	0	0	0	0
13	15	0	0	0	0	0	0	0	0	0	0
Total	100	100	100	100	100	100	100	100	100	100	100

4.2.2.4 Hourly truck distribution (HTD)

The hourly truck distribution is an average daily hour by hour representation of AADTT within the base year. The distribution is important because it increases accuracy in determining damage for different temperature gradients. This design software is provided with default factors computed from the Long Term Pavement Performance (LTPP) traffic data base. This study used the default values as shown in Table 4.3.

Table 4.3: Hourly Truck Traffic Distributions

Time	% hourly distribution	Time	% hourly distribution
Midnight	2.3	Noon	5.9
1.00 am	2.3	1.00 pm	5.9
2.00 am	2.3	2.00 pm	5.9
3.00 am	2.3	3.00 pm	5.9
4.00 am	2.3	4.00 pm	4.6
5.00 am	2.3	5.00 pm	4.6
6.00 am	5.0	6.00 pm	4.6
7.00 am	5.0	7.00 pm	4.6
8.00 am	5.0	8.00 pm	3.1
9.00 am	5.0	9.00 pm	3.1
10.00 am	5.9	10.00 pm	3.1
11.00 am	5.9	11.00 pm	3.1

4.2.2.5 Traffic growth factors

MEPDG built in traffic growth models assists the design software to estimate future traffic. The MEPDG software has three optional models of which the annual average daily traffic at a given year can be estimated. The models are described in Table 4.4.

Table 4.4: Traffic growth models

Function description	Model
No growth	$AADTT_X = 1 * AADTT_{BY}$
Linear growth	$AADTT_X = GR * AGE + AADTT_{BY}$
Compound growth	$AADTT_X = AADTT_{BY} * (GR)^{AGE}$

Where,

$AADTT_X$ = Annual Average Daily Truck Traffic at year X

$AADTT_{BY}$ = Annual Average Daily Truck Traffic at base year

GR = Annual growth rate

AGE = pavement age at year X (years)

This study used a compound growth model with a default annual growth rate of 4%.

4.2.2.6 Axle load distribution Factors

The axle load distribution factors represent the percentage of total load carried by a specific axle type of a given vehicle class. The MEPDG software is formatted with axle load distribution factors depending on the axle type. For a single axle, the distribution ranges from 3,000 lb to 40,000 lb at an interval of 1,000 lb. For a tandem axle, the distribution ranges from 6,000 lb to 80,000 lb at an interval of 2,000 lb. For a tridem and quad axles, the distribution ranges from 12,000 lb to 102,000 lb at an interval of 3,000 lb. The sum of axle distributions for any vehicle type must be 100%.

MEPDG default tandem axle load distribution factors and the distributions used for truck cases of this study are shown in Tables 4.5 and 4.6.

Table 4.5: One month tandem-axle load distribution-default values (in %)

Mean Axle load, lbs	Trucks Class									
	4	5	6	7	8	9	10	11	12	13
6000	5.88	7.06	5.28	13.74	18.95	2.78	2.45	7.93	5.23	6.41
8000	1.44	35.42	8.42	6.71	8.05	3.92	2.19	3.15	1.75	3.85
10000	1.94	13.23	10.81	6.49	11.15	6.51	3.65	5.21	3.35	5.58
12000	2.73	6.32	8.99	3.46	11.92	7.61	5.40	8.24	5.89	5.66
14000	3.63	4.33	7.71	7.06	10.51	7.74	6.90	8.88	8.72	5.73
16000	4.96	5.09	7.50	4.83	8.25	7.00	7.51	8.54	8.37	5.53
18000	7.95	5.05	6.76	4.97	6.77	5.82	6.99	7.08	9.76	4.90
20000	11.58	4.39	6.06	4.58	5.32	5.59	6.61	5.49	10.85	4.54
22000	14.20	2.31	5.71	4.26	4.13	5.16	6.26	5.14	10.78	6.45
24000	13.14	2.28	5.17	3.85	3.12	5.05	5.95	5.99	7.24	4.77
26000	10.75	1.53	4.52	3.44	2.34	5.28	6.16	5.73	6.14	4.34
28000	7.47	1.96	3.96	6.06	1.82	5.53	6.54	4.37	4.93	5.63
30000	5.08	1.89	3.21	3.68	1.58	6.13	6.24	6.57	3.93	7.24
32000	3.12	2.19	3.91	2.98	1.20	6.34	5.92	4.61	3.09	4.69
34000	1.87	1.74	2.12	2.89	1.05	5.67	4.99	4.48	2.74	4.51
36000	1.30	1.78	1.74	2.54	0.94	4.46	3.63	2.91	1.73	3.93
38000	0.76	1.67	1.44	2.66	0.56	3.16	2.79	1.83	1.32	4.20
40000	0.53	0.38	1.26	2.50	0.64	2.13	2.24	1.12	1.07	3.22
42000	0.52	0.36	1.01	1.57	0.28	1.14	1.69	0.84	0.58	2.28
44000	0.30	0.19	0.83	1.53	0.28	0.91	1.26	0.68	0.51	1.77
46000	0.21	0.13	0.71	2.13	0.41	0.59	1.54	0.32	0.43	1.23
48000	0.18	0.13	0.63	1.89	0.20	0.39	1.73	0.21	0.22	0.85
50000	0.11	0.14	0.49	1.17	0.14	0.26	0.57	0.21	0.22	0.64
52000	0.06	0.20	0.39	1.07	0.11	0.17	0.40	0.07	0.23	0.39
54000	0.04	0.06	0.32	0.87	0.06	0.11	0.38	0.13	0.20	0.60
56000	0.08	0.06	0.26	0.81	0.05	0.08	0.25	0.15	0.12	0.26
58000	0.01	0.02	0.19	0.47	0.03	0.05	0.16	0.09	0.07	0.18
60000	0.02	0.02	0.17	0.49	0.02	0.03	0.15	0.03	0.19	0.08
62000	0.1	0.01	0.13	0.38	0.06	0.02	0.09	0.06	0.09	0.14
64000	0.01	0.01	0.08	0.24	0.02	0.02	0.08	0.01	0.04	0.07
66000	0.02	0.01	0.06	0.15	0.02	0.02	0.06	0.01	0.02	0.08
68000	0.01	0.00	0.07	0.16	0.00	0.02	0.05	0.01	0.04	0.03
70000	0.01	0.02	0.04	0.06	0.00	0.01	0.11	0.00	0.12	0.01
72000	0.00	0.01	0.04	0.13	0.00	0.01	0.04	0.00	0.01	0.04
74000	0.00	0.00	0.02	0.06	0.00	0.01	0.01	0.00	0.01	0.02
76000	0.00	0.00	0.01	0.06	0.00	0.00	0.01	0.00	0.01	0.04
78000	0.00	0.00	0.00	0.02	0.00	0.00	0.01	0.00	0.01	0.02
80000	0.00	0.00	0.00	0.02	0.00	0.00	0.00	0.00	0.00	0.08
Total	100	100	100	100	100	100	100	100	100	100

Table 4.6: Monthly axle load distribution values (in %) for truck cases analyzed by MEPDG

Truck Case	Single Axle		Tandem Axle		Tridem Axle		Quadem Axle	
	Loads	%	Loads	%	Loads	%	Loads	%
L6a	12,000	100	34,000	100	0	0	0	0
L6b	12,000	100	26,000	50	0	0	0	0
			42,000	50	0	0	0	0
L6c	12,000	100	18,000	50	0	0	0	0
			50,000	50	0	0	0	0
L7a	12,000	100	0	0	51,000	100	0	0
L7b	12,000	100	0	0	39,000	50	0	0
					63,000	50	0	0
L7c	12,000	100	0	0	27,000	50	0	0
					75,000	50	0	0
L8a	12,000	100	0	0	0	0	68,000	100
L8b	12,000	100	0	0	0	0	52,000	50
							84,000	50
L8c	12,000	100	0	0	0	0	36,000	50
							100	50
L9	12,000	100	34,000	100	0	0	0	0
L10	12,000	100	22,000	100	0	0	45,000	100
L11	12,000	100	0	0	54,000	100	0	0
L12	12,000	100	0	0	48,000	50	0	0
					60,000	50	0	0
L13	12,000	100	48,000	100	0	0	57,000	100
L14	12,000	100	42,000	100	0	0	63,000	100
L15a	12,000	100	36,000	100	0	0	69,000	100
L15b	12,000	100	36,000	100	0	0	69,000	100
L15c	12,000	100	36,000	100	0	0	69,000	100

4.2.2.7 General traffic input

The inputs under this category define the axle load configuration and loading details used for calculating responses and traffic volume. The inputs used under this category are:

Mean wheel location: This is the distance between the external edge of the nearest truck wheel and the pavement edge marking. The value for mean wheel location may be derived from specific site data, or state wide data, or the national average. This study used a default value of 18 inches for the wheel mean location.

Traffic wander standard deviation: This is the standard deviation of the lateral traffic wander. The input defines the average position of the axle from the point for predicting distresses and performance. The greater the wander value, the higher the fatigue life. The default wander standard deviation of 10 inches was used in this study.

Design lane Width: This is the distance between two lane markings of a design lane. This distance may or may not be equal to slab width. This study used a default value of 12 ft for the standard lane width.

Number of axle types per truck class: This section of MEPDG software requires an insertion of average number of axles for each truck class (class 4 to 13) and each axle type (single, tandem, tridem, and quadem). MEPDG default number of axle type per truck class and values for the analyzed truck cases are shown in tables 4.6a and 4.6 b respectively.

Table 4.7: MEPDG default average number of axles per truck

Vehicle class	Single	Tandem	Tridem	Quad
4	1.62	0.39	0.00	0.00
5	2.00	0.00	0.00	0.00
6	1.02	0.99	0.00	0.00
7	1.00	0.26	0.83	0.00
8	2.38	0.67	0.00	0.00
9	1.13	1.93	0.00	0.00
10	1.19	1.09	0.89	0.00
11	4.29	0.26	0.06	0.00
12	3.52	1.14	0.06	0.00
13	2.15	2.13	0.35	0.00

Table 4.8: MEPDG-Truck class average number of axles used

Truck case	Single	Tandem	Tridem	Quad
L6	1.00	2.00	0.00	0.00
L7	1.00	0.00	2.00	0.00
L8	1.00	0.00	0.00	2.00
L9	1.00	2.00	0.00	0.00
L10	1.00	1.00	0.00	1.00
L11	1.00	0.00	2.00	0.00
L12	1.00	0.00	2.00	0.00
L13	1.00	1.00	0.00	1.00
L14	1.00	1.00	0.00	1.00
L15	1.00	1.00	0.00	1.00

Axle configuration: This is a section where decision values regarding axle configurations are inserted in order to compute pavement responses. The inputs included here are:

- *Average axle width*: This is the width covering from one outside edge of an axle to the other side. The default value of 8.5ft was used for this study.
- *Dual tire spacing*: This is the center to center distance between dual tires. The default value of 12 inches was used for this study.

- *Axle spacing*: This is the average distance between two consecutive axle of an axle group (tandem, tridem, or quadem). This study used the values as provided by NYSDOT (see Appendix A for axle definitions).
- *Tire pressure*: Tire pressure input is needed for the estimation of tires print area. The guide has a fixed tire pressure of 120 psi. Therefore the study had no other choice than using this value for the MEPDG analyses.

Wheel base: Wheel base information is used in the process of determining top down fatigue cracks. The data defines how far the steering axle is located from the drive axle of the same truck, and to what percentage is the wheel base characterized as either short, or medium, or long. The input values are applicable for vehicle class 8 and above. The values for wheel base are in two categories.

- *Average spacing*: The MEPDG default axles spacing are 12 ft, 15 ft, and 18 ft for short axle, medium axle and long axle respectively. In this study, truck case L6 to L10 had an average axle spacing of 15 ft while truck cases L11 to L15 had average axle spacing of 14 ft.
- *Percentage of truck axle spacing type*: The percentage represents the proportion of trucks with short, medium, and long axle spacing in a vehicle class. The default values provided with the guide software are 33%, 33%, and 34% for short axle, medium axle and long axle respectively. This study used 100% medium spacing for each truck analyzed because each truck has only one wheel base.

4.2.3 Climate

Climate is one the major parts of the MEPDG design guide. As explained in chapter 2, the climatic conditions have significant effects on concrete pavement performance. In the design and analysis of JPCP pavements, the temperature and moisture effects that matter are:

- A combination of permanent built-in curling during construction and permanent warping during due to differential shrinkage.
- Transient hourly negative and positive non-linear temperature differences caused by the heat of the sun.
- Transient hourly negative humidity during each month of the year.

The MEPDG design recommends use of available data base from nearly 800 weather stations in the Unites States. Some of these stations have approximately 70 months of climatic data; however the MEPDG software requires at least 24 months of actual weather station data for computational purposes. The software tracks any weather station data when its latitude (degrees), longitude (degrees) and elevation (ft) are manually inserted or called from saved weather files. This study used Albany, New York, weather station for use in the entire projects analysis. The station location was 42.45° latitudes and -73.48° longitude at an elevation of 281 ft above mean sea level.

Another important parameter to be inserted on the climate screen is *groundwater table depth*. This parameter plays a significant role in the overall accuracy of the pavement moisture content, and hence, equilibrium modulus values. The depth is measured from the pavement surface. The design software allows the user to insert either an estimate of annual average depth

or seasonal average depth (depths for all four seasons of the year are required). This study adopted a yearly average groundwater table depth of 10 ft.

4.2.4 Structure

This is one of the large set of important inputs required by the MEPDG software. The set defines pavements layer design features and properties.

4.2.4.1 JPCPC design features

Design features have significant effect in the performance of JPCP pavement. The JPCP design features required as variable inputs in the software are: slab thickness, permanent curl/warp effective temperature difference, joint design, edge support, slab-base interface, and base erodibility.

Slab thickness: Under constant conditions, thicker slabs perform better than thinner ones, but with an obvious higher initial cost. Hence, one has a tradeoff between long term costs and performance. The thickness of a pavement concrete slab may vary from 6 to 15 inches. But slab thicknesses of 9 to 12 inches are commonly used in the US. This study adopted a depth of 12 inches for all the pavement and traffic damage analysis.

Permanent curl/warp effective temperature difference: This is a sensitive value of temperature difference between top and bottom of the concrete slab. It represents the locked stresses in the concrete slab due to construction temperatures, shrinkage, creep, and the curing processes. This value is negative because the top surface is expected to be cooler than the bottom surface under these initial conditions. This study adopted a curl/warp temperature difference value of -10°F as recommended by MEPDG design guide.

Joint design: Concrete pavements joints refer to predetermined cracks designed to relieve stresses in the concrete. The design includes: type of sealant, joint spacing, and dowel sizing and spacing.

- Sealant type

The sealant type is an input to predict spalling. In turn, spalling is used in the smoothness prediction model, but the guide does not consider it as a direct effect on performance. The types of sealant available for the software analysis are liquid, silicon and preformed. This study used the *silicon type* of sealant for of the analysis.

- Joint spacing

Joint spacing in JPCP design affects structural and functional performance of the pavement, as well as construction and maintenance costs. The stresses in JPCP increase rapidly as the joint spacing increases, but the costs are reduced. Therefore a designer is also obligated to exercise tradeoff between cost and reasonable joint spacing. In this study a joint spacing of 15 ft was used in all of the analysis.

- Dowel diameter and spacing

Dowel diameter and spacing are critical inputs for predicting joint faulting. The larger the dowel diameter and the smaller the dowel spacing, the lower the concrete bearing stress and joint faulting. The typical dowel diameters and spacing are 1 to 1.75 inches and 12 inches respectively. This study used a dowel spacing of 12 inches and dowel diameter of 1.5 inches.

Edge support: The edge support inputs required by the MEPDG software are: tied concrete shoulders, or widened slab, and long-term load transfer efficiency (LTE). Tied

shoulders can significantly improve JPCP performance by reducing critical deflections and stresses along the edge. In this study, *tied concrete shoulders* with a long-term LTE of 70% which lies between the values recommended for monolithically constructed tied shoulders

Slab-base interface: The structural contribution of stabilized base under a cement concrete slab is significant if the base is fully bonded to the slab. However the effect of environmental and traffic loading tend to weaken the bond over time. This study used non-stabilized crushed stones for a base; thus, unbonded conditions were assumed throughout the design life.

Base erodibility: This input has significant effects on the initiation and development of pavement distresses. The MEPDG design guide has classified base types according to their erodability behavior as follows:

- Class 1 – Extremely erosion resistant materials
- Class 2 – Very erosion resistant materials
- Class 3 – Erosion resistant materials
- Class 4 – Fairly erodible materials
- Class 5 – Very erodible materials

This study defined the used base materials as *class 3 – erosion resistant* materials. This is the average class of erodability property of material defined by MEPDG, 2004.

4.2.4.2 JPCP design layers and properties

Essentially a well designed combination of layers form a pavement structure; hence the design and analysis of pavements is always done to assure good performance of the layers. The performances of pavements depend very much on the properties of individual layers. The

MEPDG software allows as many layers as practical to reflect the actual pavement structure in the field. The layers' properties used in this study are shown in Table 4.9.

Table 4.9: Pavement design layers and properties used in MEPDG

Layer and Mix Properties	Layers							
	Layer – 1 (12 in)		Layer – 2 (12 in)		Layer – 3 (60 in)		Layer – 4 (Semi-infinite)	
	Surface	Conc. slab	Base	Crushed stone	Subgrade	CH	Bedrock	Weathered rock
Surface absorptive	0.85							
Unit weight (pcf)	150						140	
Poisson's Ratio	0.15		0.35		0.4		0.15	
Coefficient of lateral pressure (k_o)			0.5		0.5			
Coefficient of thermal expansion (per $F^\circ \times 10^{-6}$)	5.5							
Thermal conductivity (BTU/hr-ft- F°)	1.25							
Heat capacity (BTU/lb- F°)	0.28							
Cement type	Type I							
Cementitious material content (lb/yd ³)	600							
Water/cement ratio	0.4							
Aggregate type	Limestone							
Ultimate shrinkage at 40% R.H (microstrains)	50							
Time to develop 50% ultimate shrinkage (days)	35							
Curing Method	Compound curing							
28 days modulus of rupture (psi)	700							
28 days elastic modulus (psi)	4,000,000							
Resilient modulus (psi)			35,000		5,000		500,000	

CHAPTER 5

DAMAGE ANALYSIS AND RESULTS

5.1 Truck configuration

The US Department of Transportation Federal Highway Administration (FHWA) classifies vehicles into 13 groups. Classes 1 to 3 are light vehicles with two axles, while classes 4 and higher are heavy vehicles with more than two axles. According to the FHWA, only vehicles in classes 4 to 13 significantly damage pavements. The FHWA classification of the trucks is based on the number of axles and trailer units; the other characteristics of trucks such as axle group type, suspension system, tire types, distance between axles of a given axle group, distance between centers of dual tires, tire inflation pressure and loading capacities vary base on the vehicle's manufacturers (Derastani, 2006). This section will describe characteristics of trucks proposed for this study by the New York State Department of Transportation (Appendix A).

Truck cases: The trucks provided in appendix A are classified into 35 truck cases, named L1 through L35. Each of the truck cases is made up of one or more of the following axles: single axle single tire (SAST), single axle dual tire (SADT), tandem axle dual tire (TADT), tridem axle dual tire (TRADT), and quad axle dual tire (QADT) (Figure 5.1). Cases L1 to L5 are treated as standalone axles while case L6 to 35 are considered as standalone trucks (i.e. they have an SAST front axle and one or more of the other axles as rear axles.)

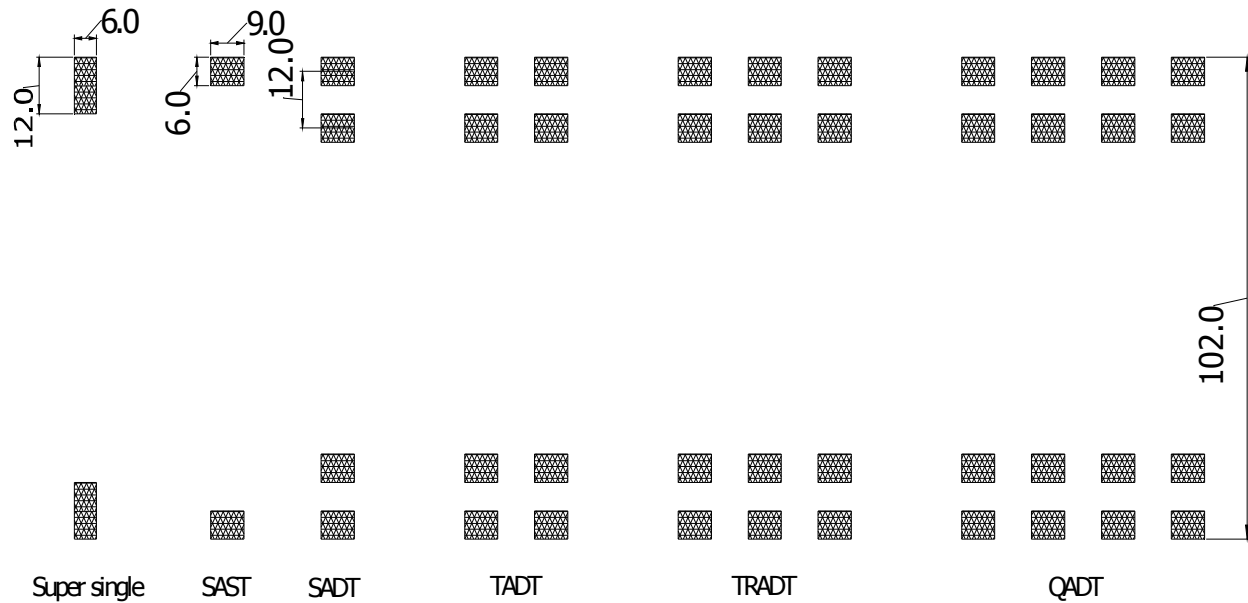


Figure 5.1: Types of axles

Distance between axles in a given axle group: This parameter also depends on the vehicle's manufacturer. The arrangement of axles in a given axle group has an impact on the pavement response. In this research, axles for cases L1 and L5 are unequally spaced; the rest of axles in all other groups of axles are equally spaced. Axles in groups for case L6 to 15 are spaced at distance of 4 ft. The distance between axles in groups of axles for truck cases L16 to 35 ranges from 4 to 10 ft.

Axle width and space between centers of dual tires: Axle width refers to the distance from the centre of dual tires of an axle to another center of dual tires of the same axle while the space between centers of dual tires mean the distance between centers of paired tires. Researchers have been using different axle width and space between dual tires for their studies. While Kim et al. (2002) assumed these distances to be 75 inches and 13 inches, Hiller et al. (2002) assumed them to be 74 inches and 13.5 inches respectively. This research assumed the

axles width and space between centers of dual tires to be 84 inches and 12 inches respectively (according to NCHRP, 2004).

Tire inflation pressure: The tire inflation pressure affects the contact area and stress when the tire is in contact with pavement surface. According to Darestani et al. (2002), the pressure of heavy trucks varies between 70 to 140 psi. For the finite element analysis, this research used an inflation pressure of 80 psi for all tires, except for super single tires where a pressure of 120 psi was used. MEPDG program uses an inflation pressure of 120 psi. Therefore all researchers and designers has to apply this value whenever using the MEPDG software.

Axle spacing: Different trucks may have different axle spacing. This parameter is inconsequential when analyzing bottom up cracks damage of concrete pavements, but has significant effects when top down cracks are considered. The axle spacing of trucks used in this research can be seen in the truck cases shown in appendix A.

Axle Loads: This is the most important parameter required for designing of pavement structures. This study used all axle loads as proposed by NYSDOT except for MEPDG analyses, where some axle loads had to be modified slightly to fit the software range of axle loads. Table 5.1 shows the modified axle loads.

Table 5.1: Modified axle loads

<div style="text-align: center;"> <div style="display: inline-block; transform: rotate(-45deg);">Axle load</div> <div style="display: inline-block;">Truck case</div> </div>	Axle1 (lbs)	Axle2 (lbs)		Axle3 (lbs)	
	<i>Original</i>	<i>Original</i>	<i>Modified</i>	<i>Original</i>	<i>Modified</i>
L10	12,000	22,700	22,000	45,300	45,000
L11	12,000	52,400	54,000	52,400	54,000
L12	12,000	47,000	48,000	58,000	60,000

5.2 Finite element results and analysis

Tensile stresses at the bottom of concrete slab obtained as results of the finite element (ABAQUS/CAE) program runs were used to calculate the allowable number axles base on Tepfer (1979) and Darter (1977) fatigue models. The two models relate the number of repetitions of loading that can cause failure to stress ratio (tensile stress divided to modulus of rupture). However, the used Darter fatigue model estimate number of axle passes at 25% conservative probability of failure limit for a zero maintenance JPCP (Gillespie et al., 1993). Tepfer's model estimates the number of axle passes at a higher probability of failure. The overall analysis after the Abaqus program runs can be considered step by step as follows.

Step 1: The critical tensile stresses at the bottom concrete slab (Figure 5.2) caused by different axle groups (i.e. single axle, tandem axles, tridem axles and quadem axles) were computed by the Abaqus program and the results were recorded in Tables 5.2 and 5.3.

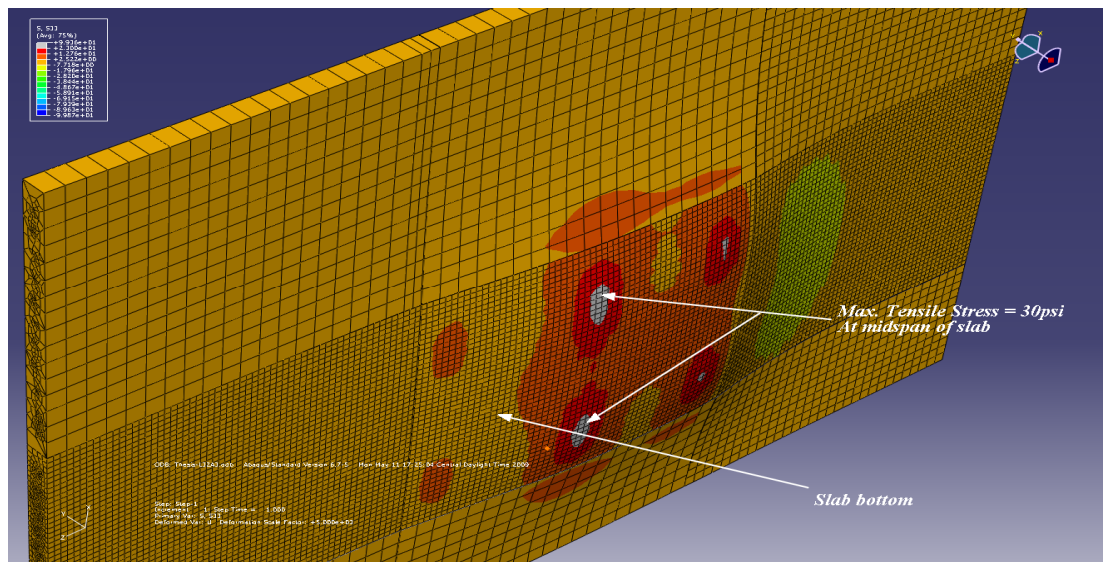


Figure 5.2: Maximum Tensile Stresses at the bottom of a Slab caused by axle A3 of Truck L32.

Table 5.2: Calculated damage relative to axle L1 (FEM)

Load case/ Truck type	Slab bottom max		Axle Loads lbs	Darter-fatigue model ⁽¹⁾		Tepfer-fatigue model ⁽²⁾	
	tensile stress (psi)	tensile strain (x10 ⁻⁶)		Allowable axles	Relative Damage	Allowable Axles	Relative Damage
L1	21	5.3	63,000	1.20698E+16	1.00	1.4474E+14	1.00
L2	28.75	7	63,000	7.70428E+15	1.57	9.976E+13	1.45
L3	13.5	3.4	48,000	1.86371E+16	0.65	2.0749E+14	0.70
L4	35	8.75	63,000	5.36414E+15	2.25	7.3895E+13	1.96
L5	22.75	5.6	50,000	1.09062E+16	1.11	1.3307E+14	1.09

(1) Darter – fatigue model = equation 2.12.

(2) Tepfer – fatigue model = equation 2.7.

Table 5.3: Calculated damage relative to truck L6a (FEM)

Load case/ Truck type	Slab bottom max		Axle Loads (lbs)	Darter-fatigue model ⁽¹⁾		Tepfer-fatigue model ⁽²⁾	
	tensile stress (psi)	tensile strain (x10 ⁻⁶)		Allowable axles	Relative Damage	Allowable Axles	Relative Damage
L6aA1	20	5	12,000	1.27896E+16		1.5186E+14	
L6aA2	25	6.25	34,000	9.57352E+15		1.1944E+14	
L6aA3	25	6.25	34,000	9.57352E+15		1.1944E+14	
Total L6a			80,000	3.48313E+15	1.00	4.2864E+13	1.00
L6bA1	20	5	12,000	1.27896E+16		1.5186E+14	
L6bA2	20	5	26,000	1.27896E+16		1.5186E+14	
L6bA3	32.5	8	42,000	6.20002E+15		8.332E+13	
Total L6b			80,000	3.14795E+15	1.11	3.9727E+13	1.08
L6cA1	20	5	12,000	1.27896E+16		1.5186E+14	
L6cA2	14	3.5	18,000	1.81051E+16		2.0257E+14	
L6cA3	39	9.8	50,000	4.25472E+15		6.0981E+13	
Total L6c			80,000	2.71404E+15	1.28	3.5816E+13	1.20
L7aA1	20	5	12,000	1.27896E+16		1.5186E+14	
L7aA2	24.5	6	51,000	9.85485E+15		1.2235E+14	
L7aA3	24.5	6	51,000	9.85485E+15		1.2235E+14	
Total L7a			114,000	3.55702E+15	0.98	4.3607E+13	0.98
L7bA1	20	5	12,000	1.27896E+16		1.5186E+14	
L7bA2	19	4.8	39,000	1.35523E+16		1.5933E+14	
L7bA3	30.5	7.5	63,000	6.96157E+15		9.1719E+13	
Total L7b			114,000	3.3827E+15	1.03	4.208E+13	1.02

Table 5.3 – Continued

L7cA1	20	5	12,000	1.27896E+16		1.5186E+14	
L7cA2	13	3.3	27,000	1.91848E+16		2.1253E+14	
L7cA3	37	9.2	75,000	4.77734E+15		6.7128E+13	
Total L7c			114,000	2.94434E+15	1.18	3.8187E+13	1.12
L8aA1	20	5	12,000	1.27896E+16		1.5186E+14	
L8aA2	22.5	5.6	52,000	1.58927E+16		1.8182E+14	
L8aA3	22.5	5.6	84,000	7.93069E+15		1.0218E+14	
Total L8a			148,000	3.74247E+15	0.93	4.5722E+13	0.94
L8bA1	20	5	12,000	1.27896E+16		1.5186E+14	
L8bA2	16.25	4	52,000	1.58927E+16		1.8182E+14	
L8bA3	28.25	6.7	84,000	7.93069E+15		1.0218E+14	
Total L8b			148,000	3.74247E+15	0.93	4.5722E+13	0.94
L8cA1	20	5	12,000	1.27896E+16		1.5186E+14	
L8cA2	11.25	3	36,000	2.12316E+16		2.3116E+14	
L8cA3	32	8	100,000	6.38221E+15		8.5345E+13	
Total L8c			148,000	3.54643E+15	0.98	4.4193E+13	0.97
L9A1	20	5	12,000	1.27896E+16		1.5186E+14	
L9A2	25	6.3	34,000	9.57352E+15		1.1944E+14	
L9A3	25	6.3	34,000	9.57352E+15		1.1944E+14	
Total L9			80,000	3.48313E+15	1.00	4.2864E+13	1.00
L10A1	20	5	12,000	1.27896E+16		1.5186E+14	
L10A2	16.25	4	22,700	1.58927E+16		1.8182E+14	
L10A3	11	3	45,300	2.15413E+16		2.3396E+14	
Total L10			80,000	5.33239E+15	0.65	6.1127E+13	0.70
L11A1	20	5	12,000	1.27896E+16		1.5186E+14	
L11A2	25	6.3	52,500	9.57352E+15		1.1944E+14	
L11A3	25	6.3	52,500	9.57352E+15		1.1944E+14	
Total L11			117,000	3.48313E+15	1.00	4.2864E+13	1.00
L12A1	20	5	12,000	1.27896E+16		1.5186E+14	
L12A2	22.5	5.6	47,000	1.10653E+16		1.3468E+14	
L12A3	27.5	6.8	58,000	8.28283E+15		1.0593E+14	
Total L12			117,000	3.45671E+15	1.01	4.2644E+13	1.01

Table 5.3 – Continued

L13A1	20	5	12,000	1.27896E+16		1.5186E+14	
L13A2	34.5	8.6	48,000	5.52177E+15		7.569E+13	
L13A3	16.5	4.2	57,000	1.56642E+16		1.7965E+14	
Total L13			117,000	3.09473E+15	1.13	3.9427E+13	1.09
L14A1	20	5	12,000	1.27896E+16		1.5186E+14	
L14A2	32.5	8.1	42,000	6.20002E+15		8.332E+13	
L14A3	18	4.5	63,000	1.43606E+16		1.6717E+14	
Total L14			117,000	3.23506E+15	1.08	4.0702E+13	1.05
L15aA1	20	5	12,000	1.27896E+16		1.5186E+14	
L15aA2	27.5	6.9	36,000	8.28283E+15		1.0593E+14	
L15aA3	19.5	4.9	69,000	1.31655E+16		1.5555E+14	
Total L15a			117,000	3.638E+15	0.96	4.4536E+13	0.96
L15bA1	20	5	12,000	1.27896E+16		1.5186E+14	
L15bA2	27.5	6.7	36,000	8.28283E+15		1.0593E+14	
L15bA3	18	4.5	69,000	1.43606E+16		1.6717E+14	
Total L15b			117,000	3.72363E+15	0.94	4.544E+13	0.94
L15cA1	20	5	12,000	1.27896E+16		1.5186E+14	
L15cA2	27.5	6.9	36,000	8.28283E+15		1.0593E+14	
L15cA3	12.5	3	69,000	1.97486E+16		2.177E+14	
Total L15c			117,000	4.0071E+15	0.87	4.85E+13	0.88
L16A1	20	5	12,000	1.27896E+16		1.5186E+14	
L16A2	32.5	8	42,000	6.20002E+15		8.332E+13	
L16A3	22.5	5.6	63,000	1.10653E+16		1.3468E+14	
Total L16			117,000	3.03167E+15	1.15	3.8444E+13	1.11
L17A1	20	5	12,000	1.27896E+16		1.5186E+14	
L17A2	28	7	37,000	8.04637E+15		1.0342E+14	
L17A3	28	7	58,000	8.04637E+15		1.0342E+14	
Total L17			107,000	3.06046E+15	1.14	3.8574E+13	1.11
L18A1	15	3.8	9,000	1.70861E+16		1.9307E+14	
L18A2	25	6.3	54,000	9.57352E+15		1.1944E+14	
L18A3	25	6.3	54,000	9.57352E+15		1.1944E+14	
Total L18			117,000	3.7392E+15	0.93	4.5613E+13	0.94

Table 5.3 - Continued

L19A1	16.5	4.2	10,000	1.56642E+16		1.7965E+14	
L19A2	28	7	35,000	8.04637E+15		1.0342E+14	
L19A3	28.5	7	18,000	7.81666E+15		1.0097E+14	
L19A4	24.4	6.1	54,000	9.9121E+15		1.2294E+14	
Total L19			117,000	2.39844E+15	1.45	3.0053E+13	1.43
L20A1	20	5	12,000	1.27896E+16		1.51858E+14	
L20A2	26.25	6.5	39,000	8.90482E+15		1.12485E+14	
L20A3	26	6.5	58,000	9.03471E+15		1.13844E+14	
Total L20			109,000	3.32037E+15	1.05	4.12216E+13	1.04
L21A1	20	5	12,000	1.27896E+16		1.5186E+14	
L21A2	32.5	8	42,000	6.20002E+15		8.332E+13	
L21A3	22.5	5.6	63,000	1.10653E+16		1.3468E+14	
Total L21			117,000	3.03167E+15	1.15	3.8444E+13	1.11
L22A1	20	5	12,000	1.27896E+16		1.5186E+14	
L22A2	32.5	8	42,000	6.20002E+15		8.332E+13	
L22A3	22.5	5.6	63,000	1.10653E+16		1.3468E+14	
Total L22			117,000	3.03167E+15	1.15	3.8444E+13	1.11
Total L23	30	7.5	62,800	7.16615E+15	0.49	9.3948E+13	0.46
L24A1	14	3.5	8,000	1.81051E+16		2.0257E+14	
L24A2	36	9	47,000	5.06224E+15		7.043E+13	
L24A3	36	9	47,000	5.06224E+15		7.043E+13	
Total L24				2.22067E+15	1.57	3E+13	1.43
L25A1	20	5	12,000	1.27896E+16		1.5186E+14	
L25A2	32.5	8.2	48,000	6.20002E+15		8.332E+13	
L25A3	35	8.8	47,000	5.36414E+15		7.3895E+13	
Total L25			107,000	2.34796E+15	1.48	3.1134E+13	1.38
Total L26	42	10.5	49,400	3.57602E+15	0.97	5.2799E+13	0.81
L27A1	34	8.5	20,000	5.68404E+15		7.753E+13	
L27A2	35.5	8.9	59,000	5.211E+15		7.2142E+13	
Total L27			79,000	2.71863E+15	1.28	3.7369E+13	1.15
L28A1	18.5	4.6	15,000	1.39506E+16		1.632E+14	
L28A2	37.8	9.45	64,000	4.561E+15		6.4598E+13	
Total L28			79,000	3.43723E+15	1.01	4.628E+13	0.93

Table 5.3 - Continued

L29A1	27	6.75	22,400	8.52623E+15		1.0851E+14	
L29A2	22.5	5.6	56,600	1.10653E+16		1.3468E+14	
Total L29			79,000	4.81562E+15	0.72	6.0092E+13	0.71
L30A1	14	3.5	8,000	1.81051E+16		2.0257E+14	
L30A2	40	10	40,500	4.01527E+15		5.8122E+13	
L30A3	19	4.8	30,500	1.35523E+16		1.5933E+14	
Total L30			79,000	2.64501E+15	1.32	3.5189E+13	1.22
L31A1	22.5	5.6	15,500	1.10653E+16		1.3468E+14	
L31A2	21	5.3	77,500	1.20698E+16		1.4474E+14	
Total L31			93,000	5.77288E+15	0.60	6.9764E+13	0.61
L32A1	20	5	12,000	1.27896E+16		1.5186E+14	
L32A2	32	8	40,000	6.38221E+15		8.5345E+13	
L32A3	30	7.5	58,000	7.16615E+15		9.3948E+13	
Total L32			110,000	2.67081E+15	1.30	3.4547E+13	1.24
L33A1	20	5	12,000	1.27896E+16		1.5186E+14	
L33A2	32.5	8.1	41,000	6.20002E+15		8.332E+13	
L33A3	27.5	6.9	67,000	8.28283E+15		1.0593E+14	
Total L33			120,000	2.77616E+15	1.25	3.568E+13	1.20
L34A1 ⁽³⁾	26	11	22,400	9.03471E+15		1.1384E+14	
L34A2	13.1	8.1	46,100	1.9074E+16		2.1151E+14	
L34A3	32.5	6.9	51,500	6.20002E+15		8.332E+13	
Total L34			120,000	3.0826E+15	1.13	3.9195E+13	1.09
L35A1 ⁽³⁾	26	5	22,400	9.03471E+15		1.1384E+14	
L35A2	17	8.1	34,600	1.5217E+16		1.7539E+14	
L35A3	29	6.9	63,000	7.59352E+15		9.857E+13	
Total L35			120,000	3.24579E+15	1.07	4.06E+13	1.06

(3) Super single tire

Step 2: The allowable number passes for different axle groups of the 35 truck cases were calculated based on Darter and Tepfer's fatigue models (see chapter 2) using the critical tensile stresses computed in step 1.

Step 3: The allowable number passes of different truck cases were calculated using the allowable number of axle passes obtained in step 2. The following equation demonstrates how the allowable numbers of trucks were calculated.

$$T = \frac{1}{\sum_{i=1}^k \frac{1}{N_i}} \quad [5.1]$$

Where;

T = Allowable number of passes of a truck case

N_i = Allowable number of passes of any axle group of a truck case

i = Axle group of a truck case ($i = 1, 2, 3 \dots k$)

k = Total axle groups of a truck case

Step 4: The relative damage for each truck case was calculated using the allowable number passes of different truck cases calculated in step 3. The relative damage for truck cases L1 to L5 were calculated based on the allowable number of passes of truck case L1, while relative damages for truck case L6 to L35 were calculated base on the allowable number of passes truck case L6. The following is a mathematical presentation of step 4 operations.

$$\text{Relative damage} = \frac{\text{Allowable passes of any truck case}}{\text{Allowable passes of base truck case}} \quad [5.2]$$

Step 5: The comparison of trucks damages was done base on the relative damages calculated in step 4. This step is further described in the next section.

5.3 Discussion of the results of the FE

As explained in previous chapters, two concrete fatigue models, Darter and Tepfer's, were used for calculating the allowable number of axles for different truck cases. Then the trucks

relative damages were calculated based on the allowable number of axles. The difference in relative damage calculated base on Darter's fatigue model and Tepfer's fatigue models were small, though the allowable number of axles calculated by Darter's fatigue models tends to be higher than those calculated by the Tepfer's fatigue model.

5.3.1 Effect of changing the loads and position of axles in a group

Five types of axle configurations, L1 (63,000 lb), L2 (63,000lb), L3 (48,000lb), L4 (63,000lb), and L5 (50,000lb) were used to investigate the effects of varying load distribution and axle position in an axle group. Axle group L1 was composed of four individual axles, while the remaining axle groups were composed of three axles each. Also, the axle group L1, L2 and L3 had equally spaced individual axles while axle groups L4 and L5 had the middle axle moved closer to one end.

The damage evaluated due to static load of the above mentioned axles are presented in Figure 5.3. Two important results can be drawn from Figure 5.3. The first result is that the reduction of axles in a group without changing the total load increased the pavement damage. This was seen when axles in case L1 were reduced to form axle L2, the damage increased by 57%. The second result is that the unequal arrangement of axles in a group increases pavement damages significantly. This was seen when truck case L3 rearranged to L5 and L2 rearranged to L4 caused truck damage increase by 55% and 35% respectively.

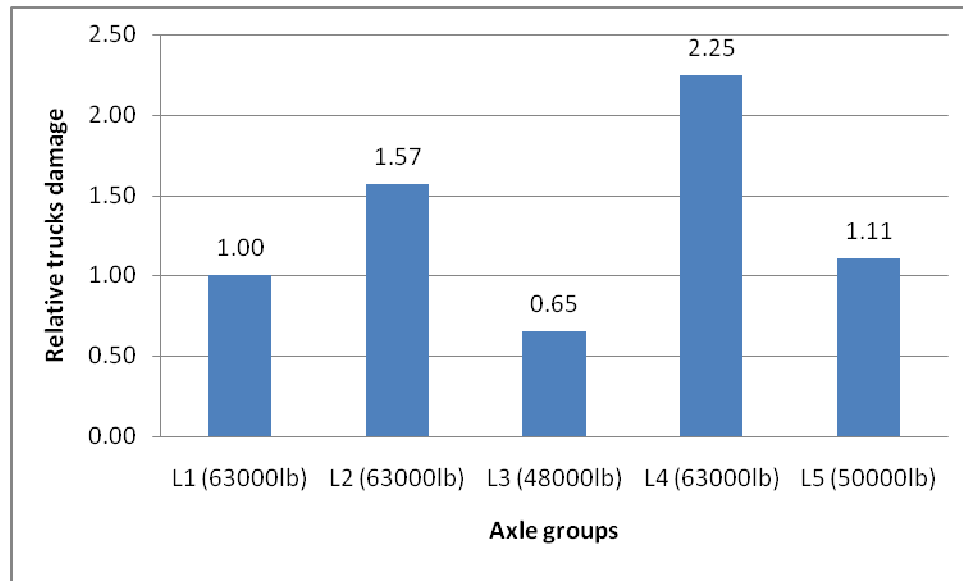


Figure 5.3: Effect of changing axle position in a group of axles (FEM)

5.3.2 Effect of increasing the number of axles in a group while maintaining the axle load distribution

This part of the analysis was done in order to get a comparison of truck damage to the concrete pavement when an axle with an equal load as individual axles in a group was added. The added axles changed the axle groups from tandem to tridem and tridem to quadem axles. Also, each of the added axles increased a load of 17,000 lbs to the formed group. In this study truck case L6 (80,000 lbs) with two tandem axles was changed to case L7 (114,000 lbs) with two tridem axles and L7 with two tridem axles was changed to case L8 (148,000 lbs) with two quadem axles. This study considered three sets (a, b, and c) of axle load distribution for the three case analyzed. The three trucks analyzed are shown in Appendix A and their relative damage based on truck case L6a are shown in Tables 5.2 and 5.3.

Figures 5.4, 5.5 and 5.6 presents relative damage due to increasing number of axles from truck cases L6 (tandems) to L7 (tridems) and L8 (quadems). The results indicate that when axles

were added, the damage reduced even though the load increased too. Under this consideration truck case L8 was found to be less damaging than truck cases L7 and L6. Truck case L7 was less damaging than truck case L6.

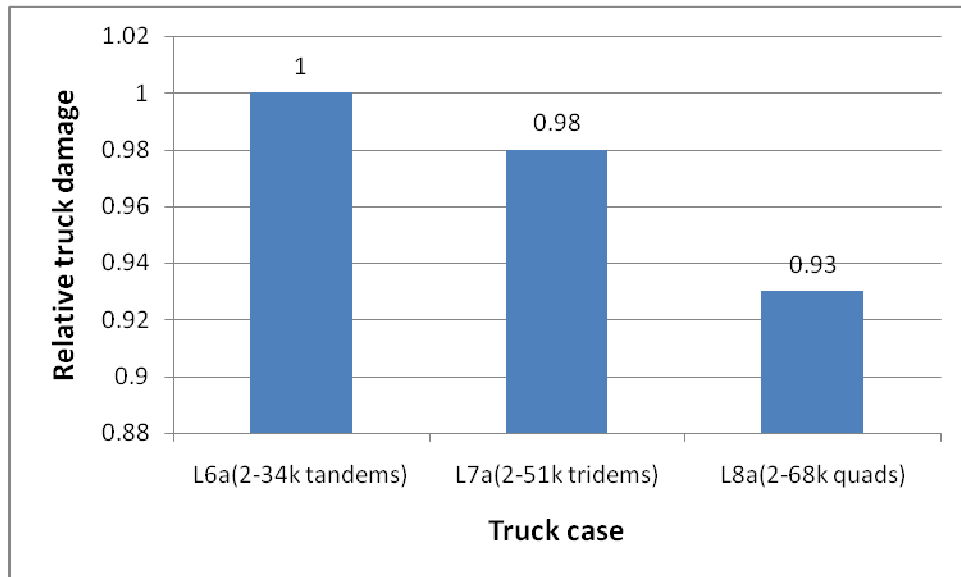


Figure 5.4: Set a-Effect of increasing axle and loads to axle groups of a truck (FEM)

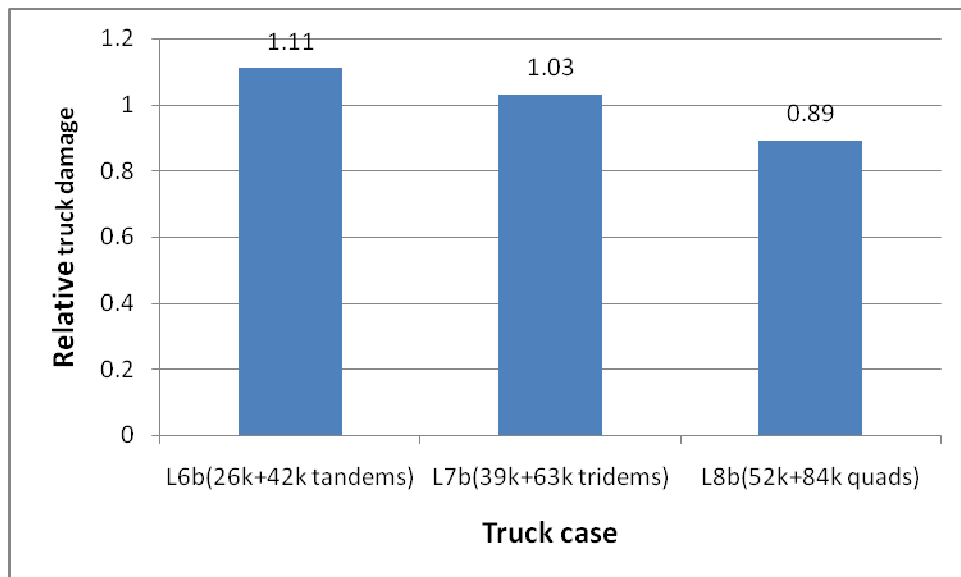


Figure 5.5: Set b-Effect of increasing axle and loads to axle groups of a truck (FEM)

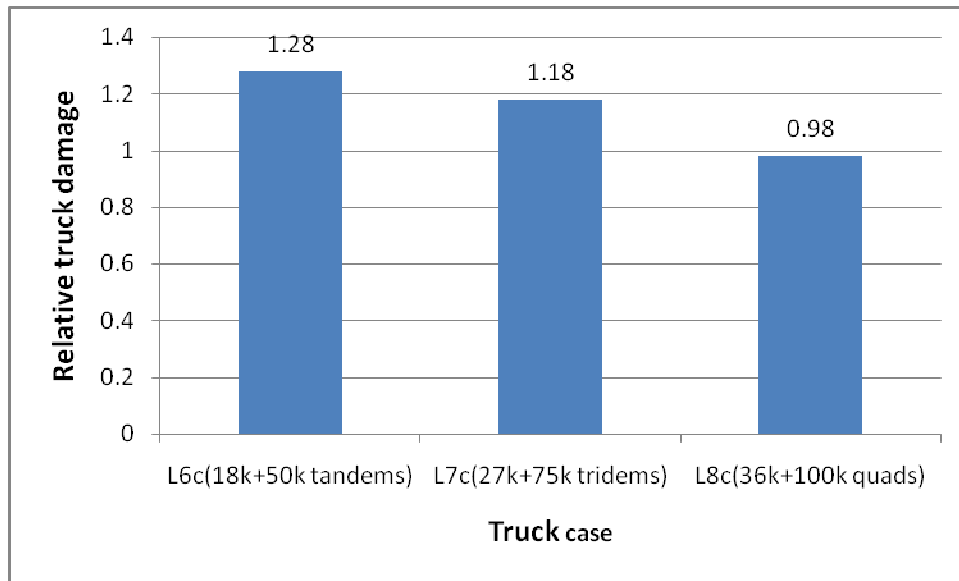


Figure 5.6: Set c-Effect of increasing axle and loads to axle groups of a truck (FEM)

5.3.3 Effect of shifting loads from one axle to another axle of the same size.

The analysis was conducted to establish a trend of rigid pavement damages when trucks were loaded unevenly. Three sets of load shifting for truck case L6, L7, and L8 were used to demonstrate shifting of loads from tandem to tandem axles, tridem to tridem axles and quadem to quadem axles respectively. For truck case L6, the loads were shifted two times at intervals of 8,000 lb and the truck case presented in three sets as L6a (no shift), L6b (shift = 8,000 lbs), and L6c (shift = 8,000 lbs). For truck case L7, the loads were shifted two times at intervals of 8,000 lb and the truck case presented in three sets as L7a (no shift), L6b (shift = 13,000lbs), and L6c (shift = 26,000 lbs).). For truck case L8, the loads were shifted two times at intervals of 8,000 lb and the truck case presented in three sets as L7a (no shift), L6b (shift = 16,000 lbs), and L6c (shift = 32,000 lbs).

The results presenting the effect of axle load shifting for trucks L6, L7 and L8 are shown in figures 5.7, 5.8, and 5.9. The results indicate that the damages for all trucks increased as the

shift loads were increased. Also, the rate of increase of loads shifting damages due to truck L6 (tandem axles) was noted to be the highest followed by truck trucks L7 (tridem axles) then L8 (quadem axles) as shown in figure 5.11.

Other trucks that can be distinguished from each other base on effects of load shifting for equal sized axles are; trucks L11 and L12. Both have two tridem axles and one front single axle. The overall weight for each truck was 80,000 lb while a shift of 5,500 lb was noted on truck L12 base on loads of truck L11 (see figures L11 and L12 in Appendix A). The results in Table 5.3 show that the shift was too small to cause any significant change in trucks damages. In general Trucks L11 and L12 have similar damage effects.

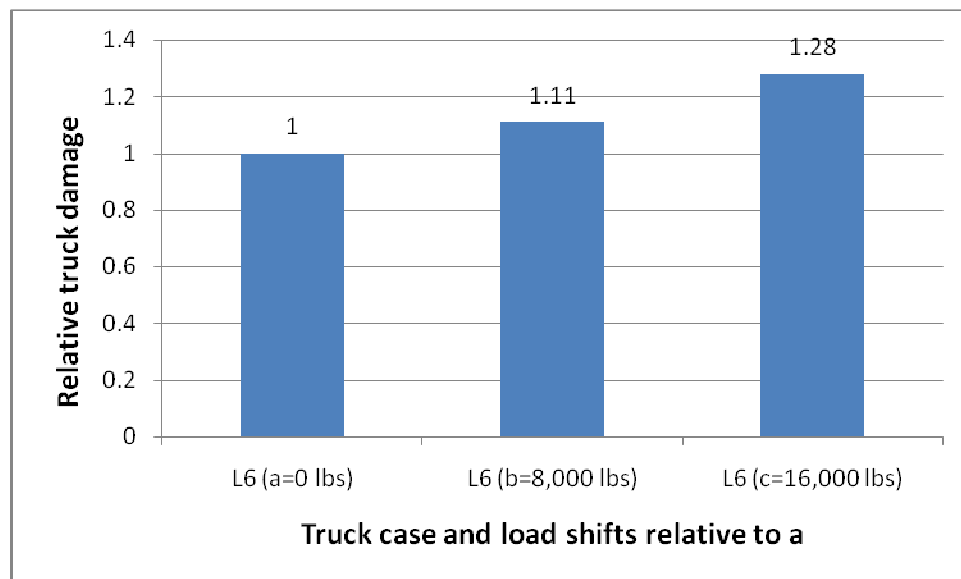


Figure 5.7: Truck L6 – Effect of shifting loads between equal axles (FEM)

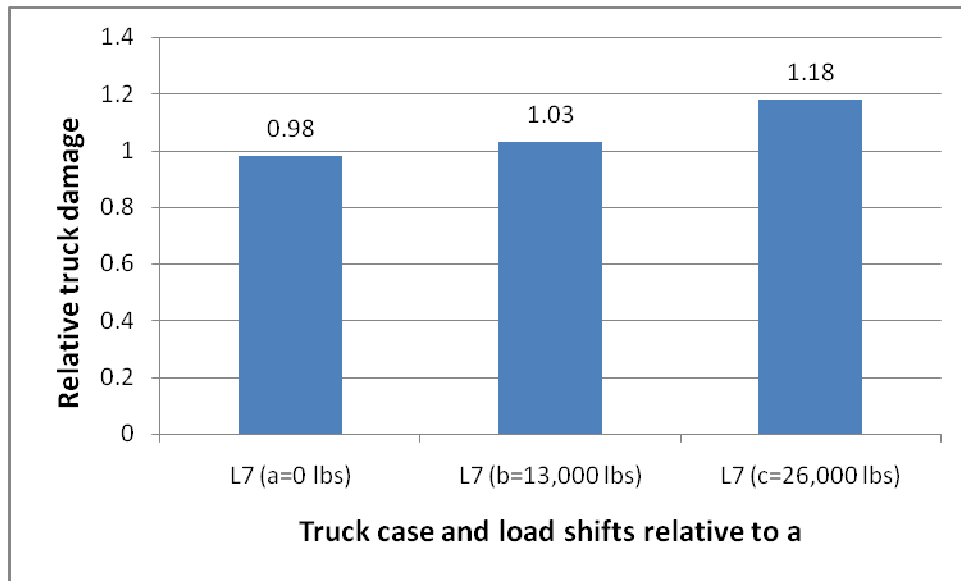


Figure 5.8: Truck L7 – Effect of shifting loads between equal axles (FEM)

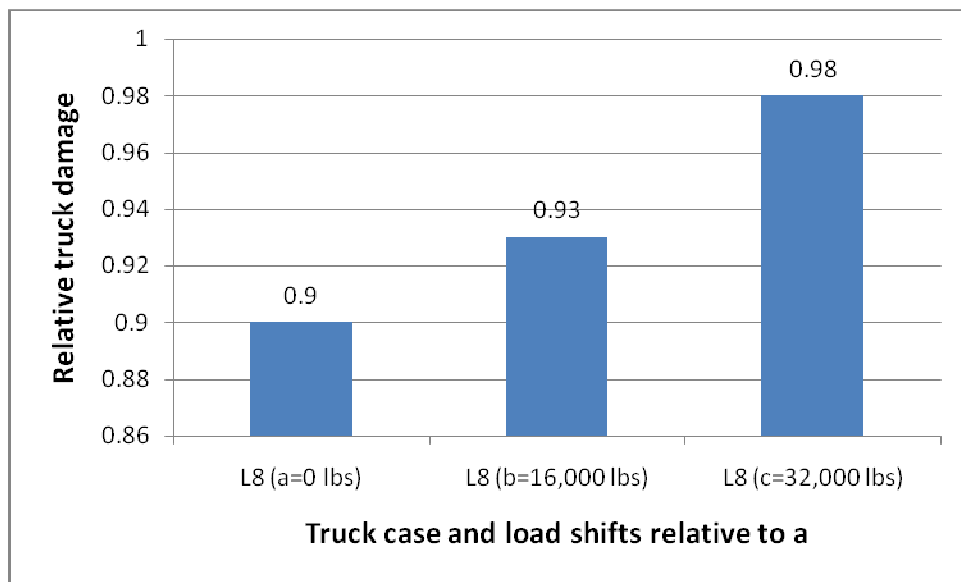


Figure 5.9: Truck case L8 – Effect of shifting loads between equal axles (FEM)

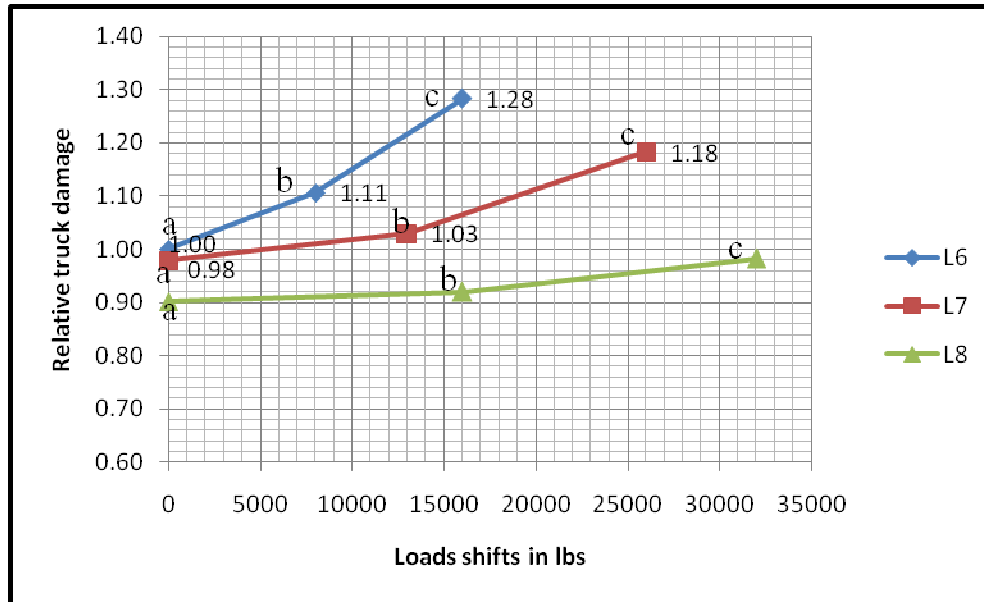


Figure 5.10: Rate of change of damage due to trucks L6, L7 and L8

5.3.4 Effect of load shifting for axles of unequal sizes (from a tandem to quadem axle)

Trucks cases L13, L14, and L15 (as shown in appendix A) were compared in terms of load shifting from a tandem axle to a quad one. Both trucks had a total weight of 117,000 lbs contributed by a front single axle, one tandem and one tridem axle. The loads shifting base on truck L13 were 6,000 lb and 12,000 lb for trucks L14 and L15 respectively (i.e. increment of 6,000 lb).

The relative damages presenting axle load shifting for trucks L13, L14 and L15 are shown in figure 5.11. The results show that shifting of loads from small axle to a larger axle (i.e. from tandem to quadem) decreases truck damages. In this case truck L13 was 1.05 and 1.18 times damaging than truck L14 and L15 respectively.

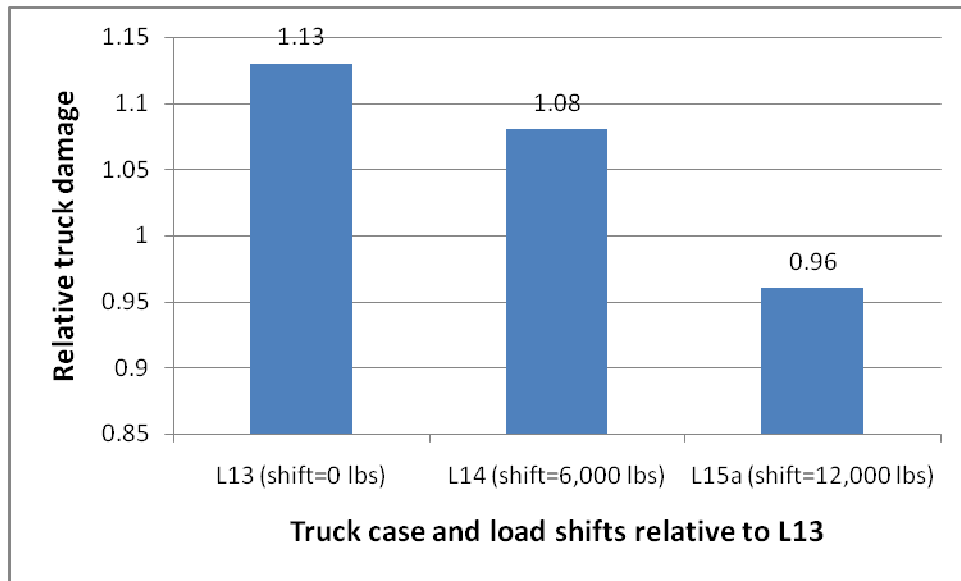


Figure 5.11: Effect of load shifting from tandem to quadem axles (FEM)

5.3.5 Effect of increasing spacing in an axle group of a truck

This analysis was conducted to get a sense of truck damages effects to rigid pavements when distances between individual axles in a group (i.e. quadem axle group) were changed. The only truck involved in this case of analysis was truck L15. The truck has one single axle, tandem axle and a quadem axle. The distances between axles of the quadem group were changed to make three sets, a, b, and c. The space increments for set L15a, L15b and L15c were 0'', 12'' and 42'' respectively (see figure L15 in Appendix A).

The Figure 5.12 presents the behavior of truck damage as a result of increasing spaces between individual axles in a group. The results indicate that when axle's spaces increases, the truck damage reduces. In terms of less damage, set L15c and L15b are 90% and 97% of set L15a respectively.

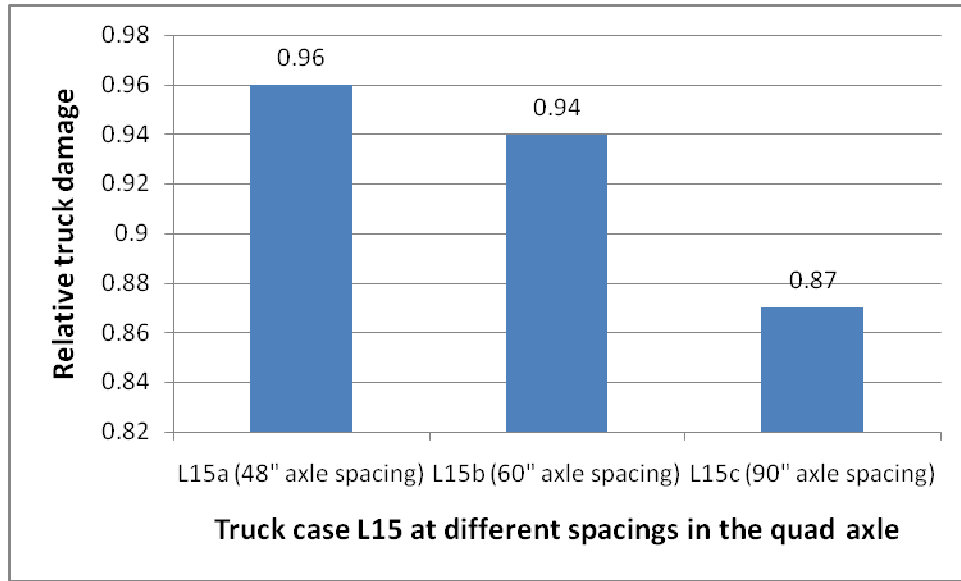


Figure 5.12: Effect of increasing spacing of a tandem axle (FEM)

5.3.6 Truck damage comparison under undesirable axles loading configuration

Under this category of the analysis, trucks with most damaging loading configurations were assessed. The trucks had unevenly loaded axles (i.e. unequal load distribution in an axle group). This group of trucks included a range of trucks from L16 to truck L35 whereby truck L24 (relative damage = 1.57) was the highest damaging of all, and truck L23 (relative damage = 0.49) was the least damaging in the group. These two trucks relative damages and other damages of trucks in this category are all recorded in Table 5.3.

5.4 Analysis and Results of MEPDG

For this study, the outputs of interest in the MEPDG analysis are predicted levels of cracking, joint faulting and roughness. Both top-down and bottom-up fatigue cracking, along with joint faulting are predicted in MEPDG. Then, the roughness of the pavement surface,

expressed in term of International Roughness Index (IRI), is computed from the cracking and joint faulting data.

The figures in the Appendix C contain pavement performance outputs for transverse cracking, faulting and roughness calculated by MEPDG software. A summary of damages calculated by the MEPDG as a result of 10 different truck cases is presented in Table 5.4. The next section concentrates on bottom up cracks, the only distress considered in the Finite Element approach.

Table 5.4: Summary of MEPDG performance output

Truck case	Bottom-up cracking		Top down cracking		Transverse cracking (% slab)		Faulting		IRI		
	Dam. at year 40	Relative damage	Dam. at year 40	Relative damage	Dam. at year 40	Relative damage	Dam. at year 40	Relative damage	Dam. at year 40	Δ IRI	Relative damage
L6a	0.0023	1.00	0.11	1.00	1.3	1.00	0.18	1.00	201	138	1.00
L6b	0.0073	3.17	0.14	1.23	1.9	1.46	0.18	1.01	203	140	1.01
L6c	0.0302	13.13	0.21	1.87	4.4	3.38	0.19	1.04	208	145	1.04
L7a	0.0026	1.13	0.21	1.87	4.3	3.31	0.18	1.01	204	141	1.02
L7b	0.0083	3.61	0.21	1.87	4.3	3.31	0.18	1.01	205	142	1.03
L7c	0.0339	14.74	0.21	1.87	4.4	3.38	0.19	1.03	207	144	1.04
L8a	0	0	0	0	0	0	0.23	1.29	228	165	1.19
L8b	0	0	0	0	0	0	0.21	1.18	218	155	1.12
L8c	0	0	0	0	0	0	0.21	1.19	218	155	1.12
L9	0.0023	1.00	0.11	1.00	1.3	1.00	0.18	1.00	201	138	1.00
L10	0.0001	0.04	0.02	0.18	0	0.00	0.16	0.87	189	126	0.91
L11	0.0043	1.87	0.02	0.21	0.1	0.08	0.19	1.04	204	141	1.02
L12	0.0062	2.70	0.02	0.21	0.1	0.08	0.19	1.04	204	141	1.02
L13	0.0218	9.48	0.21	1.88	13.8	10.62	0.21	1.16	227	164	1.18
L14	0.0072	3.13	0.26	2.36	6.6	5.08	0.21	1.14	219	156	1.13
L15a	0.0019	0.83	0.16	1.41	2.5	1.92	0.2	1.12	214	151	1.09
L15b	0.0019	0.83	0.16	1.41	2.5	1.92	0.2	1.12	214	151	1.09
L15c	0.0019	0.83	0.16	1.41	2.5	1.92	0.2	1.12	214	151	1.09

*Dam. = damage

5.5 MEPDG - Discussion of the results

5.5.1 General

As explained in section 5.4, the distress criteria considered in MEPDG are; transverse cracking, faulting and IRI. A difficulty encountered in setting up the MEPDG input files was to assign the number of axle configurations. The software requires as input the number of single, tandem, tridem and quad axle for each truck class. For the trucks that did not have all of the four axle types, 0.00001 percent was assigned for the missing axle types, when the truck configuration is described.

Also, this part of analysis found that out of the ten trucks cases analyzed by MEPDG, truck case L13 was causing more damages than the rest of the trucks. More detailed comparisons of trucks damages base on MEPDG analysis follows in the next sections.

5.5.2 Effect of load shifting (equal sized axles)

Figures 5.13 and 5.14 presents the MEPDG damage analysis results for trucks L6 (tandem to tandem axles load shifting), L7 (tridem to tridem axles load shifting), as shown in appendix A. The results indicates that shifting of loads (from a to b and b to c) increases bottom up damage to JPCP pavements for both truck L6 and L7. The rate of increase of top down cracking is very minimal for both truck cases.

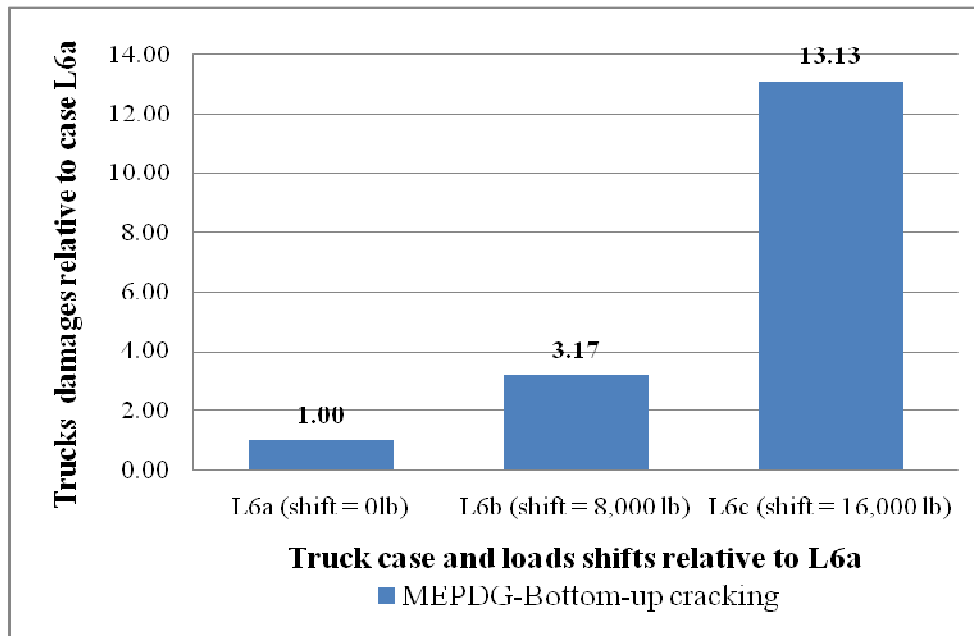


Figure 5.13: Truck case L6– Effect of shifting loads between equal axes (MEPDG)

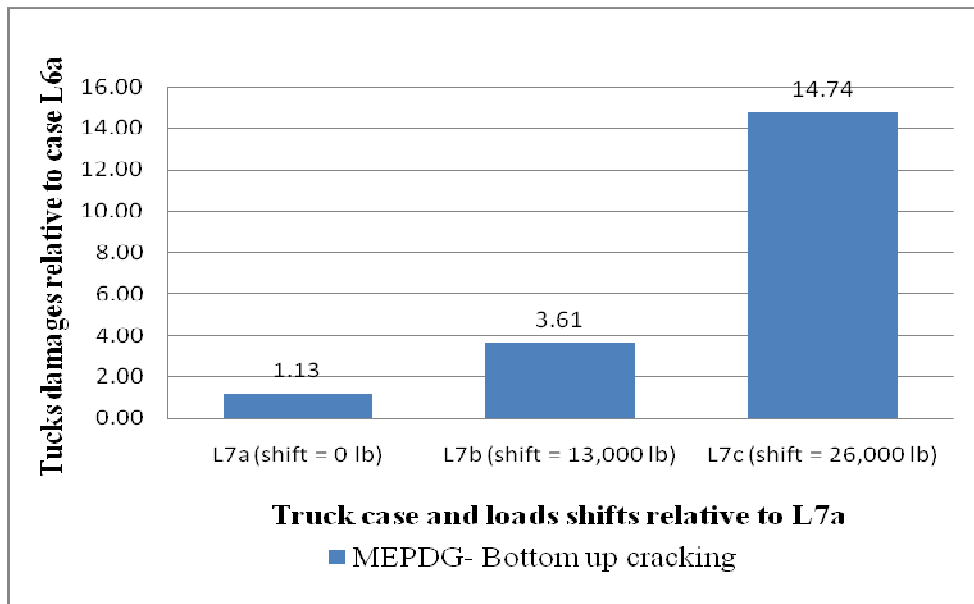


Figure 5.14: Truck case L7– Effect of shifting loads between equal axes (MEPDG)

5.5.3 Effect of load shifting (unequal sized axles)

Figure 5.15 shows the MEPDG damage analysis results for trucks case L13, L14, and L15a as shown in Appendix A. The truck cases present the effects of load shifting for unequal sized axles (from tandem axle to quadrum axle). Base on bottom up cracking, the results indicate a decrease in damages when load shifts from tandem to quadrum axle. In general figure 5.9 shows that truck case L13 is more damaging than L14 and L15.

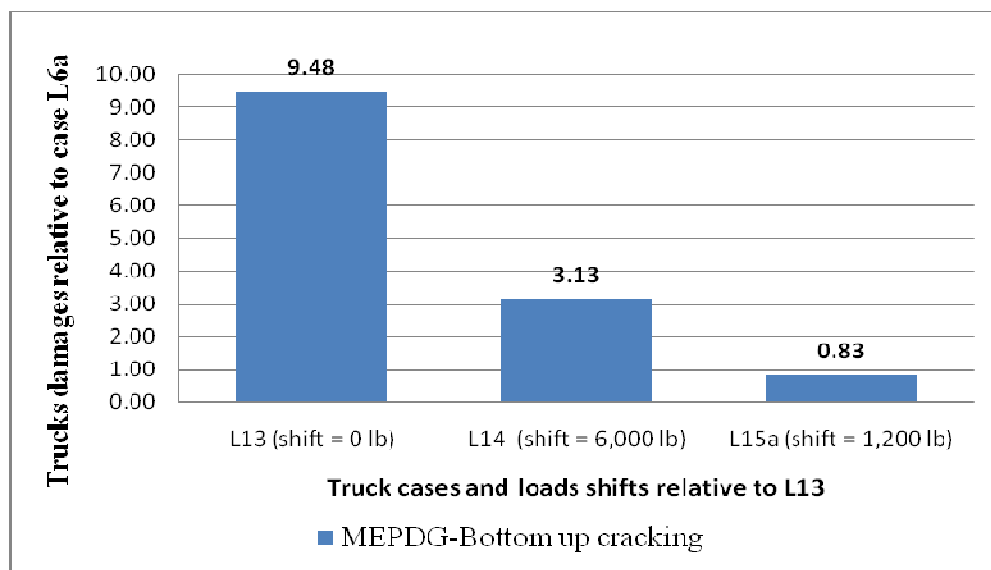


Figure 5.15: Effect of load shifting from tandem to quadrum (MEPDG)

5.5.4 Effect of increase spaces between axles of an axle group

Figure 5.16 shows damages to JPCP pavement due to increase in axle's spaces of trucks case L15 as calculated by the MPDG version 1.00 analysis software. The increase in spacing between axles changed the truck from L15a to L15b and L15c. The MEPD damage analysis results show the same damage even if spacing between axles was changing.

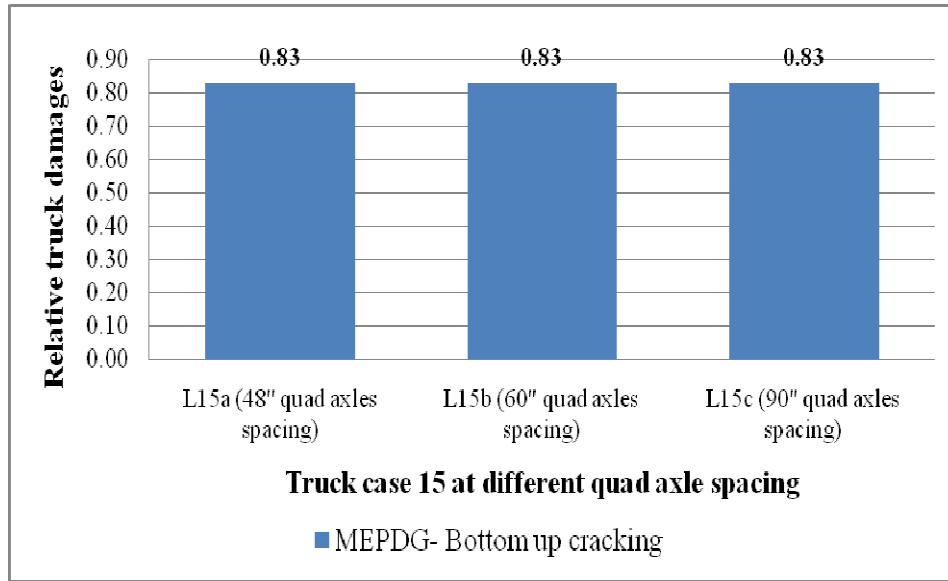


Figure 5.16: Effect of changing axle spacing for truck L15 (MEPDG)

5.6 Comparison between MEPDG and FE truck damages

A comparison between MEPDG and FE relative truck damages for Jointed Plain Concrete Pavement base on bottom up cracking are shown in Figures 5.17 to 5.20. Four cases of truck relative damages were considered for comparison:

- Effects of loads shift from tandem to tandem axles (Figure 5.17)
- Effects of loads shift from tridem to tridem axles (Figure 5.18)
- Effects of loads shift from tandem to quad axles (Figure 5.19)
- Effects of increasing space between axles a quad group of truck 15 (Figure 5.20).

As expected, in both MEPDG and FE approaches the trucks relative damages due to load shifting were increasing when loads were shifted from tandem to tandem axles, and tridem to tridem axles. Also, when the loads were shifted from tandem to quadem axle the damage decreased in both approaches. However, the relative damages based on the MEPDG were

changing faster than the relative damages calculated by 3D-FEM and its associated fatigue model.

Another aspect of comparison was on axle space increase. Figure 5.20 shows that increase in axle spaces of a group of axles (i.e. quad axle group) does not change the magnitude of trucks damages when analyzed by MEPDG. Meanwhile, the truck damages decrease with the increase of the axle spaces when the analysis was done by FE method.

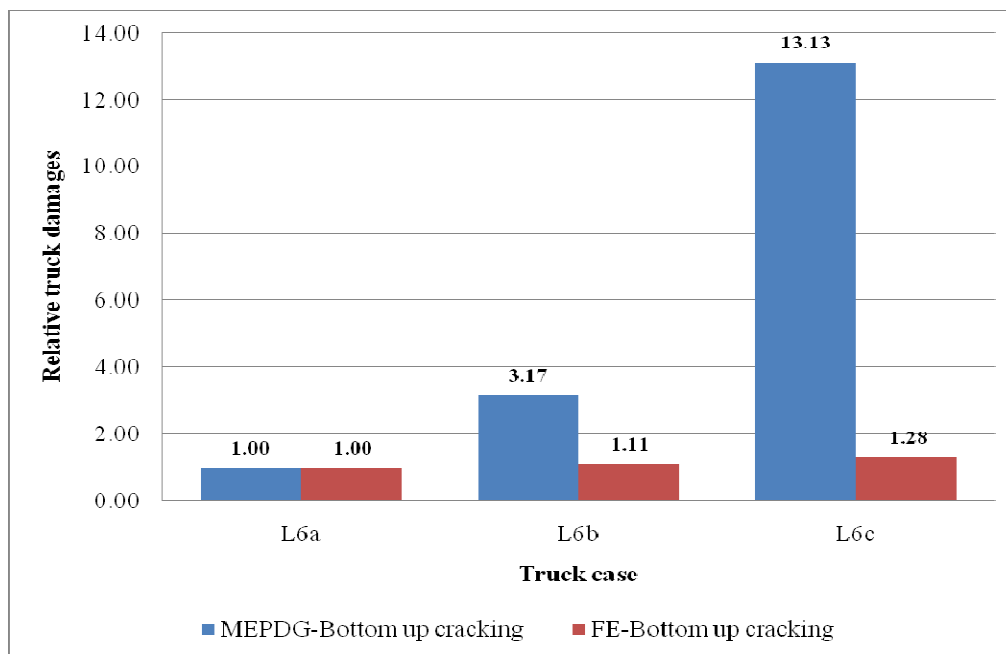


Figure 5.17: MEPDG – FE comparison: Effect of load shifting (Tandem to tandem)

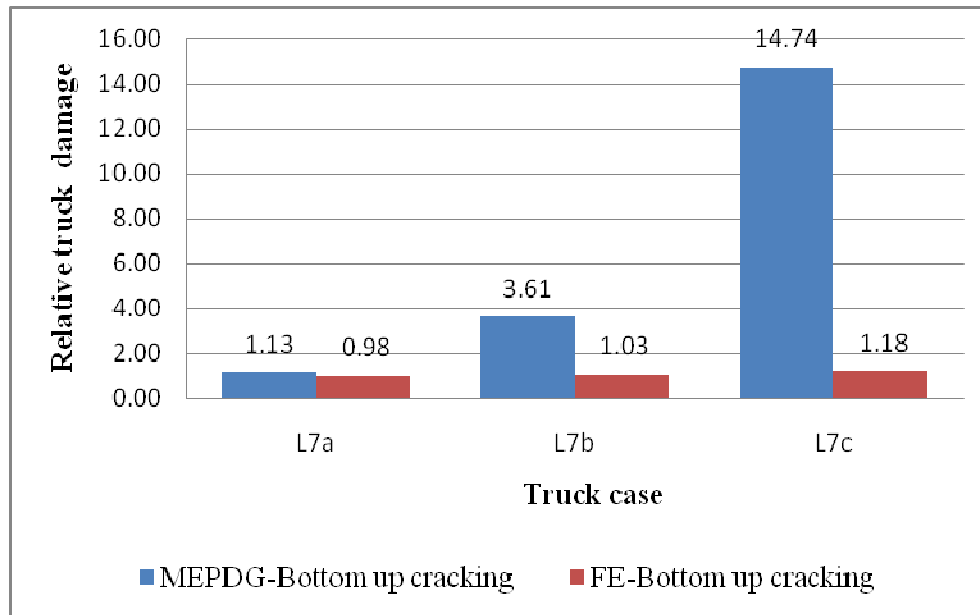


Figure 5.18: MEPDG – FE comparison: Effect of load shifting (Tridem to tridem)

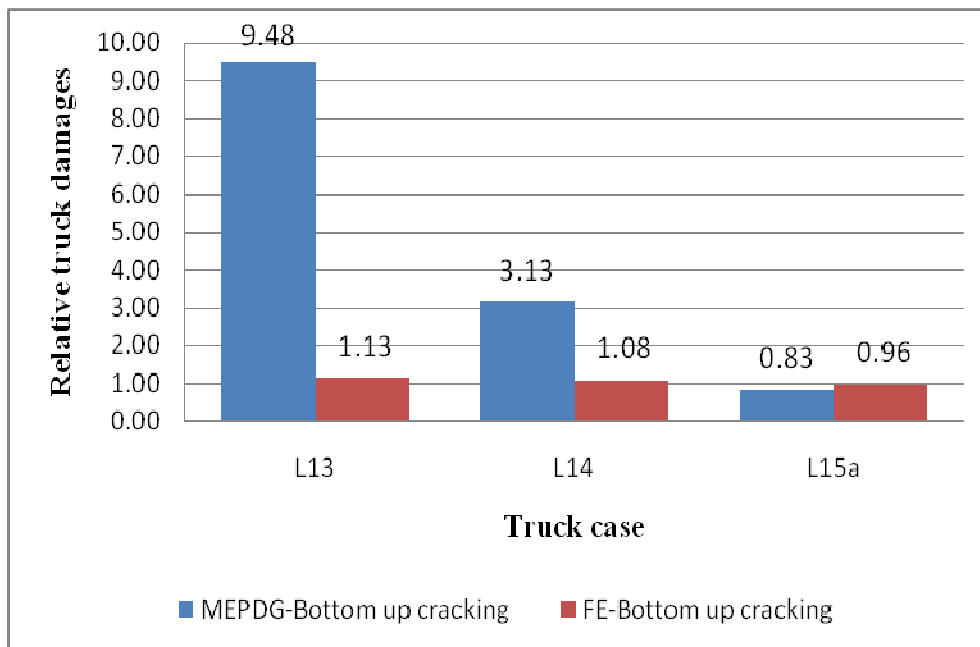


Figure 5.19: MEPDG – FE comparison: Effect of load shifting (tandem to quad)

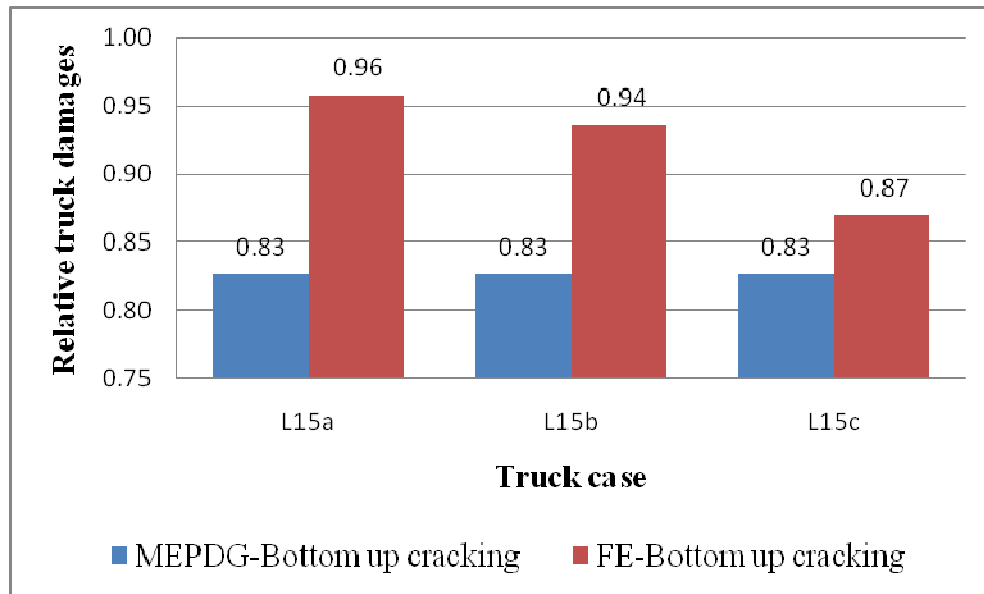


Figure 5.20: MEPDG – FE comparison: Effect of changing axle spacing

CHAPTER 6

SUMMARY, CONCLUSION AND RECOMMENDATIONS

6.1 Summary and conclusion

In this thesis, a 3D generalized Finite Element program, Abaqus/CAE, was used to simulate Jointed Concrete Plain Pavement responses under the action of axle loads from 35 different truck cases proposed by New York State Department of Transportation, the sponsor of this research. Each truck case axle's loads in form of pressure were placed at a critical position on the surface of the pavement model to cause maximum tensile stresses at the bottom of the concrete slabs. The maxima tensile stresses were then used into Darter fatigue model to calculate allowable number of axles. The aim of this exercise was to compare trucks in terms of bottom up damages caused to the concrete pavement. The exercise was a success not only at identifying the most damaging trucks cases, but also establishing trends of truck damages when axle loads were shifted, axles were added in axle's group, or axles position in an axle's group were changed. Base on the results, the following conclusions can be made:

- Base on the relative trucks damages values (in brackets), the truck cases proposed by NYSDOT can be arranged in descending order as follows: L24(1.57), L25(1.48), L19(1.45), L30(1.32), L32(1.30), L6c(1.28), L27(1.28), L33(1.25), L7c(1.18), L16(1.15), L21(1.15), L22(1.15), L17(1.14), L13(1.13), L34(1.13) L6b(1.11), L14(1.08), L35(1.07), L20(1.05), L7b(1.03), L28(1.01), L12(1.01), L6a(1.00), L9(1.00), L11(1.00), L8c(0.98),

L7a(0.98), L26(0.97), L15a(0.96), L15b(0.94), L18(0.93), L8a(0.93), L8b(0.89), L15c(0.87), L29(0.72), L10(0.65), L31(0.60), L23(0.49). Cases L1 to L5 are not reported here because they don't constitute complete trucks.

- When axles were reduced from a group of axles (i.e. quad axle reduced to tridem axle), the relative damages of the formed axle group increased. This was observed when truck case L1 was reduced to truck case L2, where L2 the damage increased by almost 50%.
- Rearranging the axles in an axle group from equally spaced to unequally spaced increases significantly the damage to the rigid pavement. When truck case L3 was converted to truck case L5, the damage increased by 71%, while when truck case L2 was converted to case L4, the damage increased by 43%.
- Increasing number of wheels and the total axle load proportionally reduces the damage. This behavior was observed when truck case L6 (with 34,000 lbs load tandem axles) was changed to truck case L7 (with 51,000 lbs tridem axles) and truck case L8 (with 68,000 lbs load quad axles).
- When loads are shifted between the axles of the same size, on the same truck, the damages increases as shifted load increases; the minimum damage is when the axles are loaded equally. Three sets of trucks cases L7 (tandems), L8 (tridem) and L8 (quad) were used to demonstrated this behavior.
- The rate of increase of truck damages due to loads shifting between equal axles of the same size is highest for truck L6 (tandem axles) followed by truck case L7 (tridem axles) then case L8 (quad axles).

- As expected, at the same axle load, when a tandem axle is replaced by a tridem or quad axle, the damage to the pavement decreases. This was indicated by reduction in trucks damages when truck case L13, having tandem axles, was replaced by truck cases L14 and L15, which have tridem and quad axles, respectively.
- When the spacing between the axles of a quad group (truck case L15) were increased the damage reduced.

For ten truck case the relative damage was evaluated with the Mechanistic Empirical Design Guide. The MEPDG predicts fatigue cracks, faulting and roughness. For this research, only the extent of bottom-up fatigue cracking was calculated and the relative damage was computed as the ratio between the predicted extend of bottom-up fatigue cracking expressed in percent of the lane area. The MEPDG performance prediction results lead to the following conclusions:

- The MEPDG analysis confirmed that, when loads are shifted between the axles of the same size, on the same truck, the damages increases as shifted load increases; the minimum damage is when the axles are loaded equally. Also, the program confirmed that when the loads are shifted from tandem to quad axle, the truck damage decreases.
- The changes in truck configuration have a much more pronounced effect on the MEPDG-based relative damages, which are computed based on the predicted fatigue cracking. In the FEM approach, the relative damages was calculated based on the number of repetitions to fatigue failure which was derived from the computed maximum strains at the bottom of the concrete slab and a fatigue model.

- Increasing spacing in an axle group (i.e. quad axle group) does not change the extent of fatigue cracking when analyzed by MEPDG. But the truck damages decreases with the increase of the axle spaces when analyzed with 3D-FEM.

6.2 Recommendations

The following recommendations are drawn base on the truck damage results and the analysis procedure in this study:

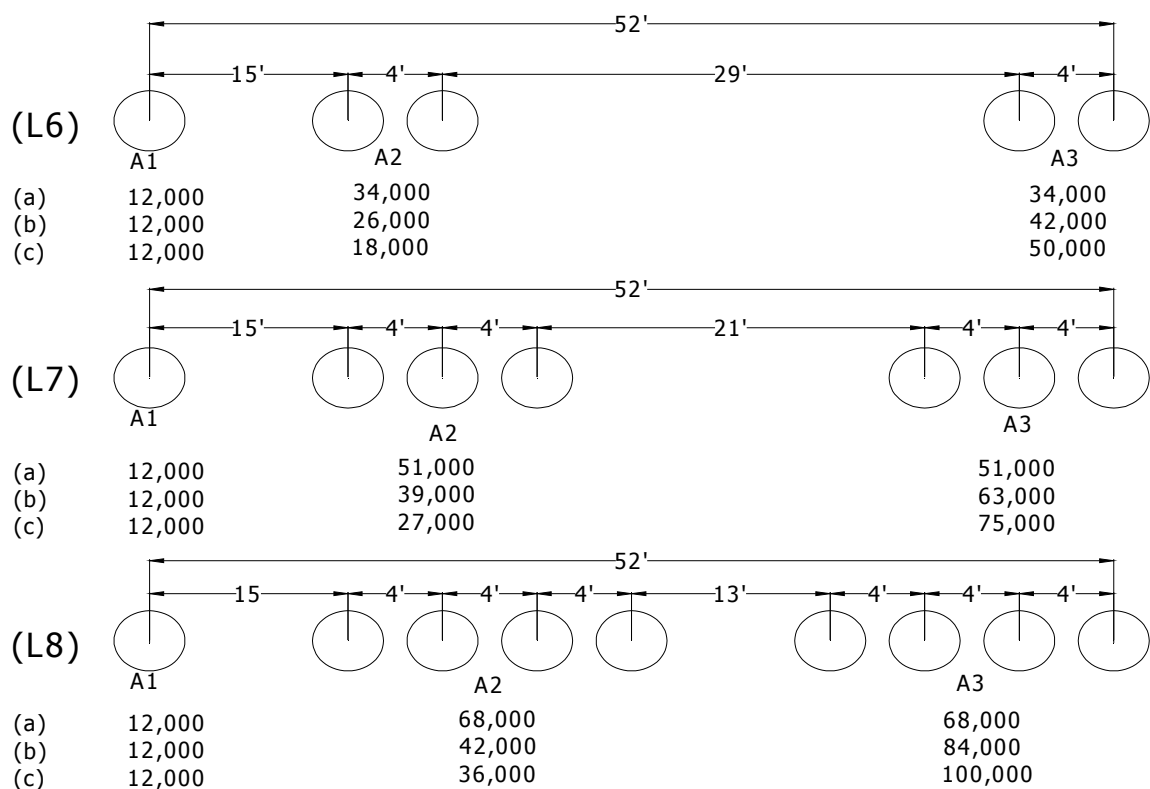
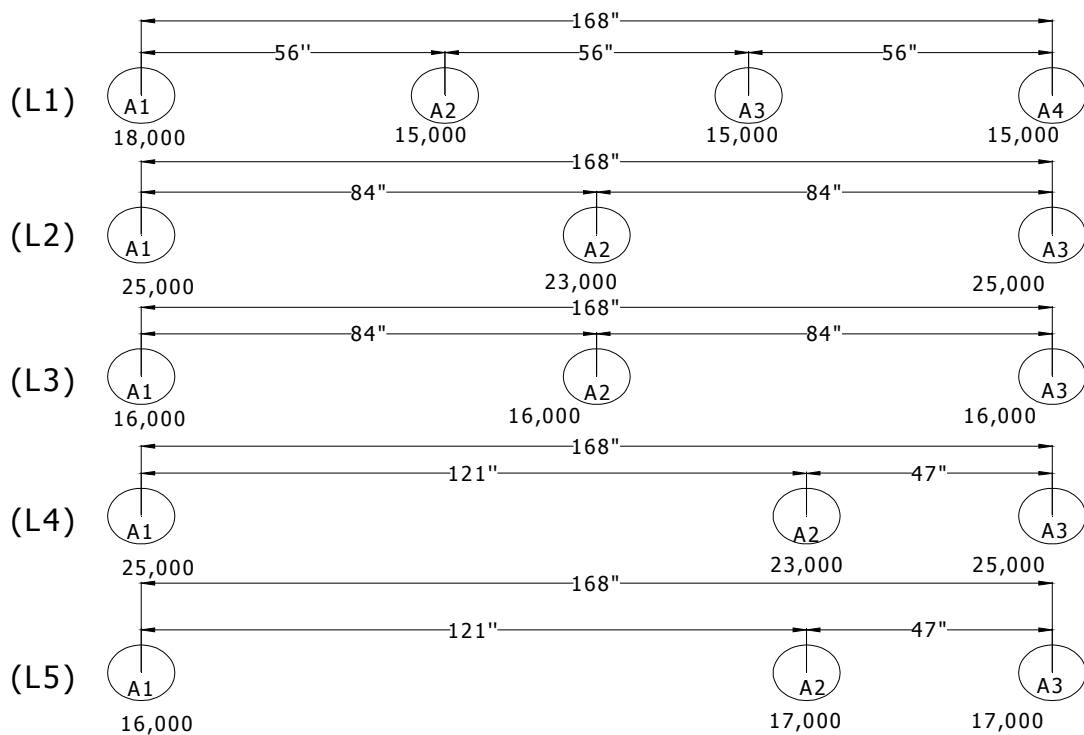
- The finite element model and analysis presented in this study considers fatigue damage evaluation focused on stress and strains at the bottom of the concrete slab induced by the load, without considering the strains caused by curling and warping of the slab. Therefore further studies are needed to consider the effects of curling and warping.
- The damage factors were computed for a concrete pavement with a slab thickness of 12 inches that yielded small stress-strain levels at the bottom of the slab. Therefore further studies are needed to consider thinner slabs.
- The MEPDG does not analyze group of axles with unequal load distributions and unequal axle spacing within an axle group. Also, it does not analyze trucks with axle configurations missing a group of axles with a size less than the truck largest group of axles and greater than the smallest size of axles of the truck (e.g. truck case L13). Therefore the MEPDG software needs to be improved to accommodate more complex truck configurations.

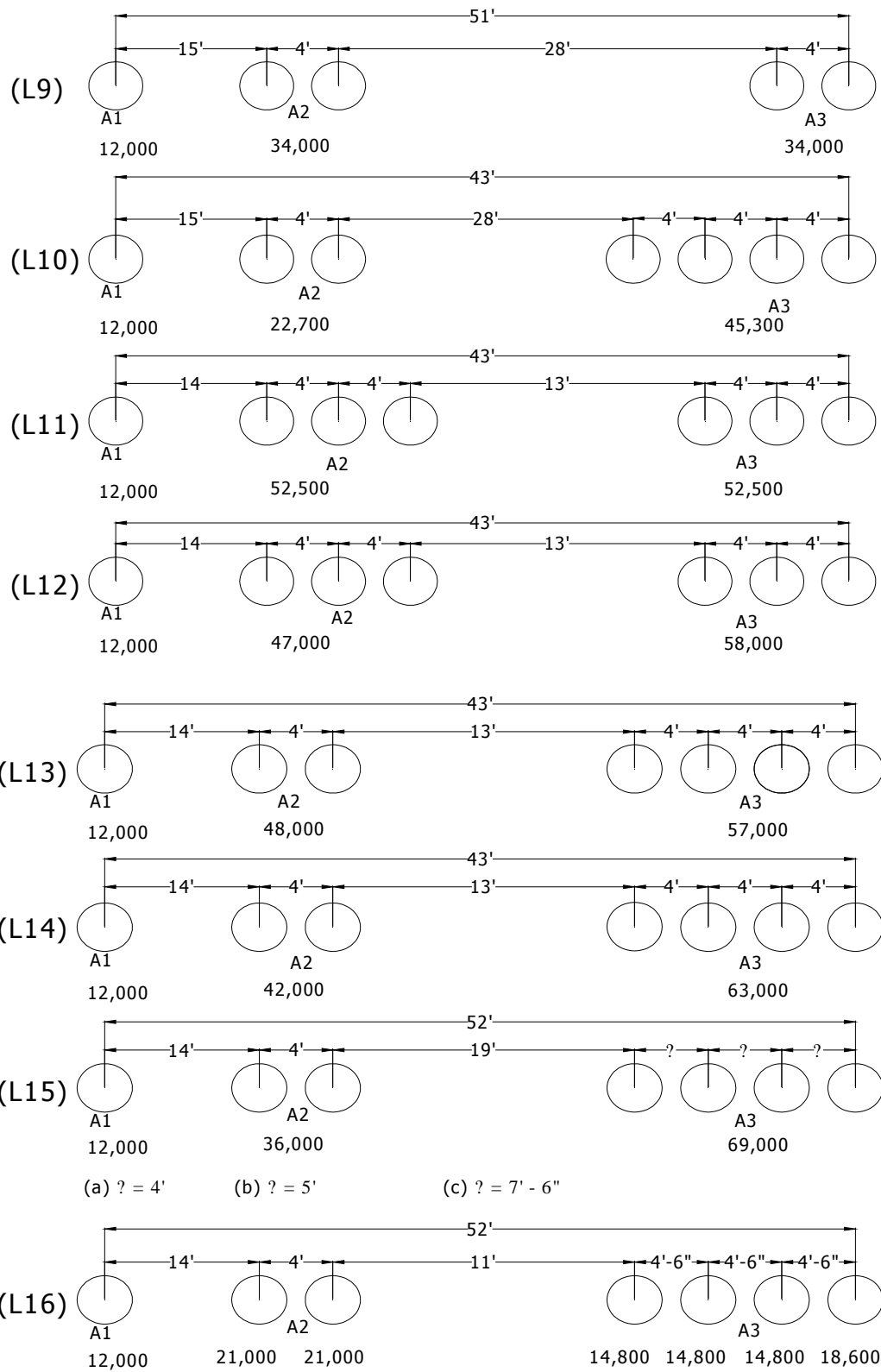
APPENDIX A

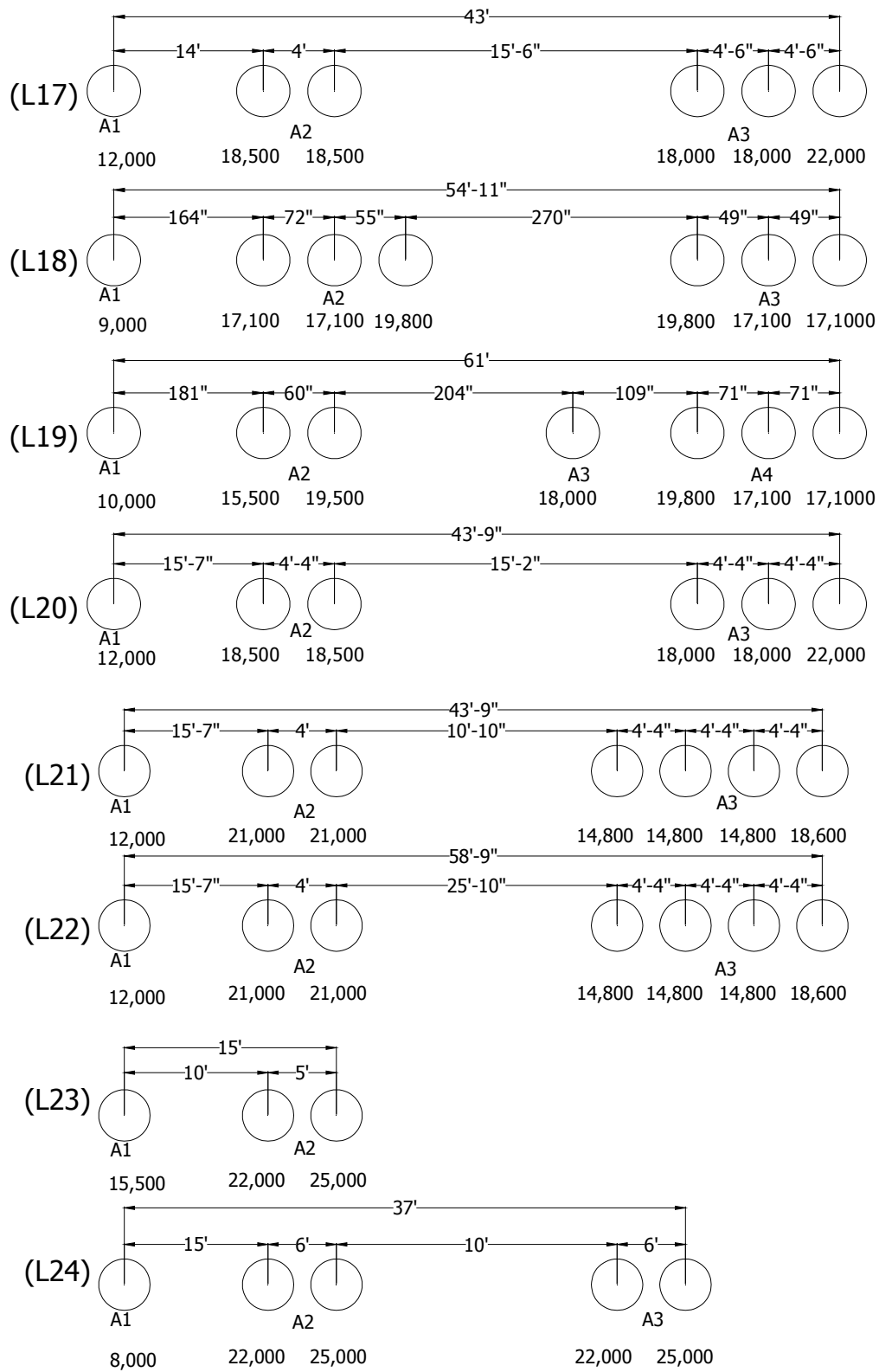
TRUCKS/AXLES CONFIGURATIONS AND LOADING

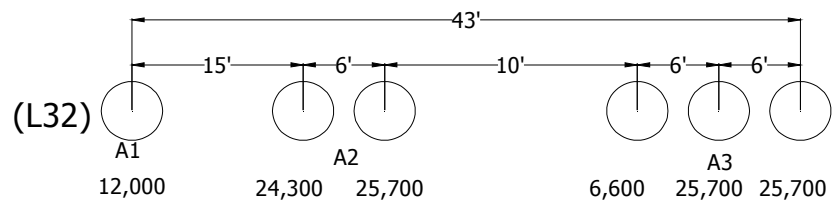
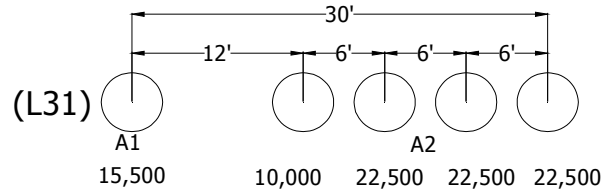
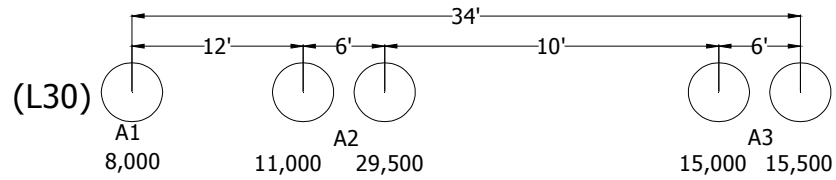
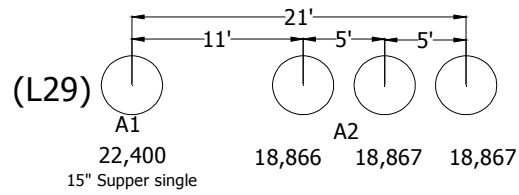
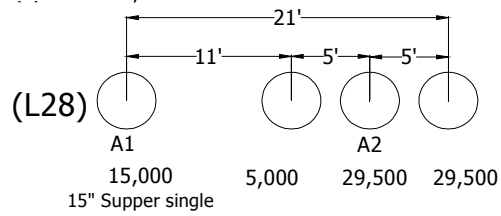
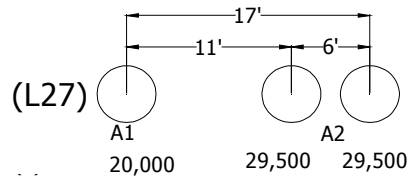
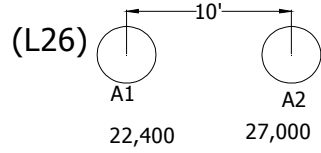
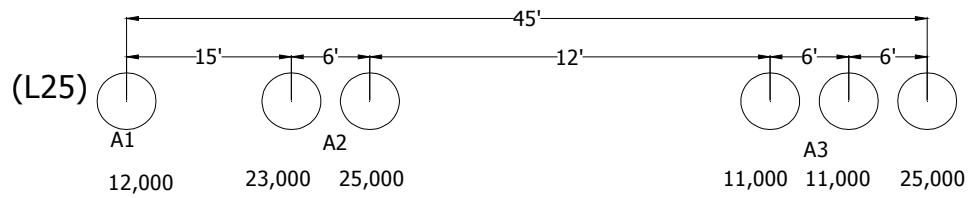
IMPORTANT NOTES

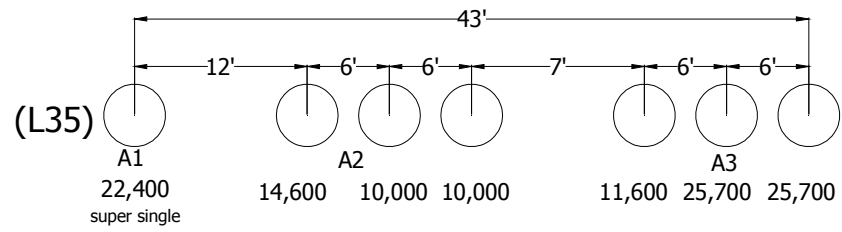
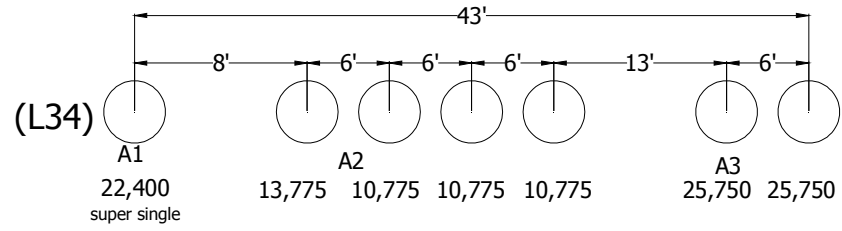
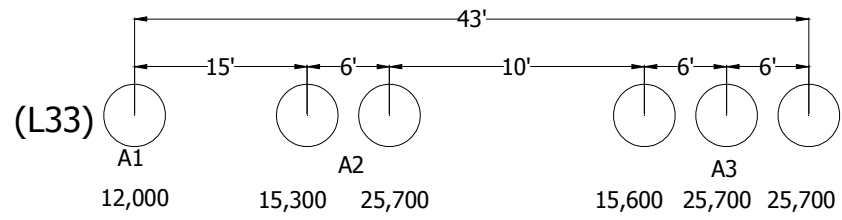
1. TRUCK CASES L1 TO L5 ARE STAND ALONE GROUP OF AXLES (i.e. EACH DRAWING IS ONE AXLE GROUP)
2. TRUCK CASES L6 THROUGH L35 WERE CONSIDERED AS FULL TRUCKS WITH MORE THAN ONE AXLE.
3. ALL THE DRAWINGS ARE NOT TO SCALE.
4. ALL DIMENSIONS ARE AS SHOWN ON THE DRAWINGS











APPENDIX B

MEPDG – PERFORMANCE OUTPUT FOR JOINTED PLAIN CONCRETE PAVEMENT

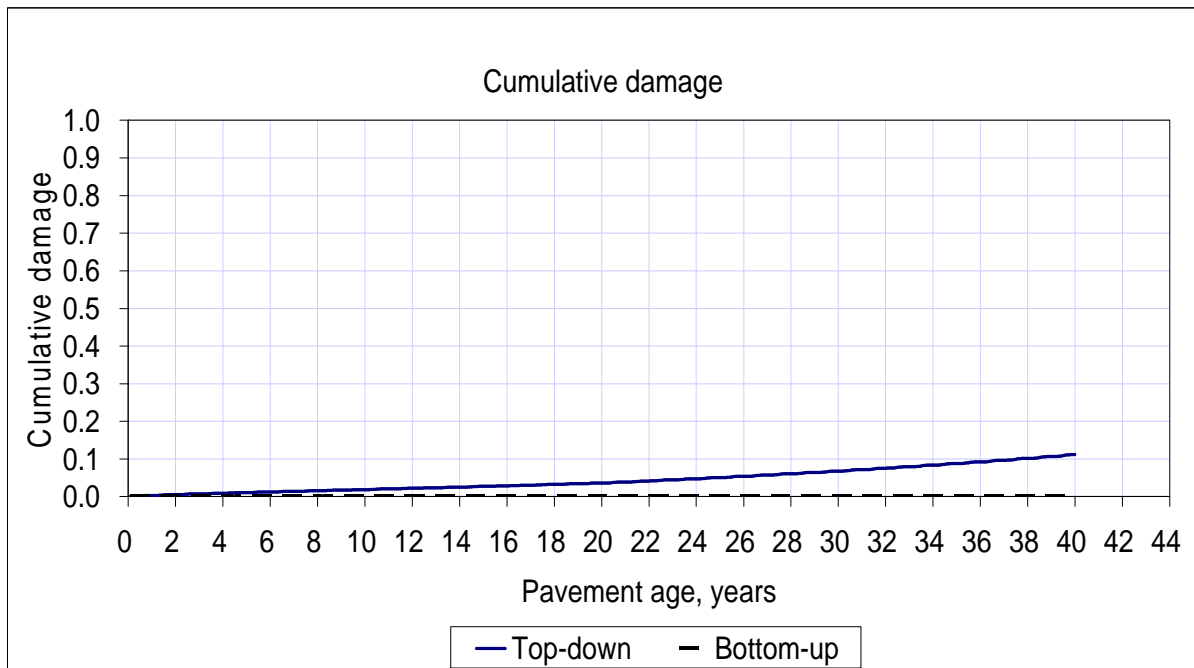


Figure B-1: Top down and bottom-up cracking for truck case L6a

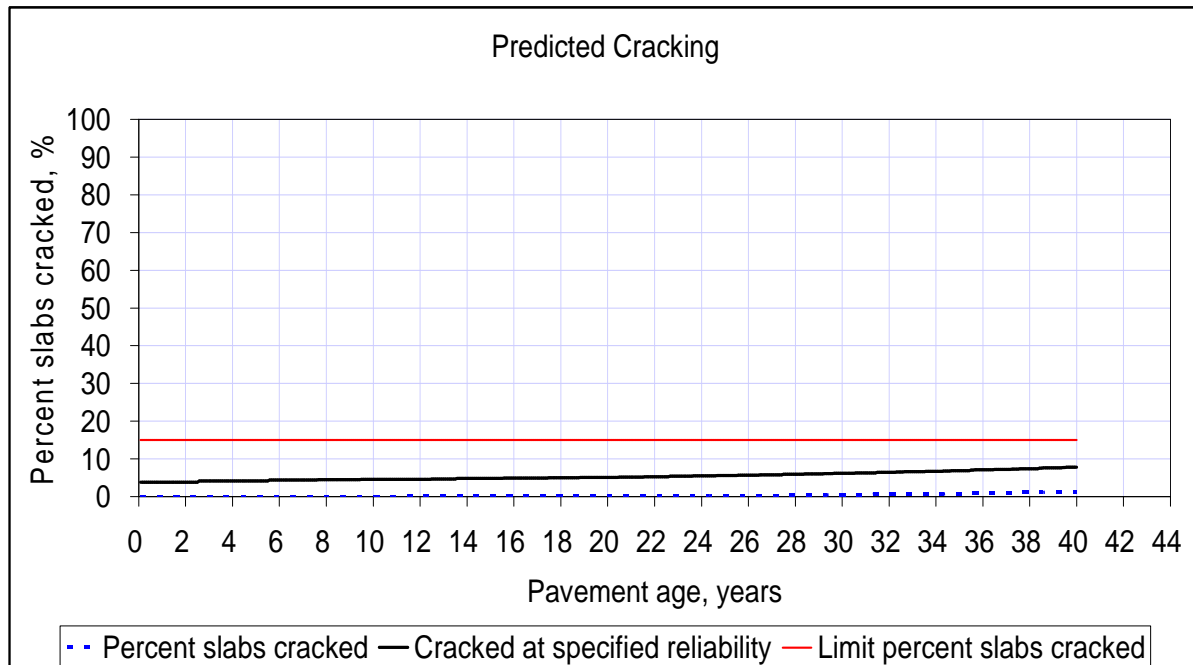


Figure B-2: % slab cracked for truck case L6a

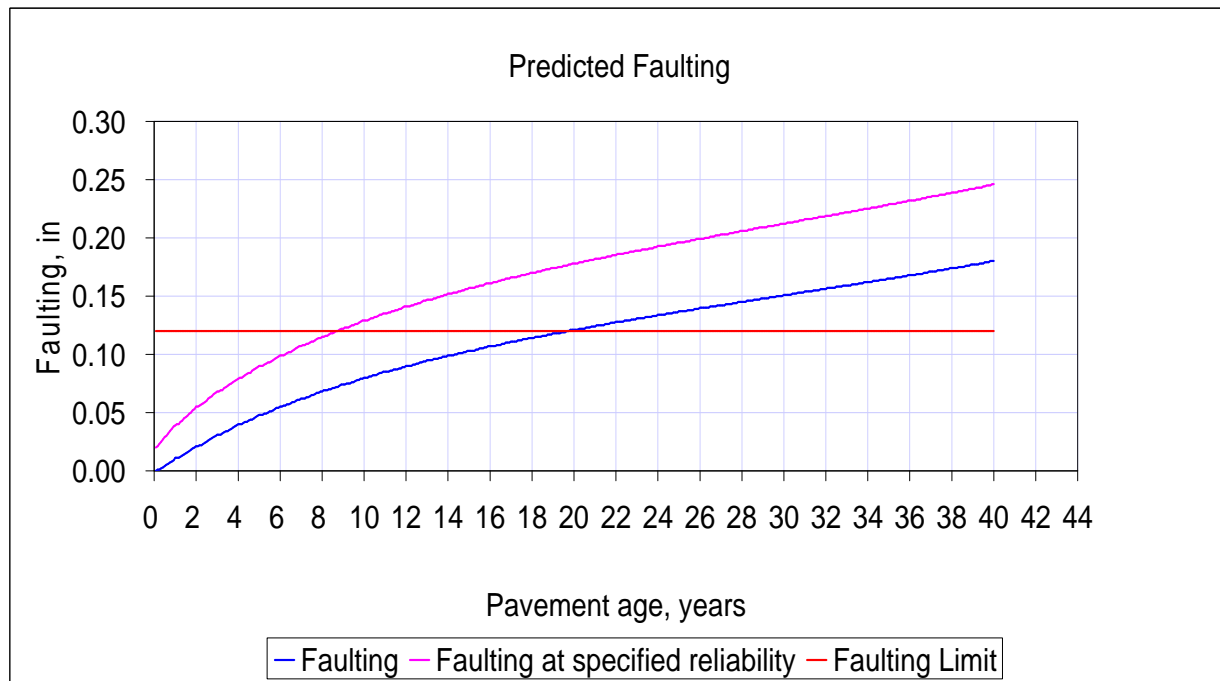


Figure B-3: Faulting for truck case L6a

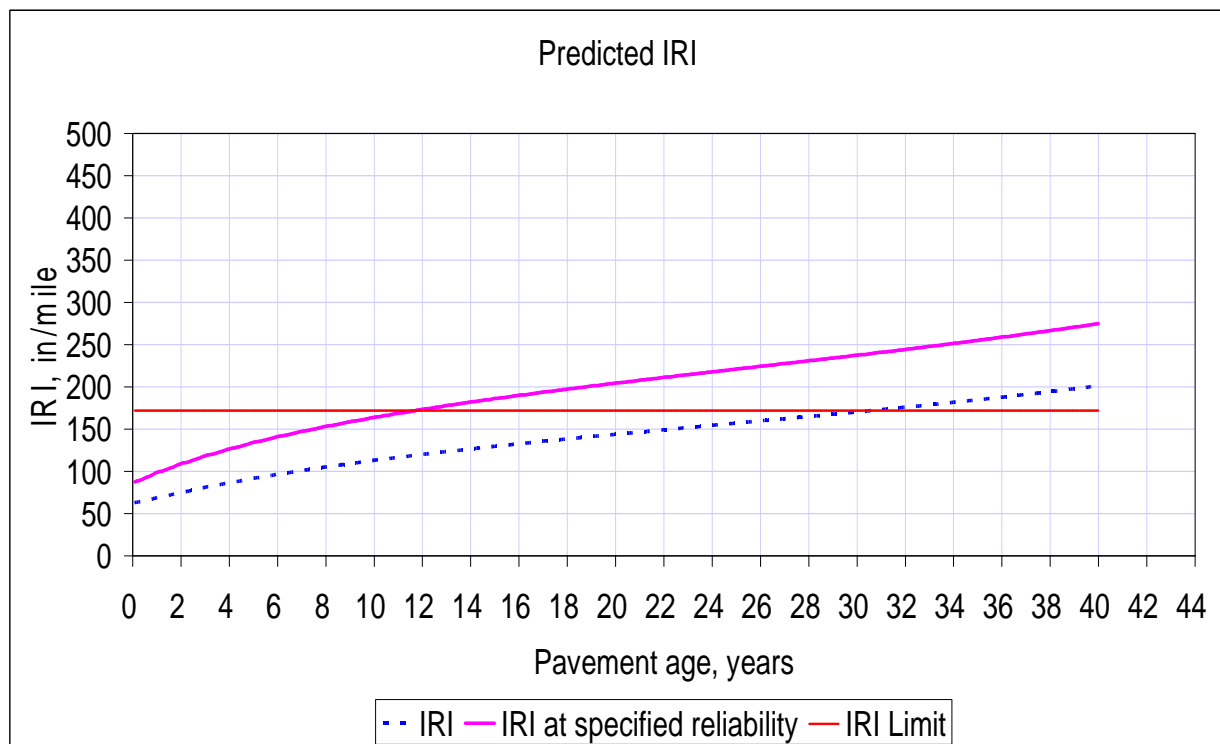


Figure B-4: IRI for truck case L6a

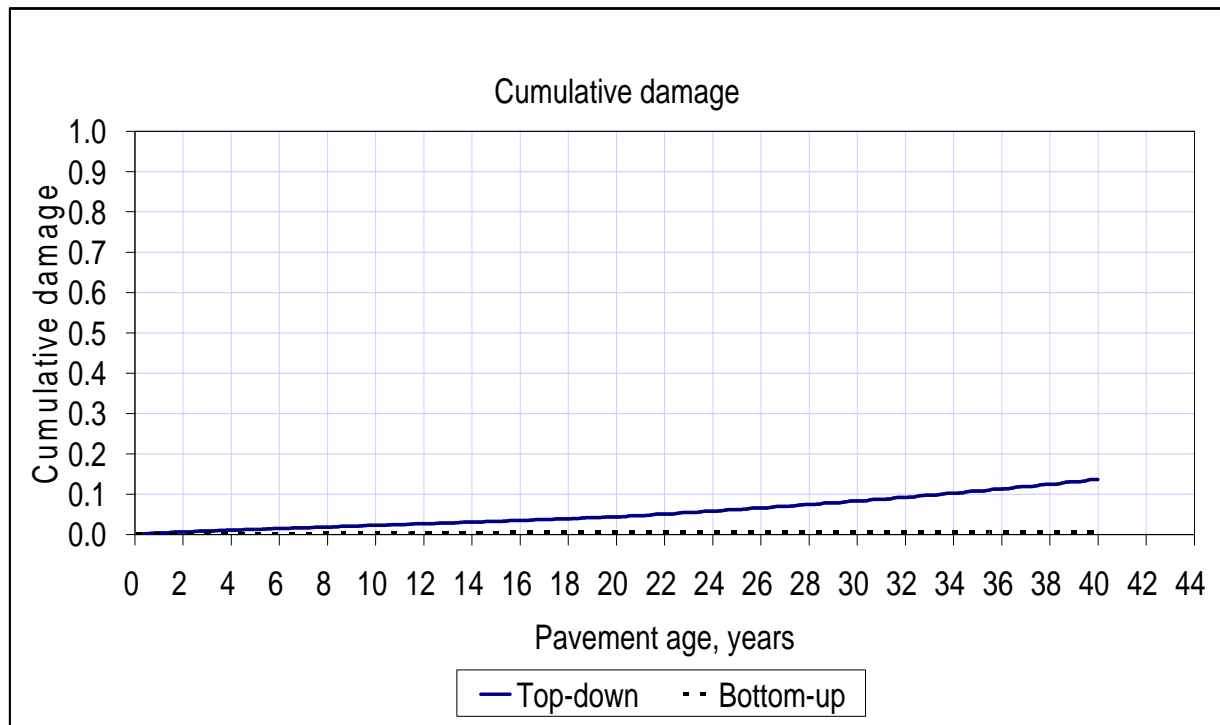


Figure B-5: Top-down and bottom-up cracking for truck case L6b

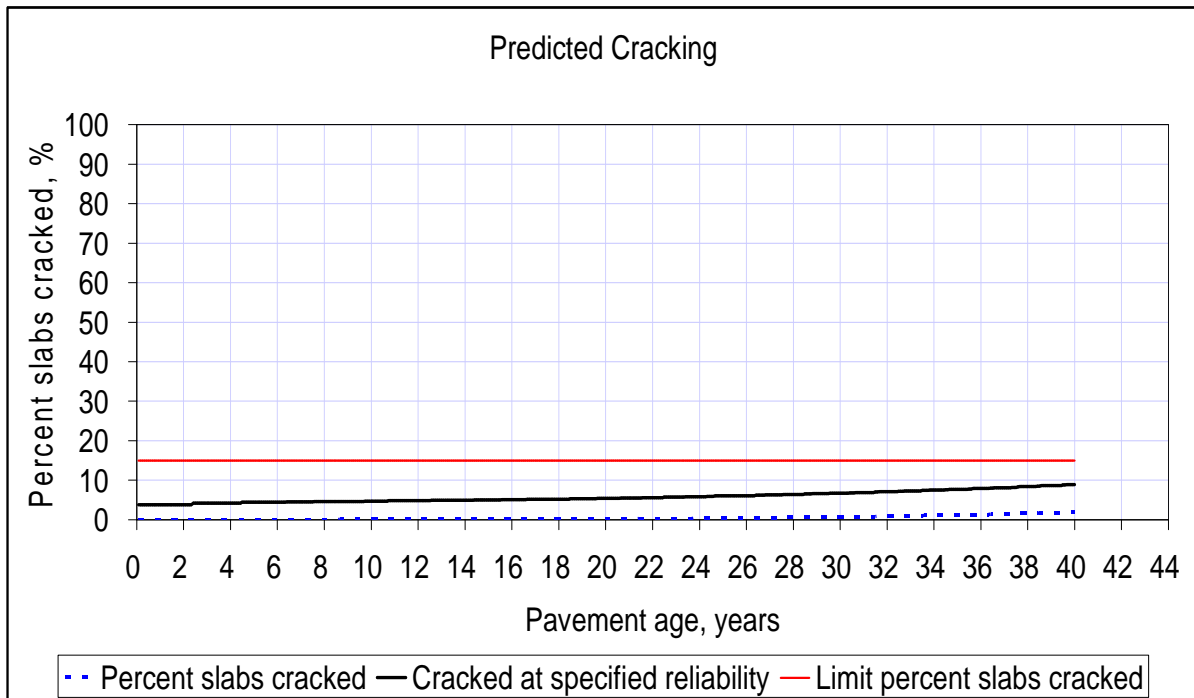


Figure B-6: % slab cracked for truck case L6b

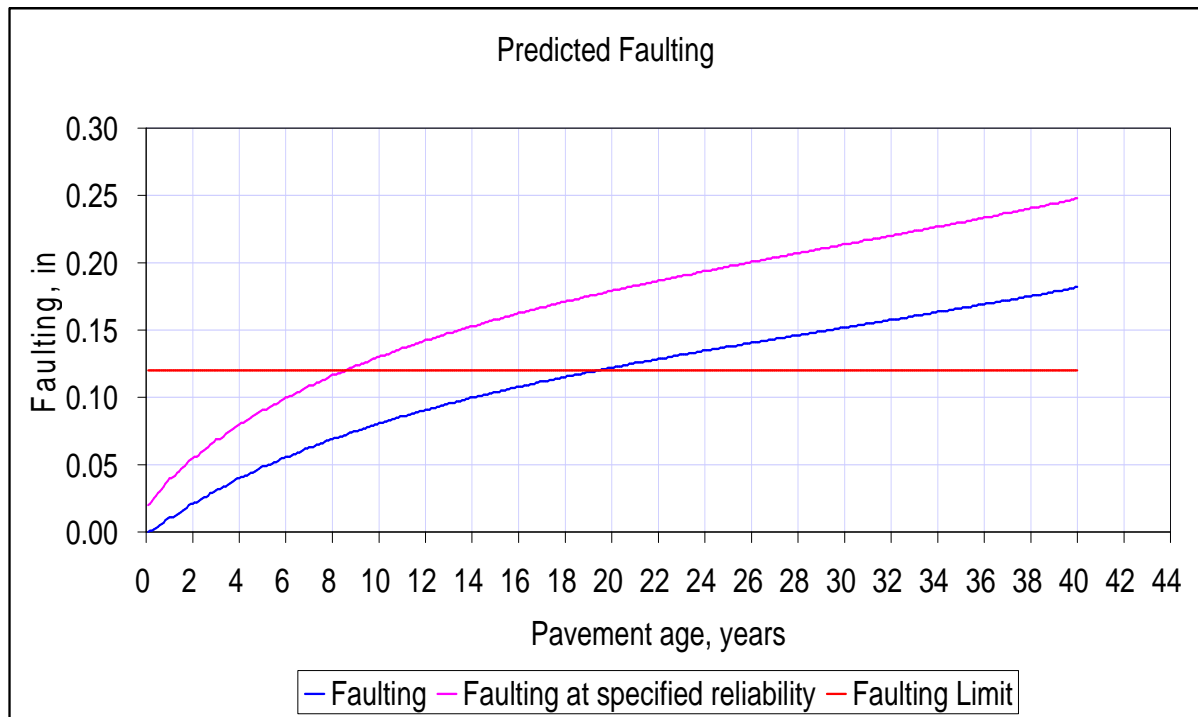


Figure B-7: Faulting for truck case L6b

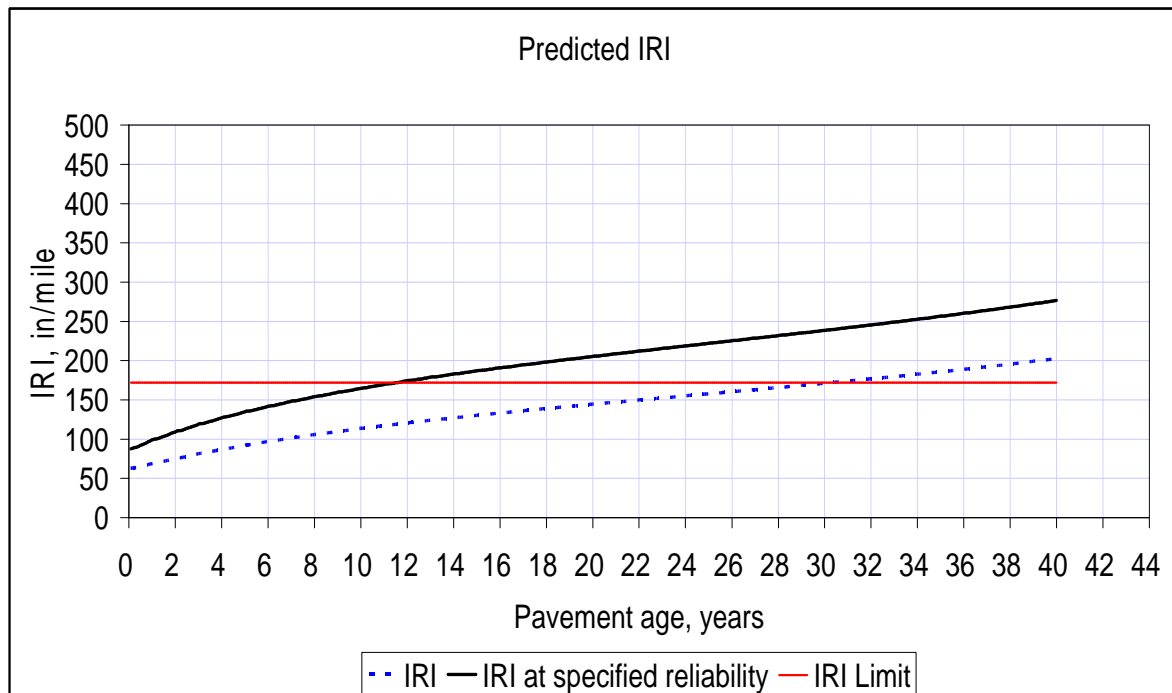


Figure B-8: IRI for truck case L6b

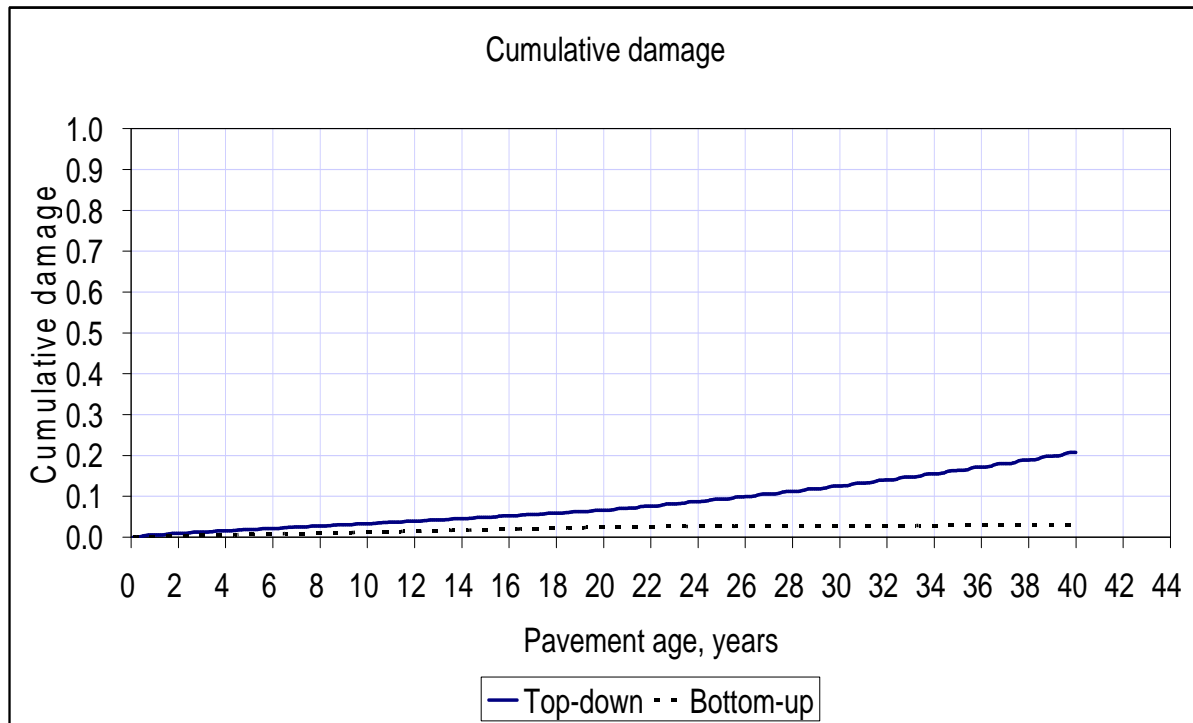


Figure B-9: Top down and bottom-up cracking for truck case L6c

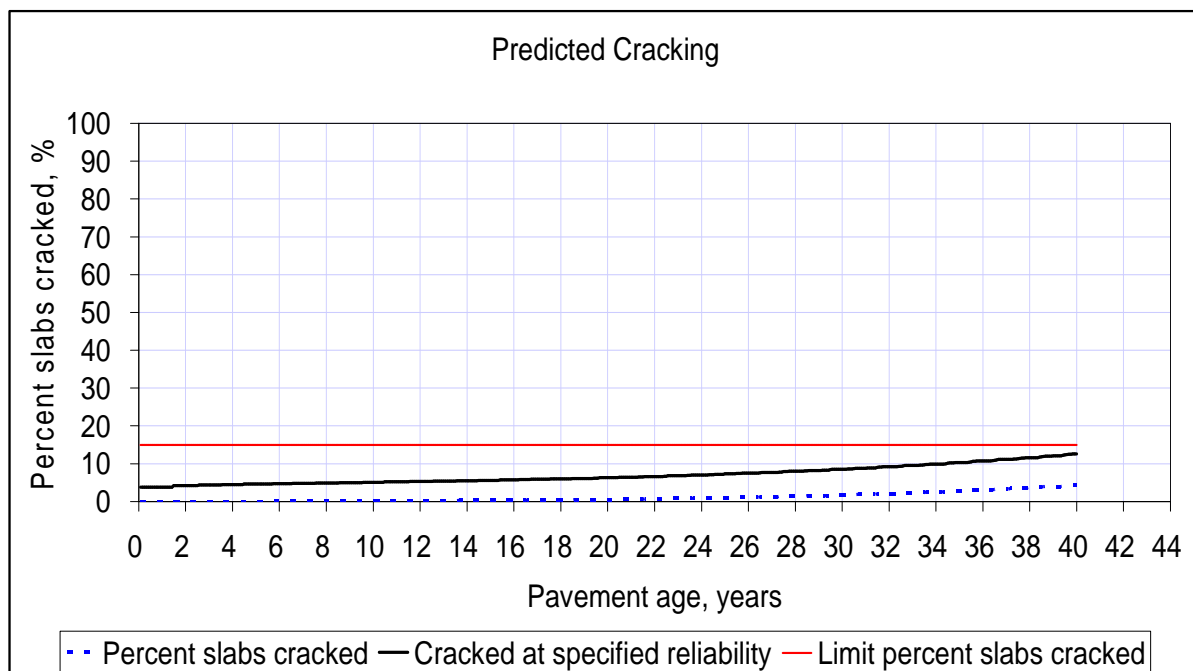


Figure B-10: % slab cracked for truck case L6c

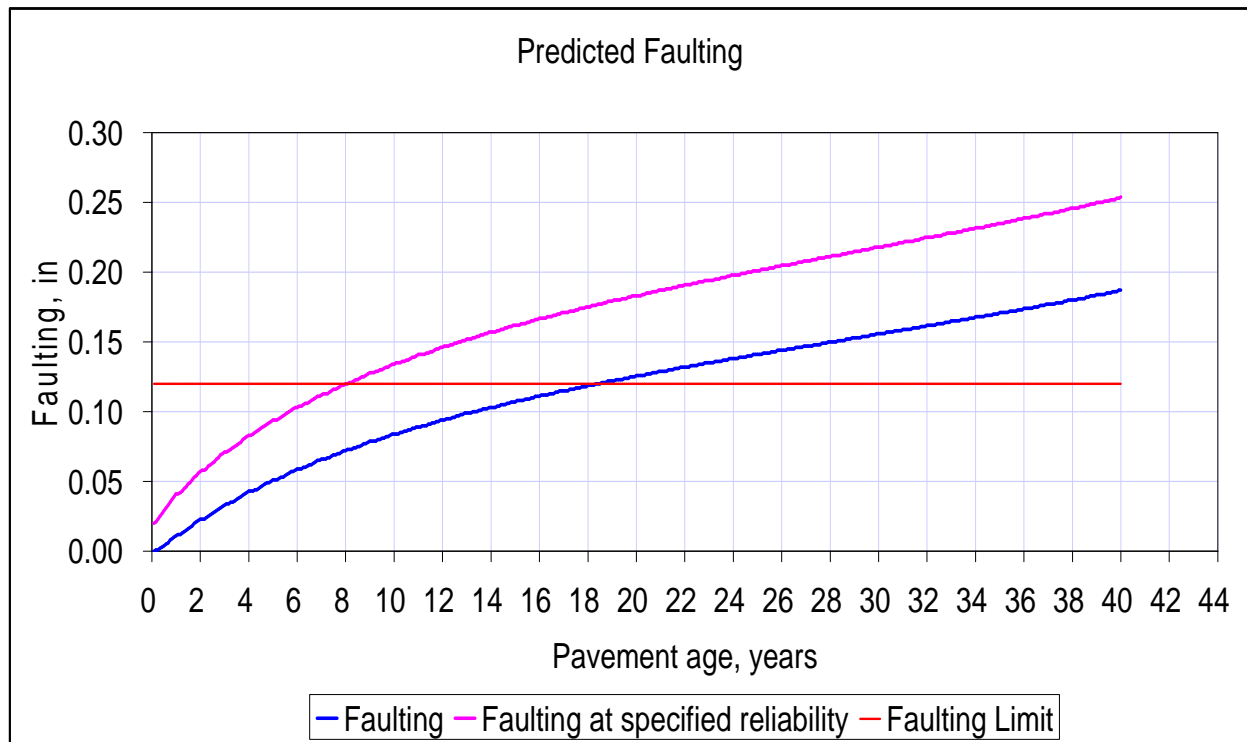


Figure B-11: Faulting for truck case L6c

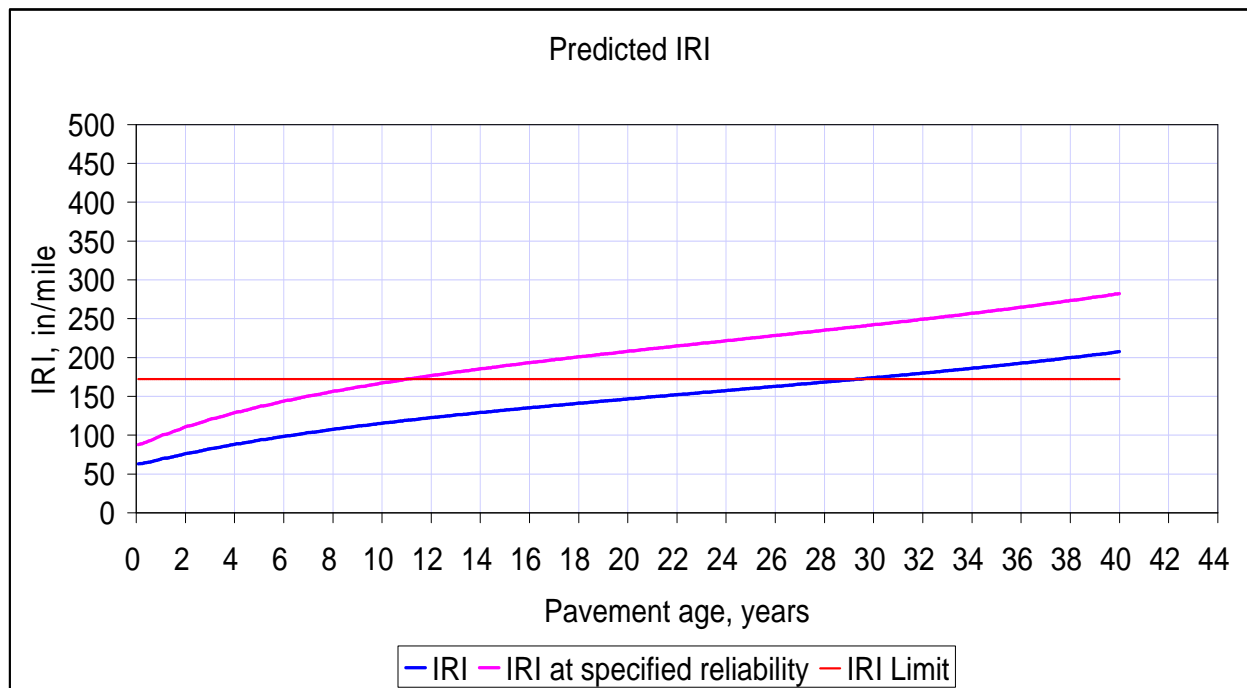


Figure B-12: IRI for truck case L6c

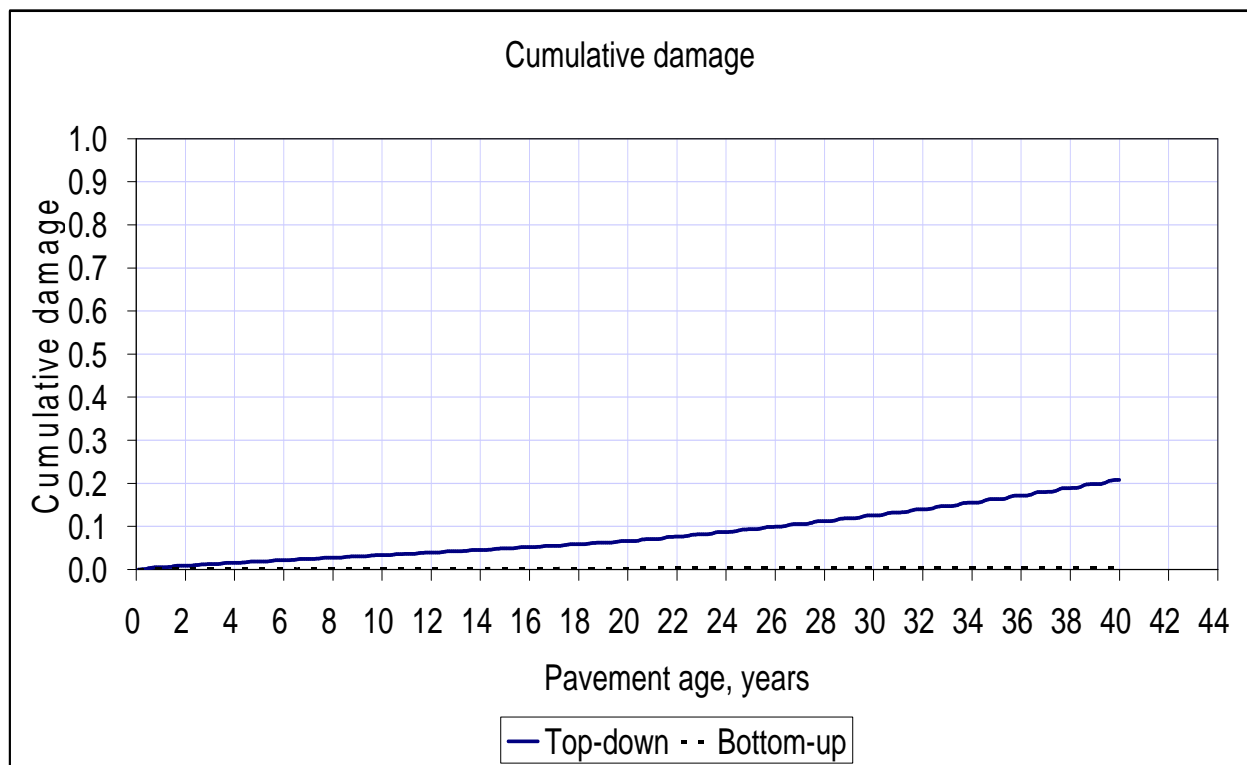


Figure B-13: Top down and bottom-up cracking for truck case L7a

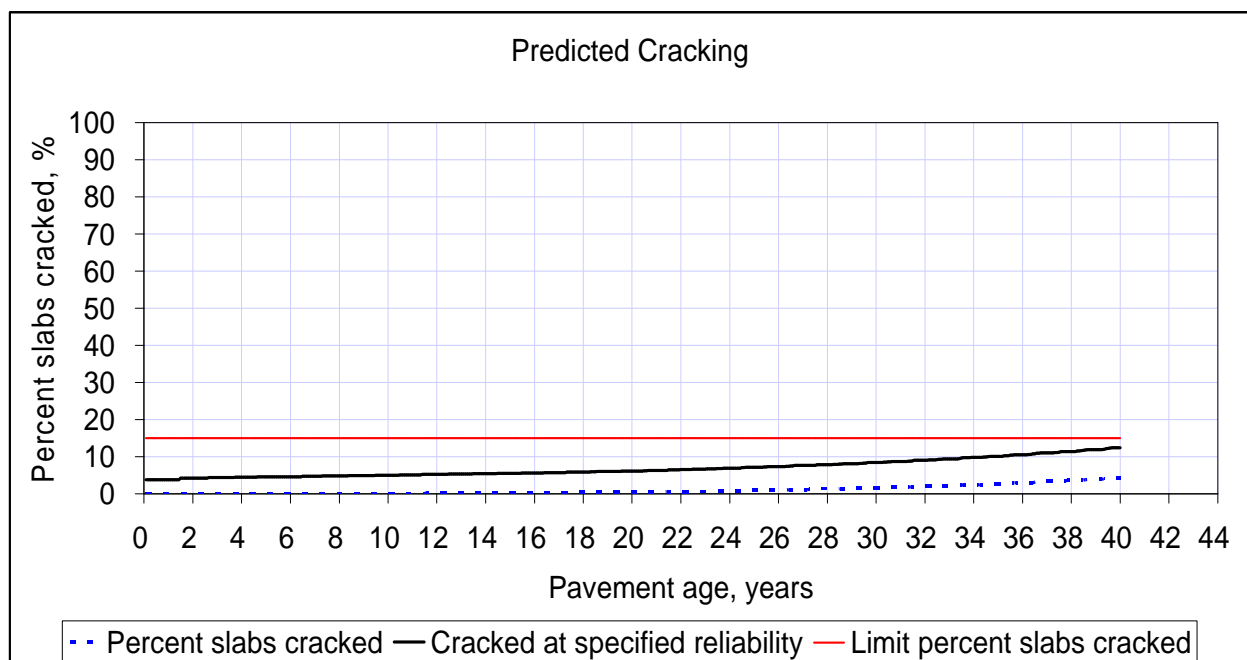


Figure B-14: % slab cracked for truck case L7a

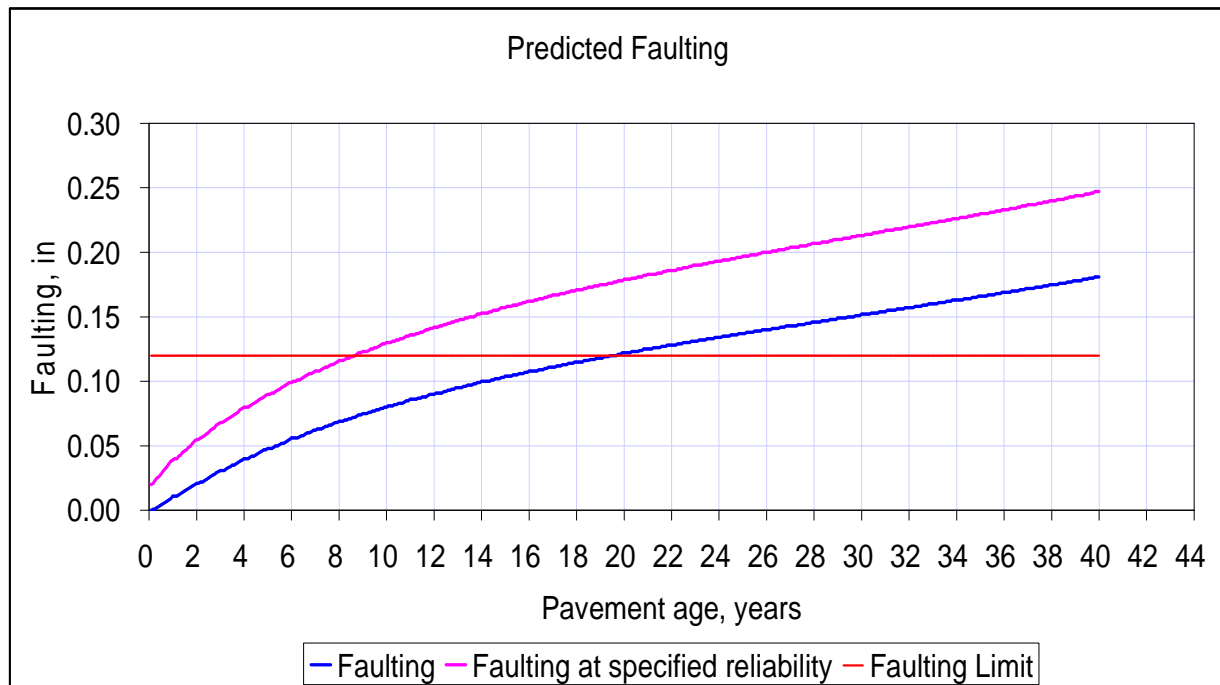


Figure B-15: Faulting for truck case L7a

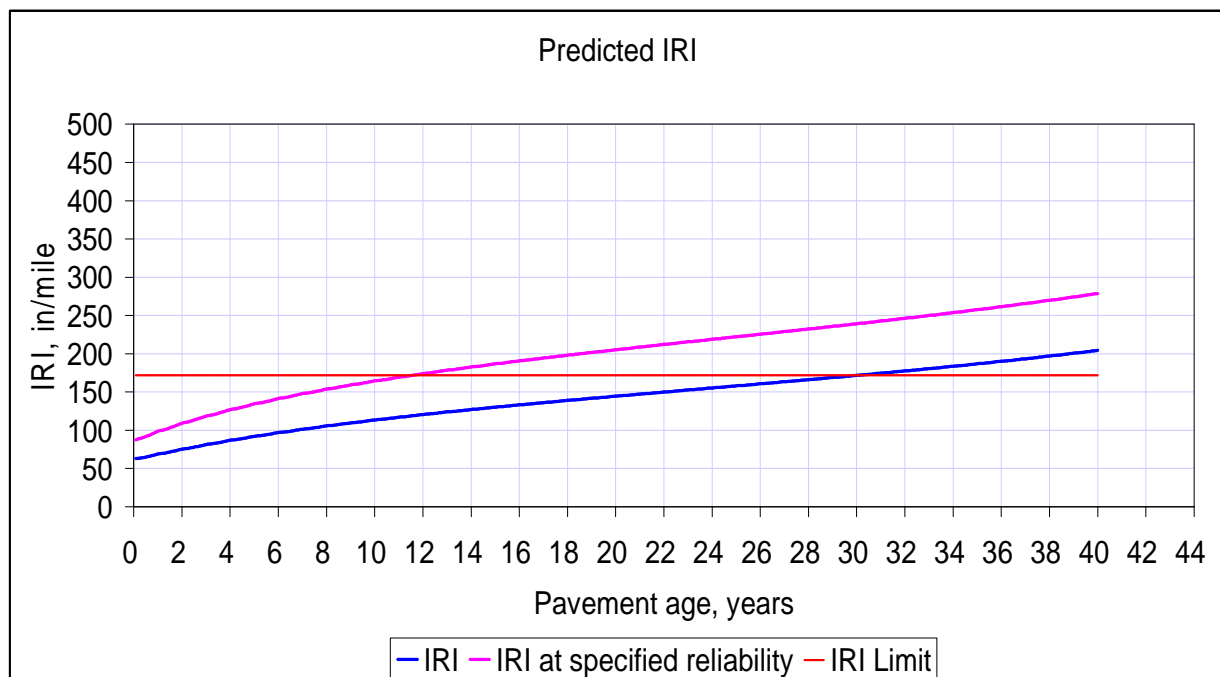


Figure B-16: IRI for truck case L7a

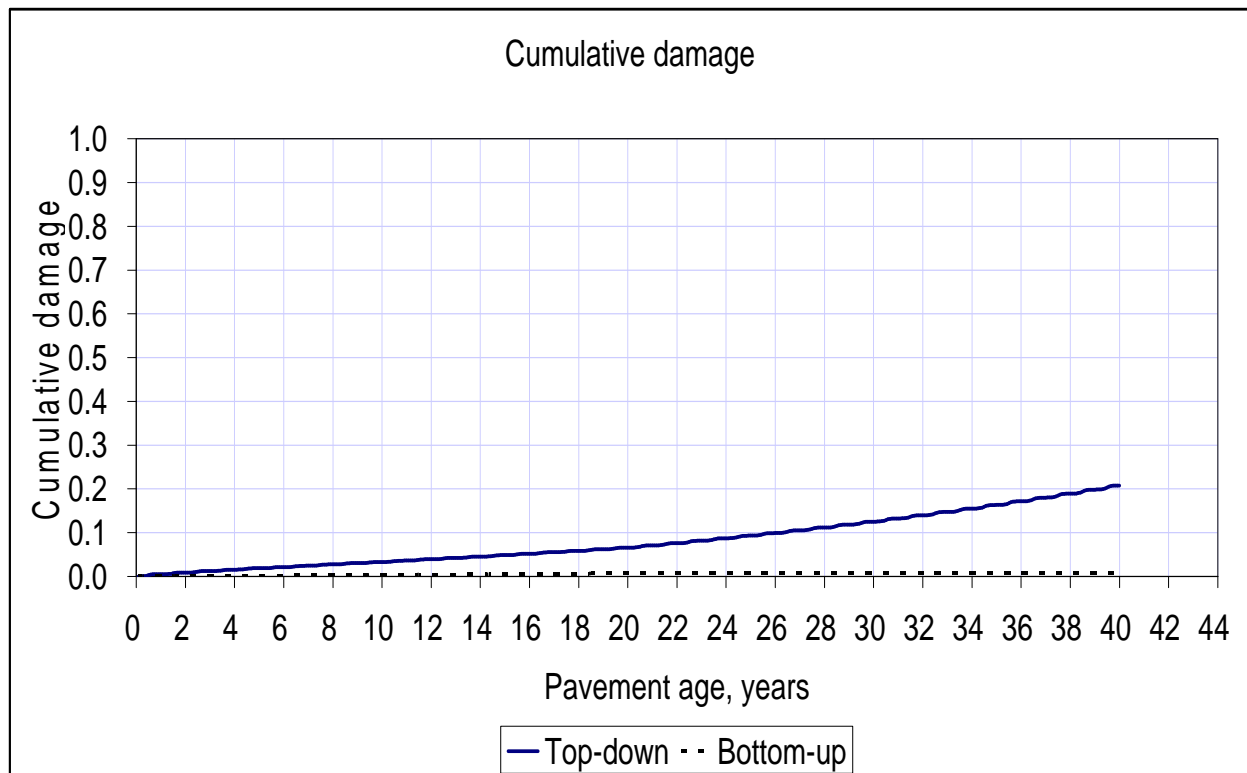


Figure B-17: Top down and bottom-up cracking for truck case L7b

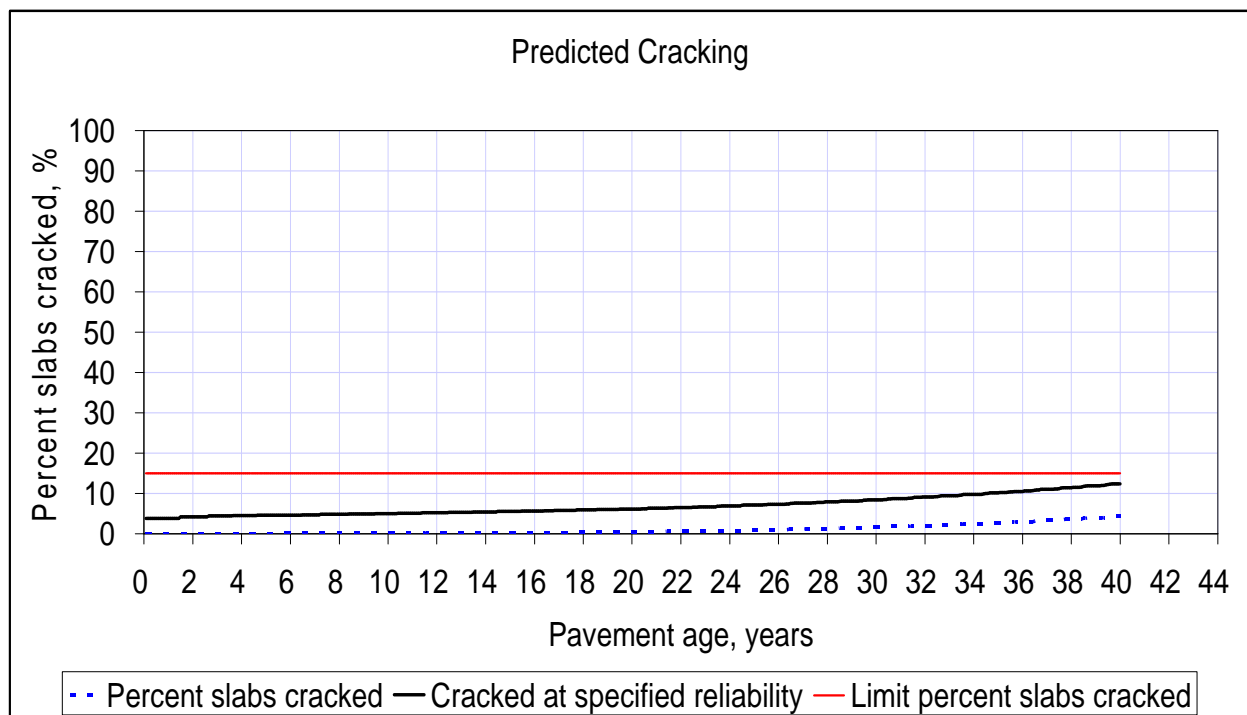


Figure B-18: % slab cracked for truck case L7b

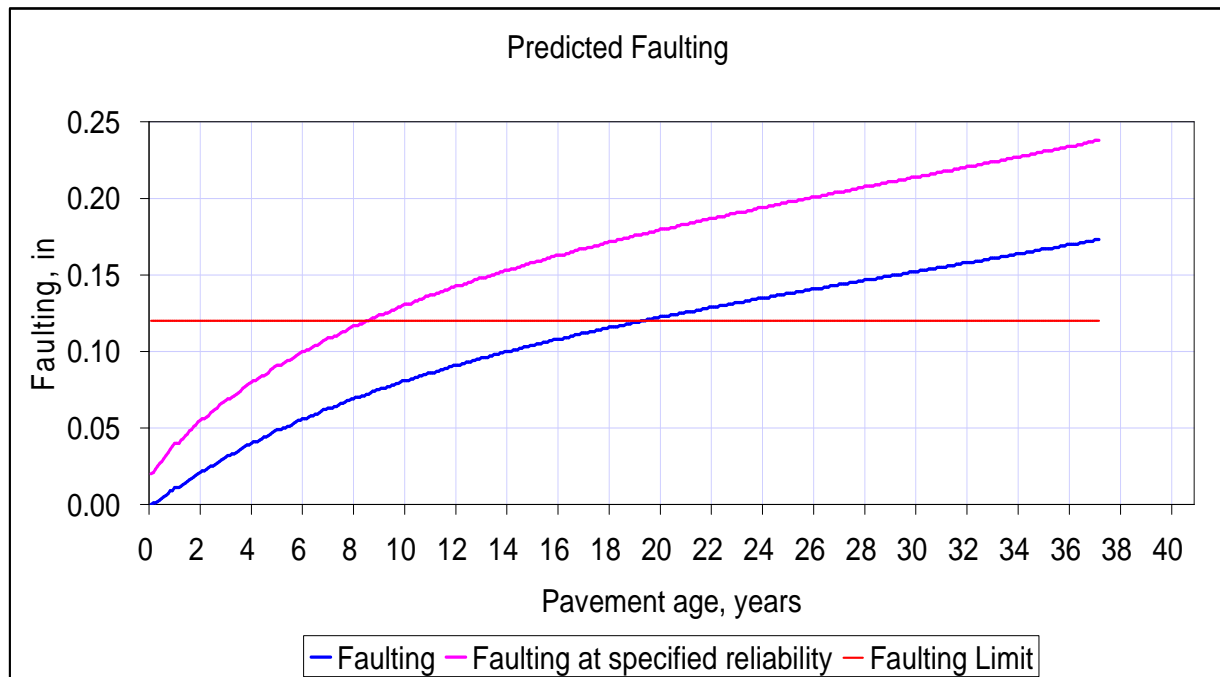


Figure B-19: Faulting for truck case L7b

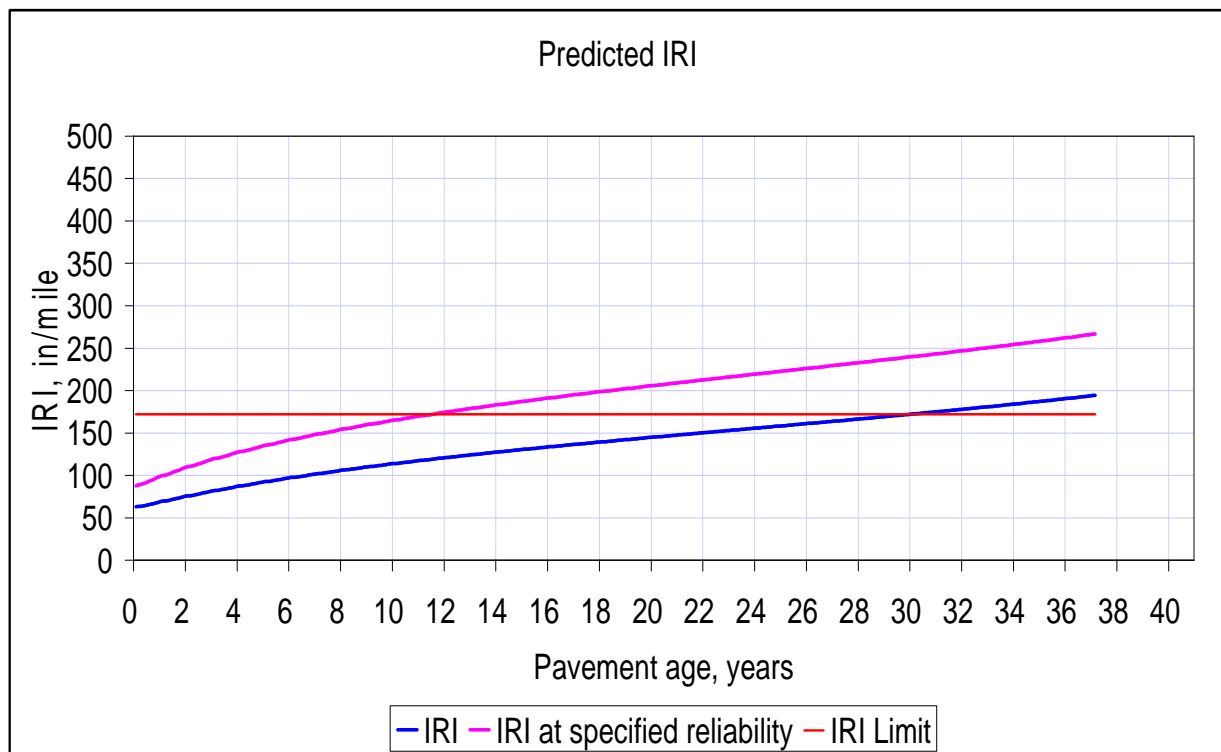


Figure B-20: IRI for truck case L7b

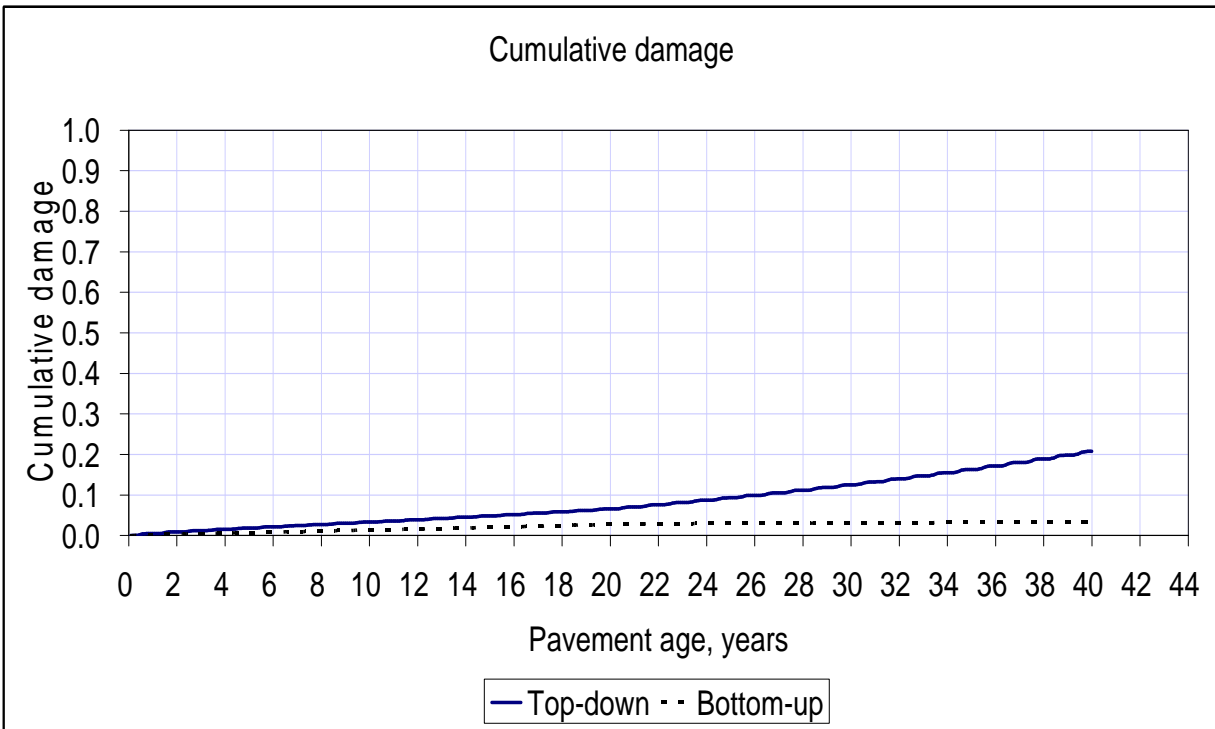


Figure B-21: Top down and bottom-up cracking for truck case L7c

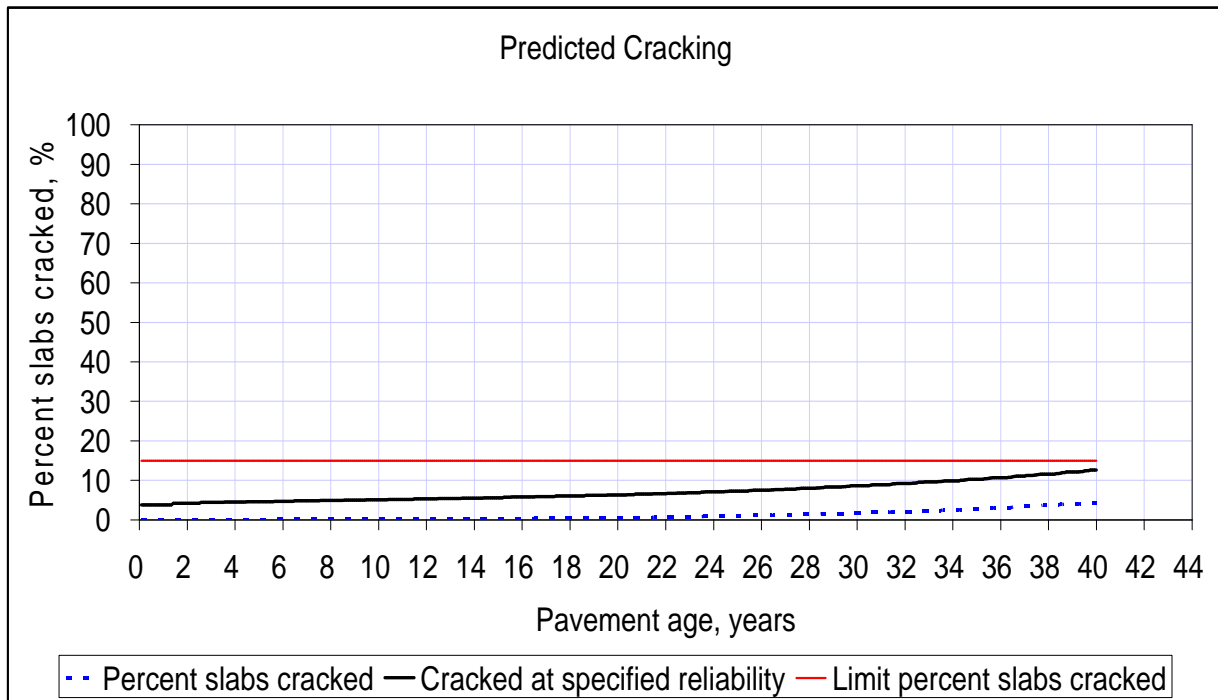


Figure B-22: % slab cracked for truck case L7c

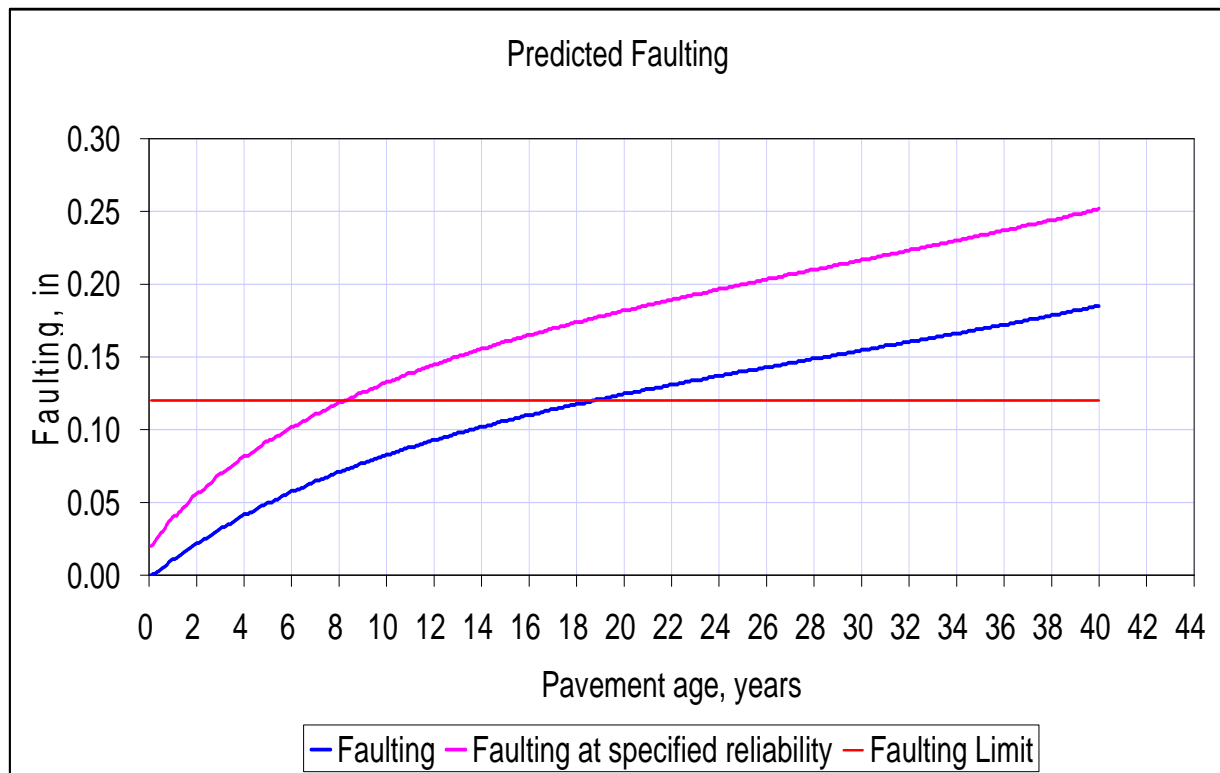


Figure B-23: Faulting for truck case L7c

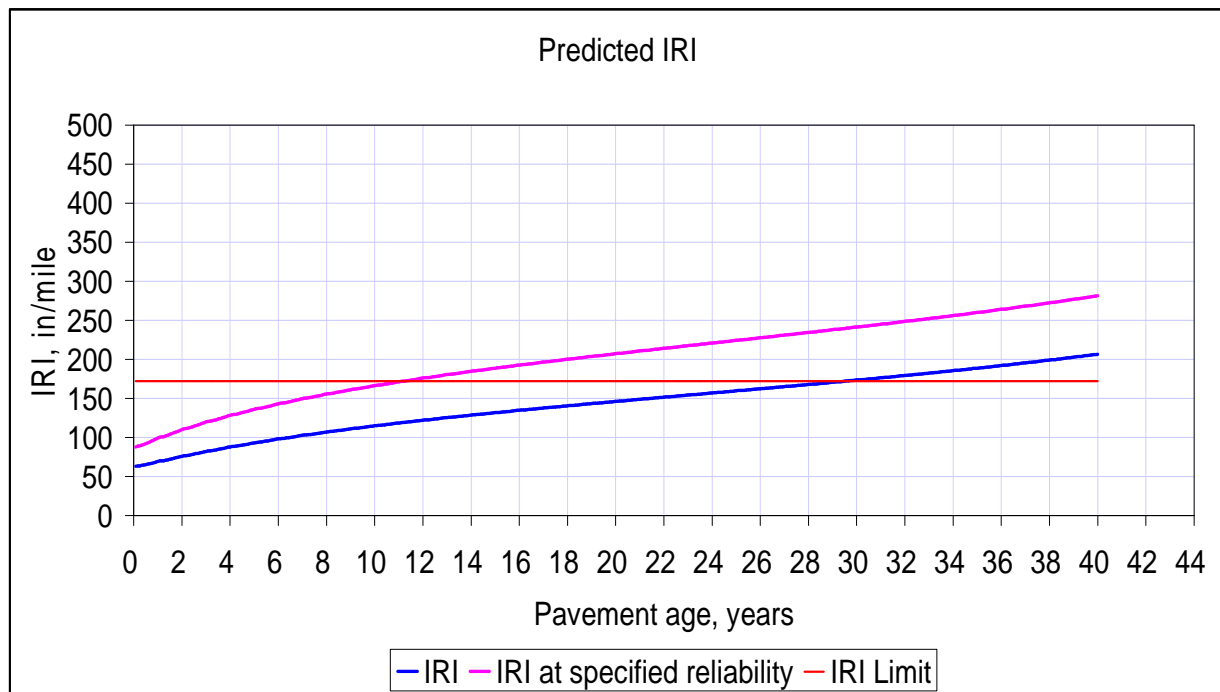


Figure B-24: IRI for truck case L7c

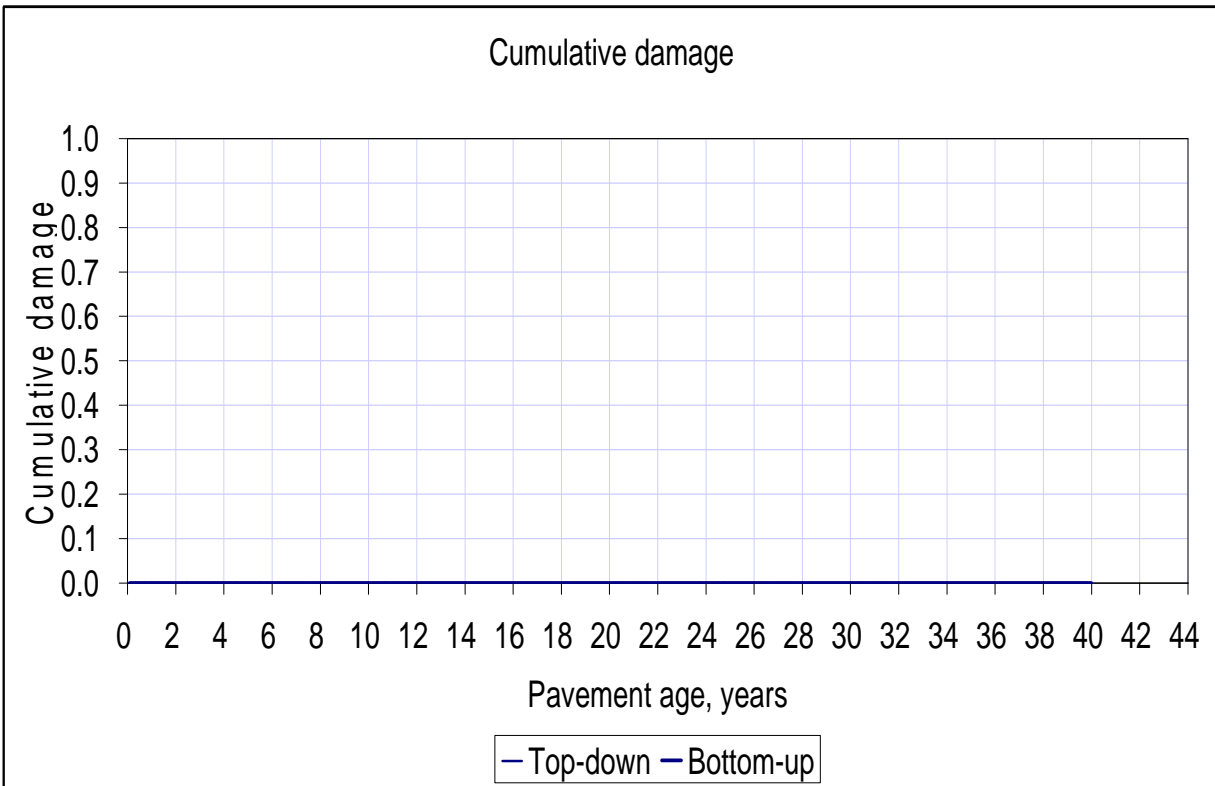


Figure B-25: Top down and bottom-up cracking for truck case L8a

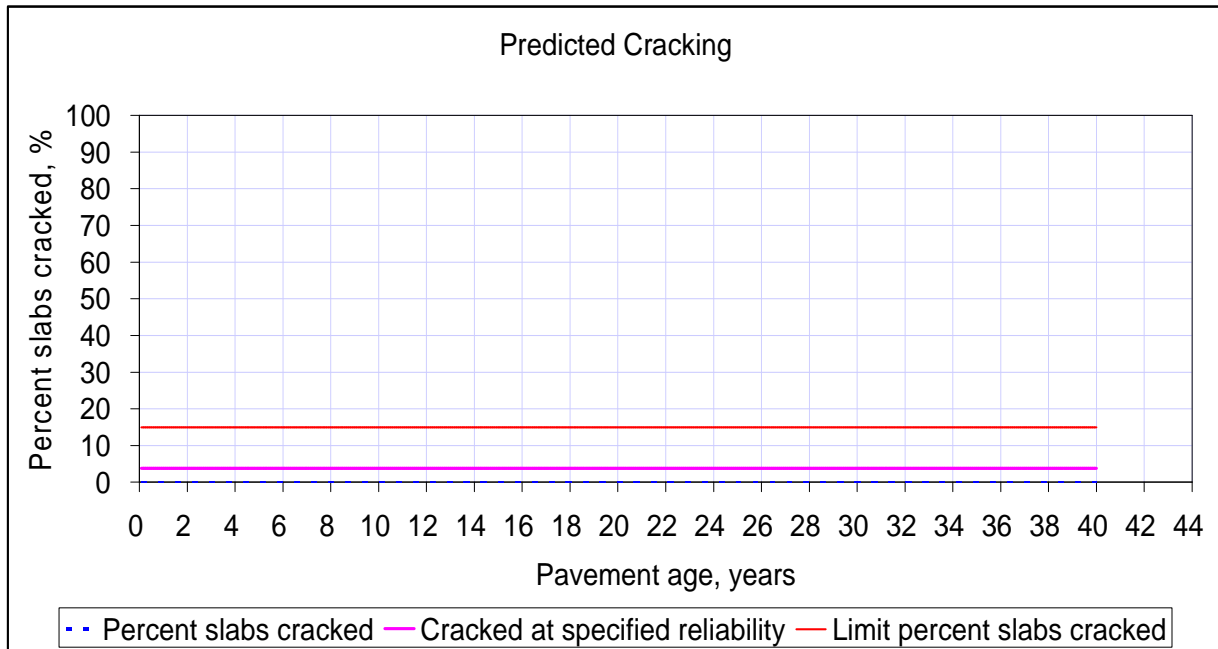


Figure B-26: % slab cracked for truck case L8a

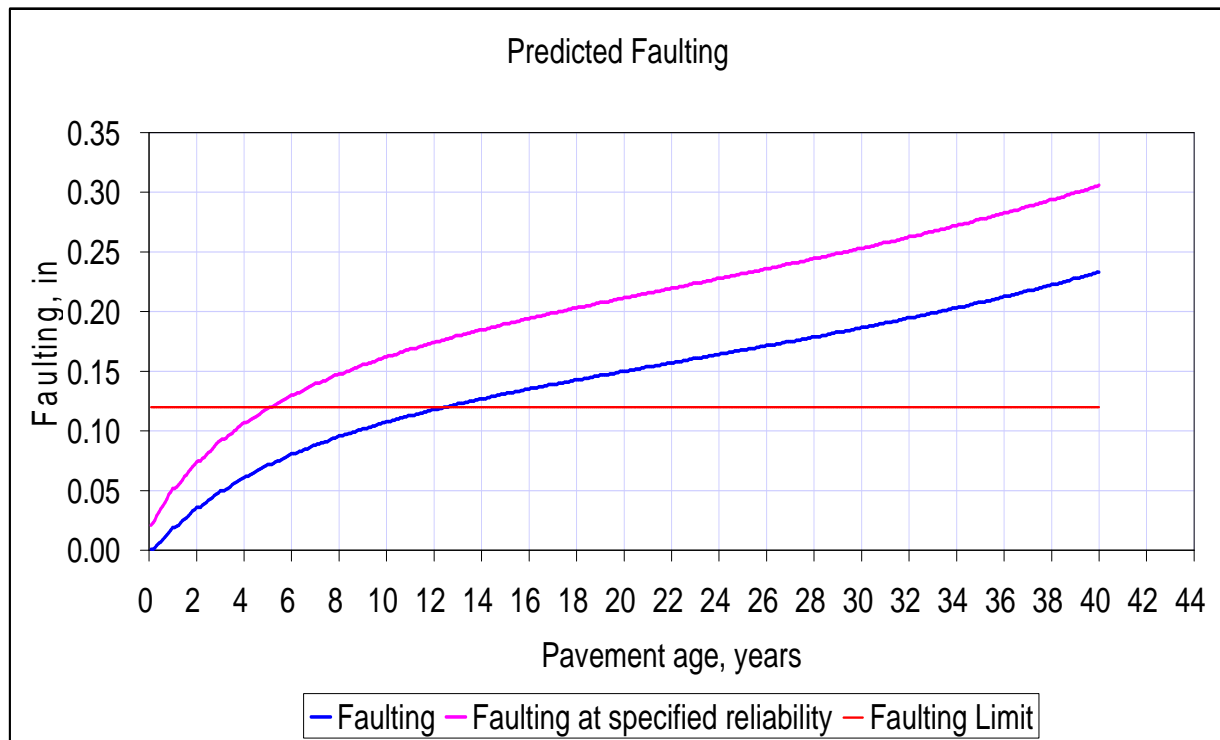


Figure B-27: Faulting for truck case L8a

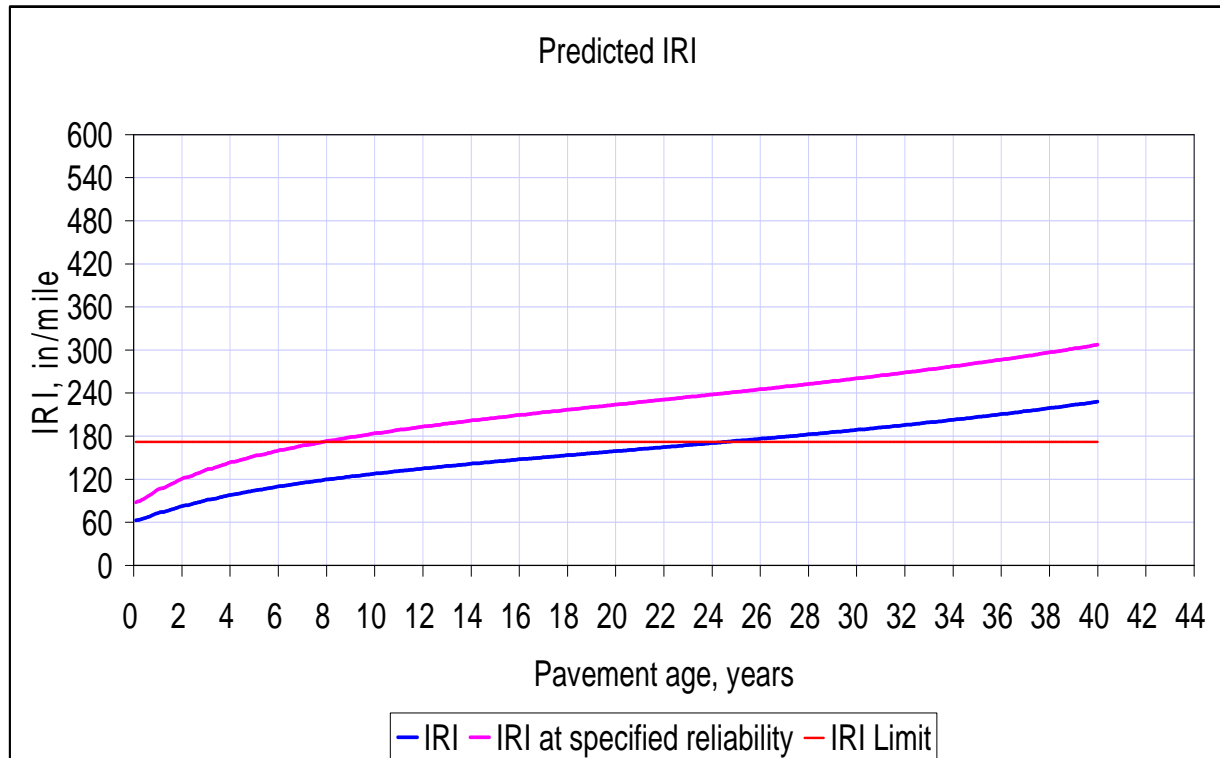


Figure B-28: IRI for truck case L8a

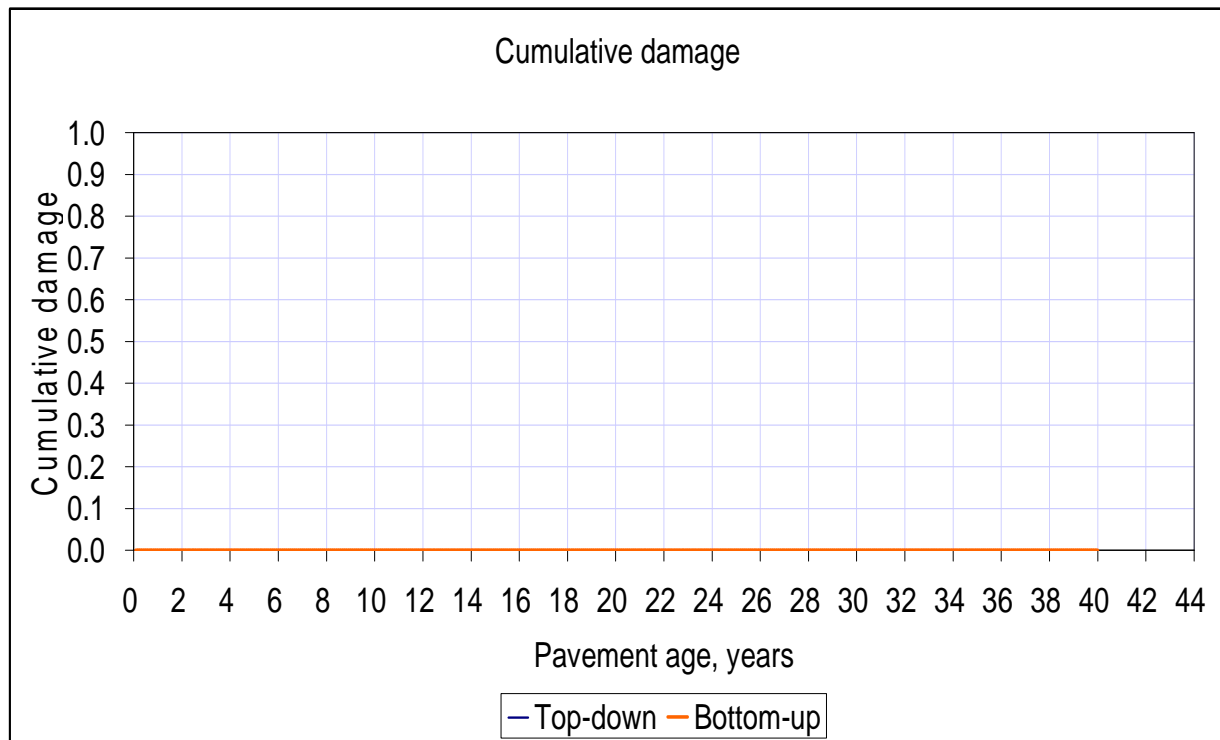


Figure B-29: Top down and bottom-up cracking for truck case L8b

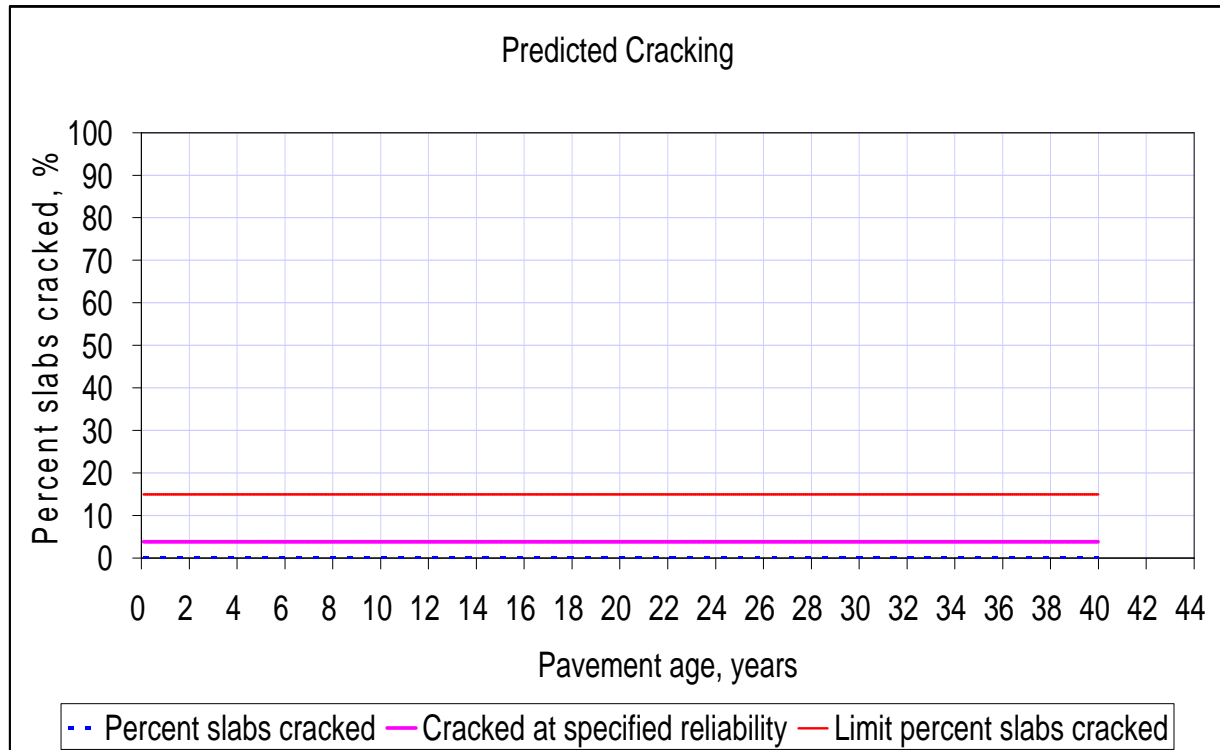


Figure B-30: % slab cracked for truck case L8b

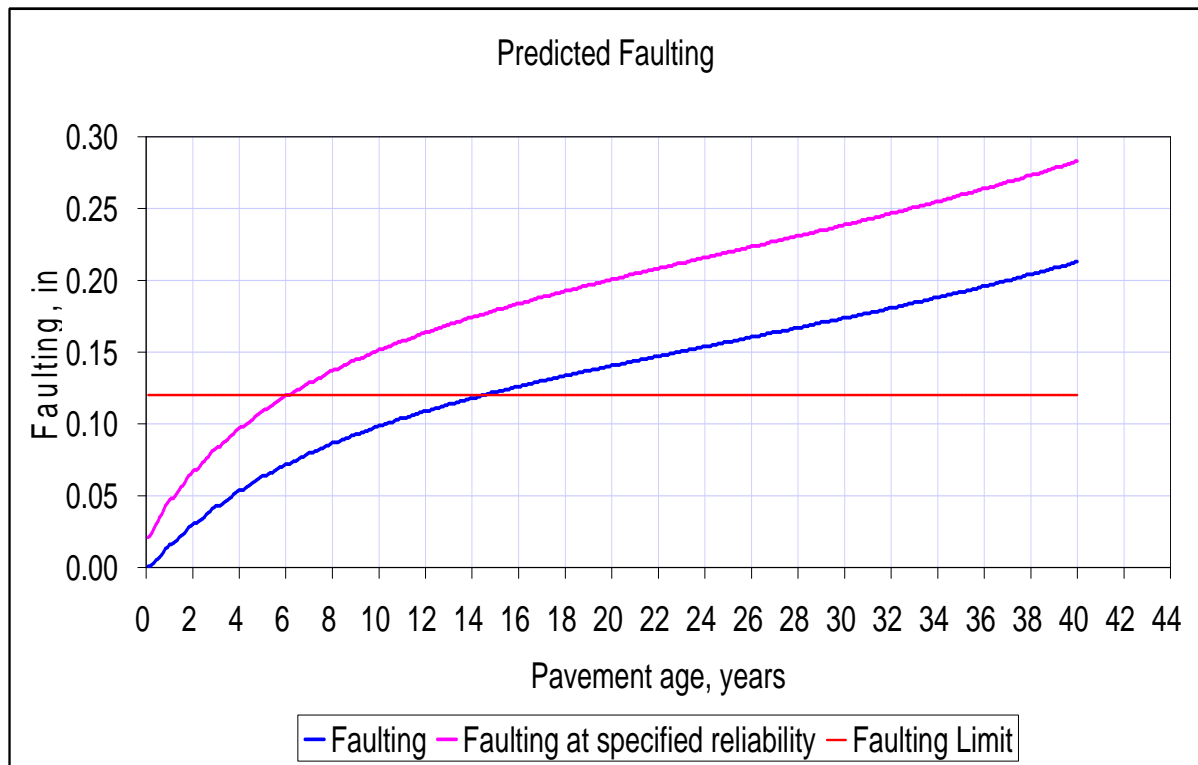


Figure B-31: Faulting for truck case L8b

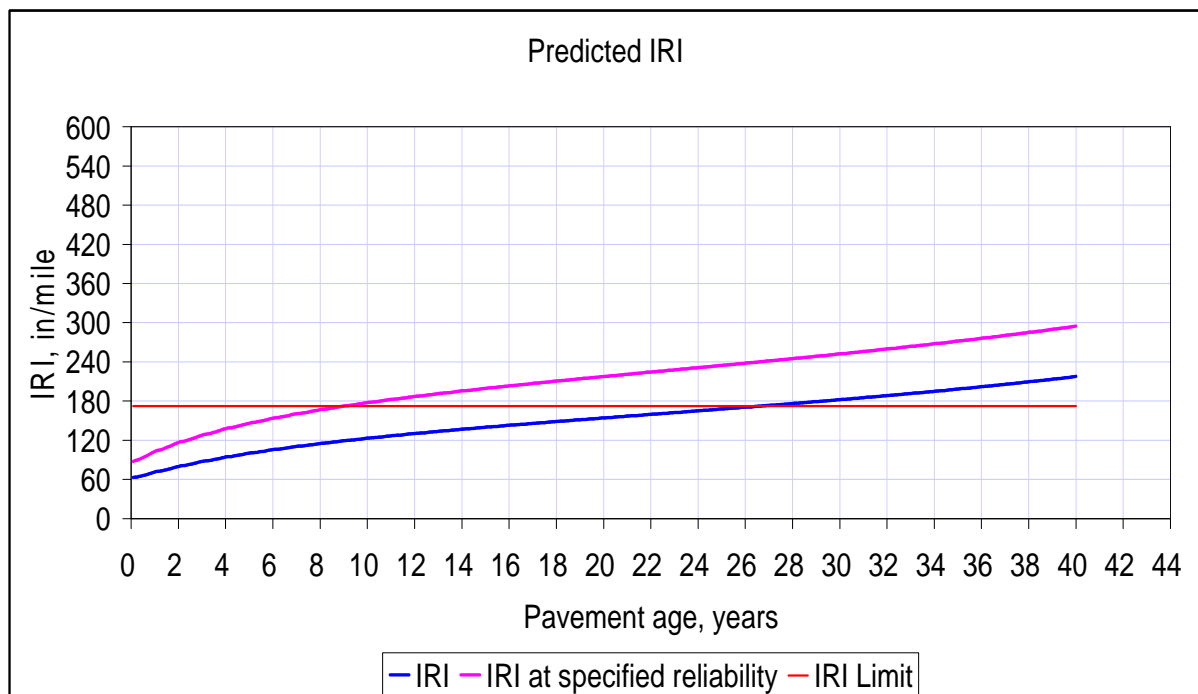


Figure B-32: IRI for truck case L8b

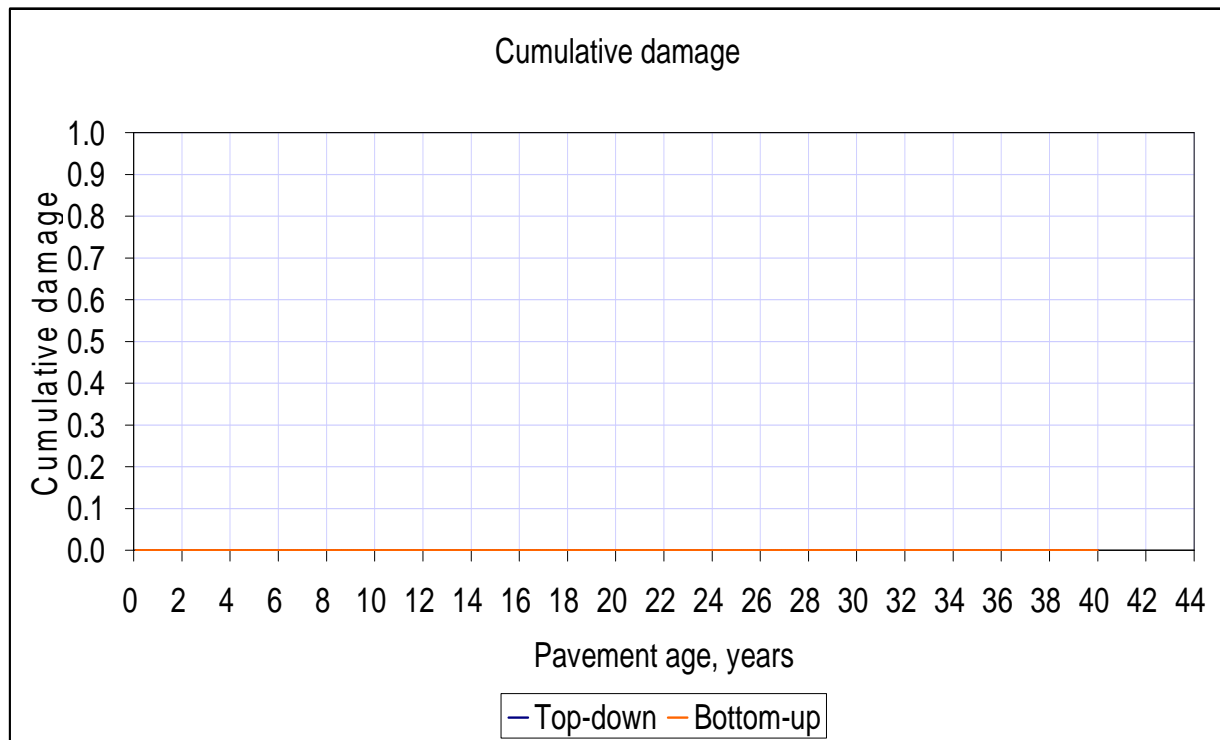


Figure B-33: Top down and bottom-up cracking for truck case L8c

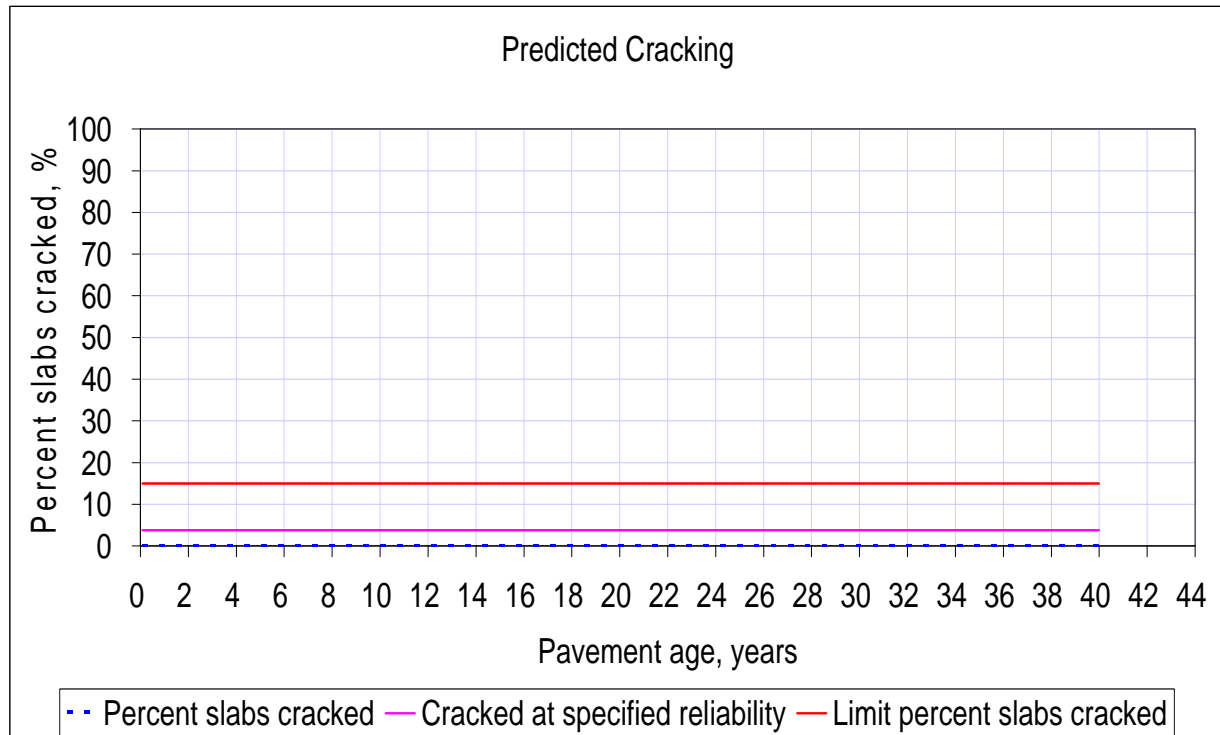


Figure B-34: % slab cracked for truck case L8c

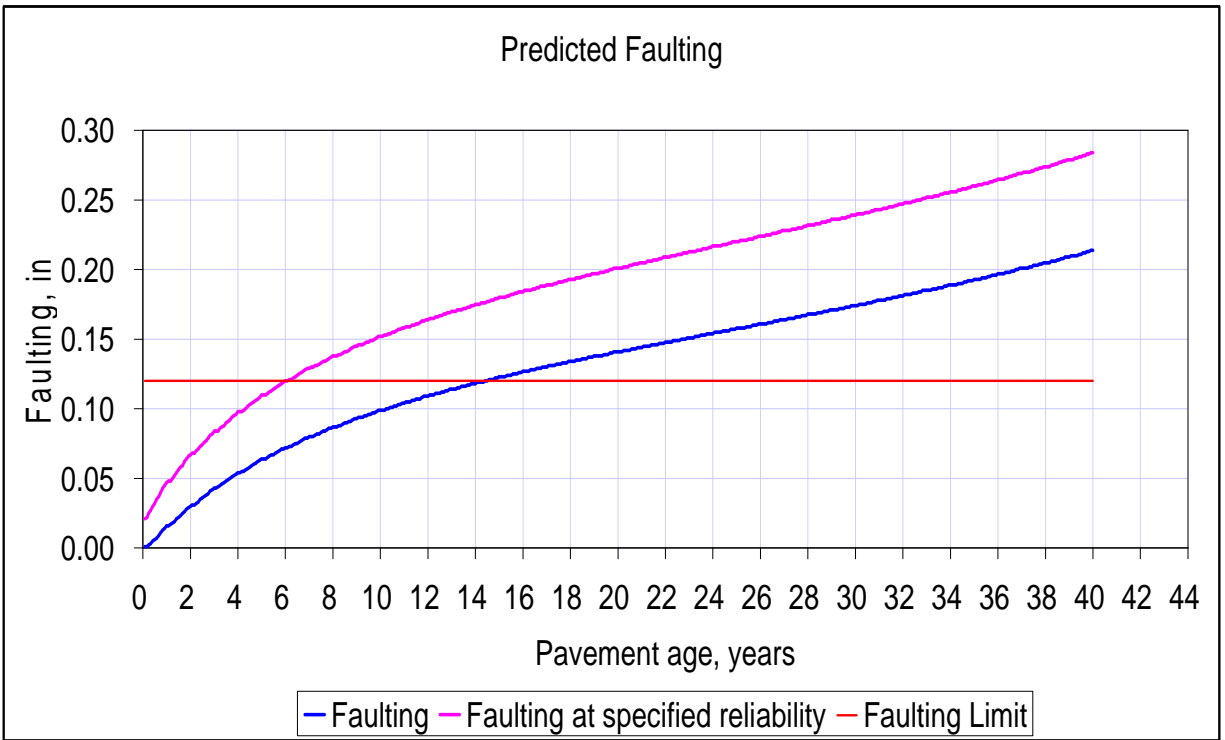


Figure B-35: Faulting for truck case L8c

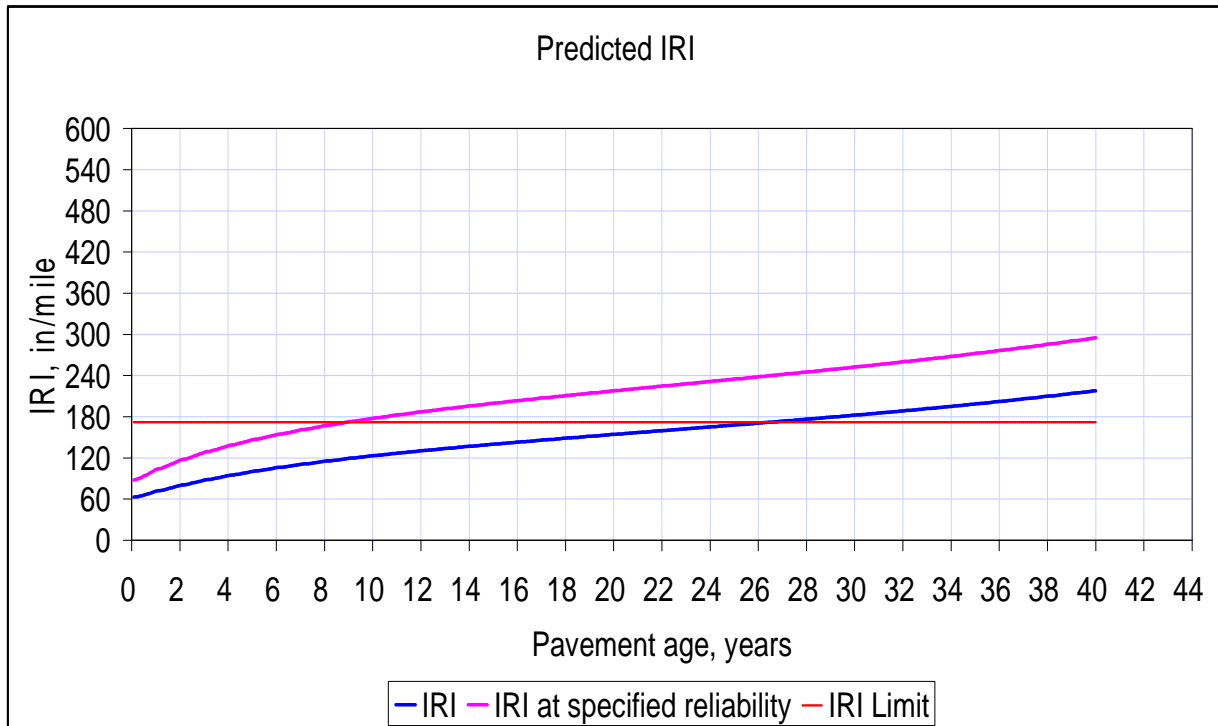


Figure B-36: IRI for truck case L8c

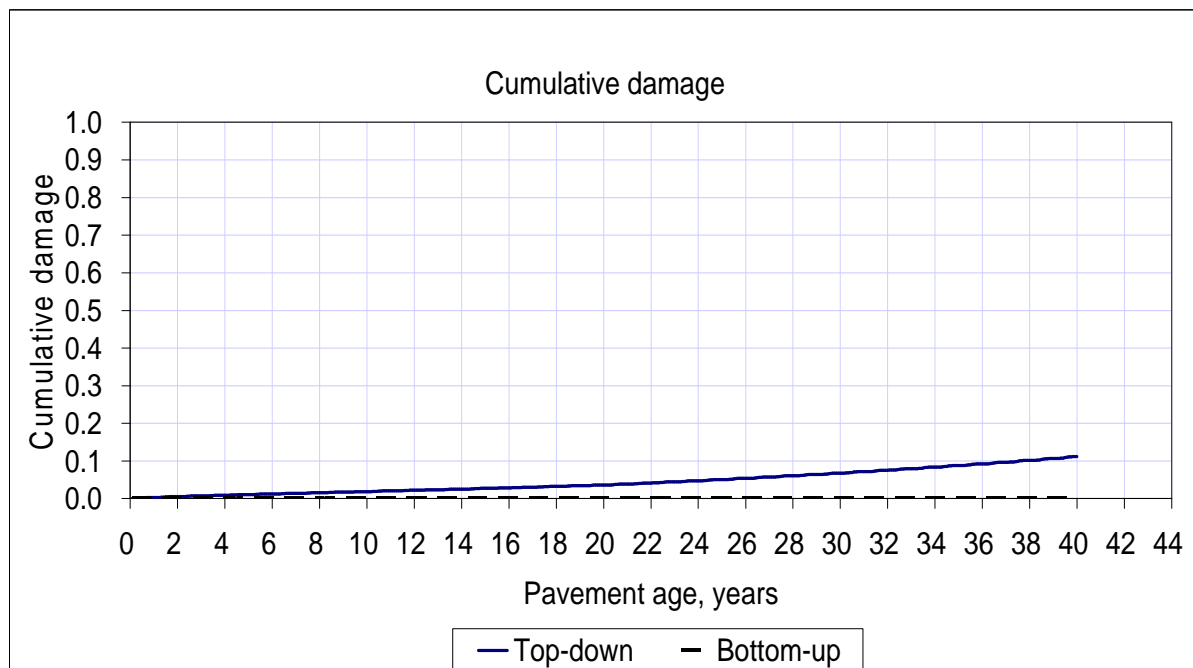


Figure B-37: Top down and bottom-up cracking for truck case L9

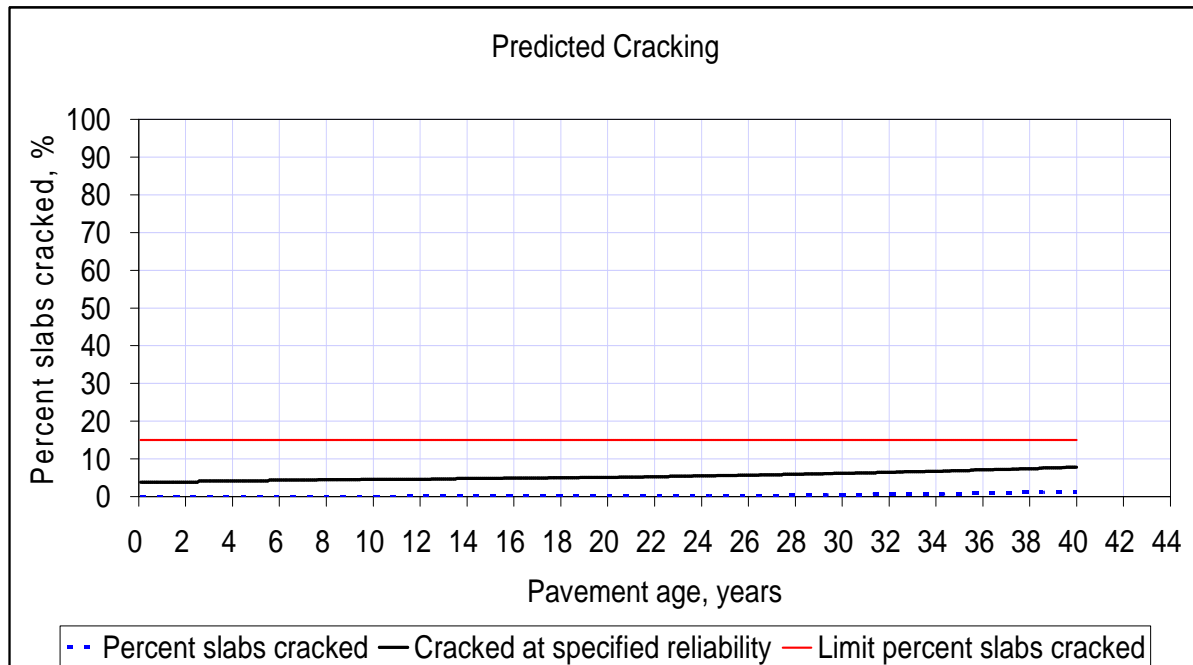


Figure B-38: % slab cracked for truck case L9

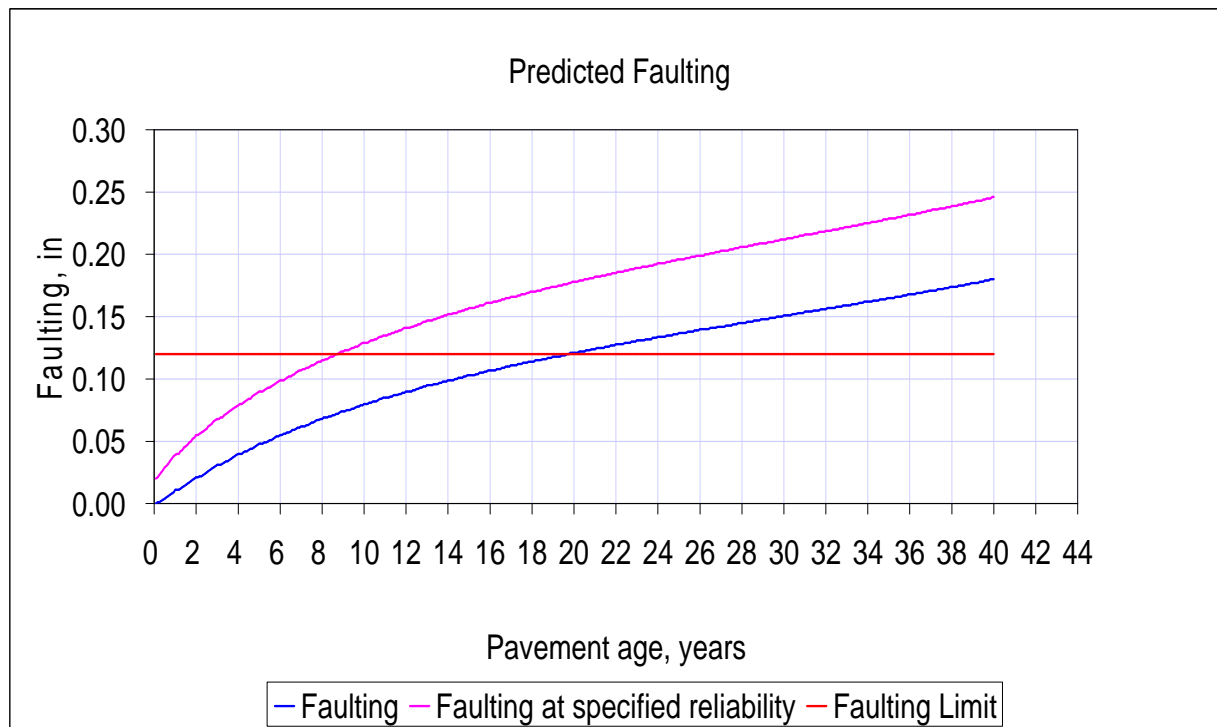


Figure B-39: Faulting for truck case L9

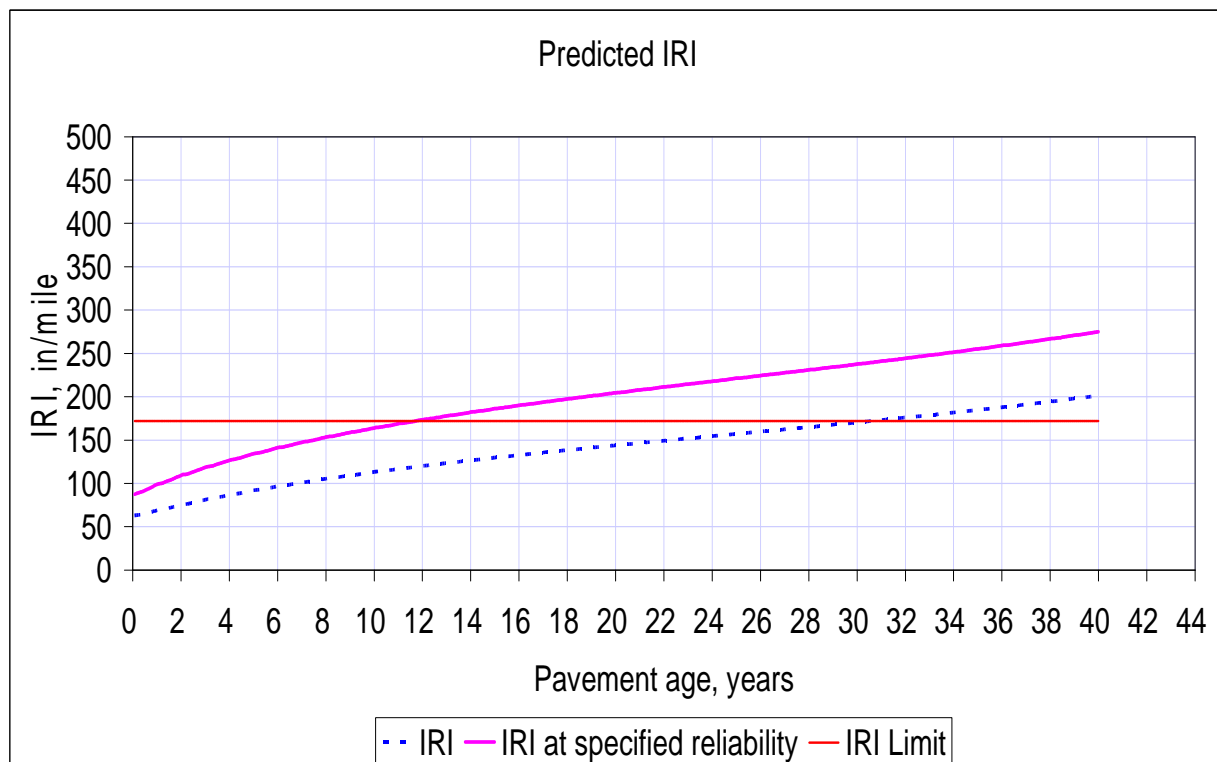


Figure B-40: IRI for truck case L9

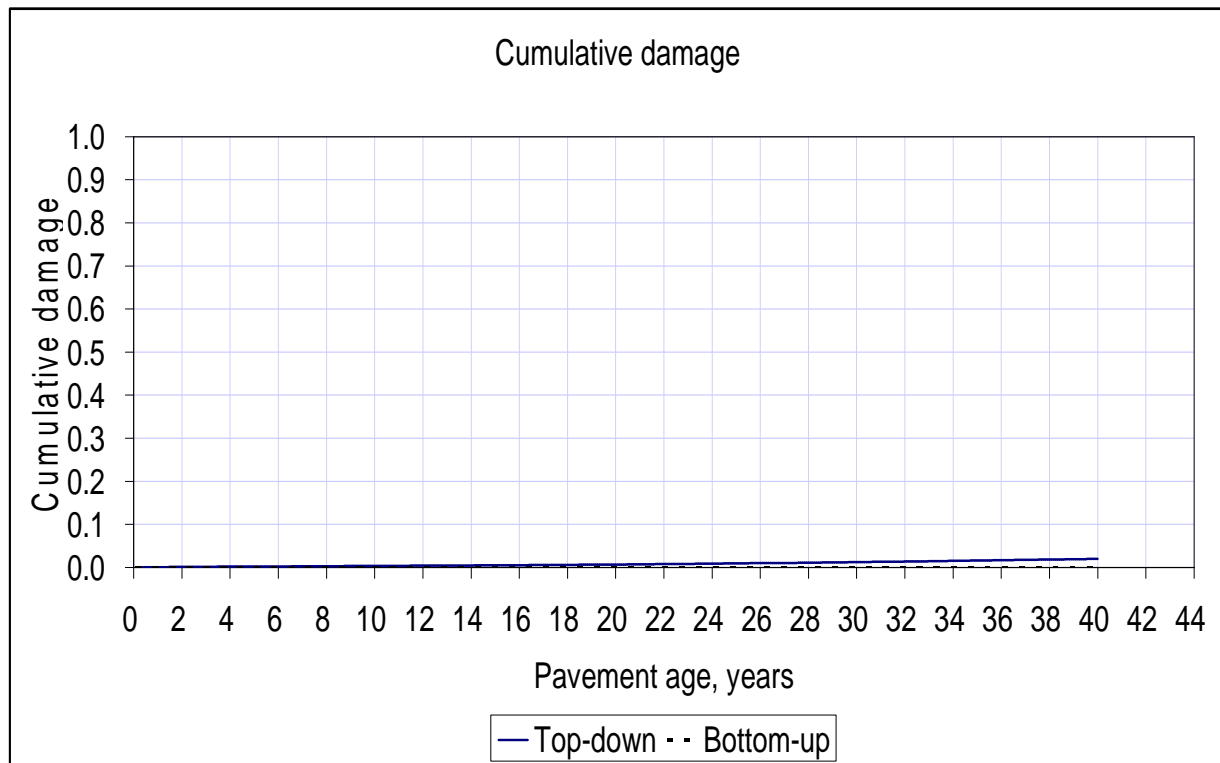


Figure B-41: Top down and bottom-up cracking for truck case L10

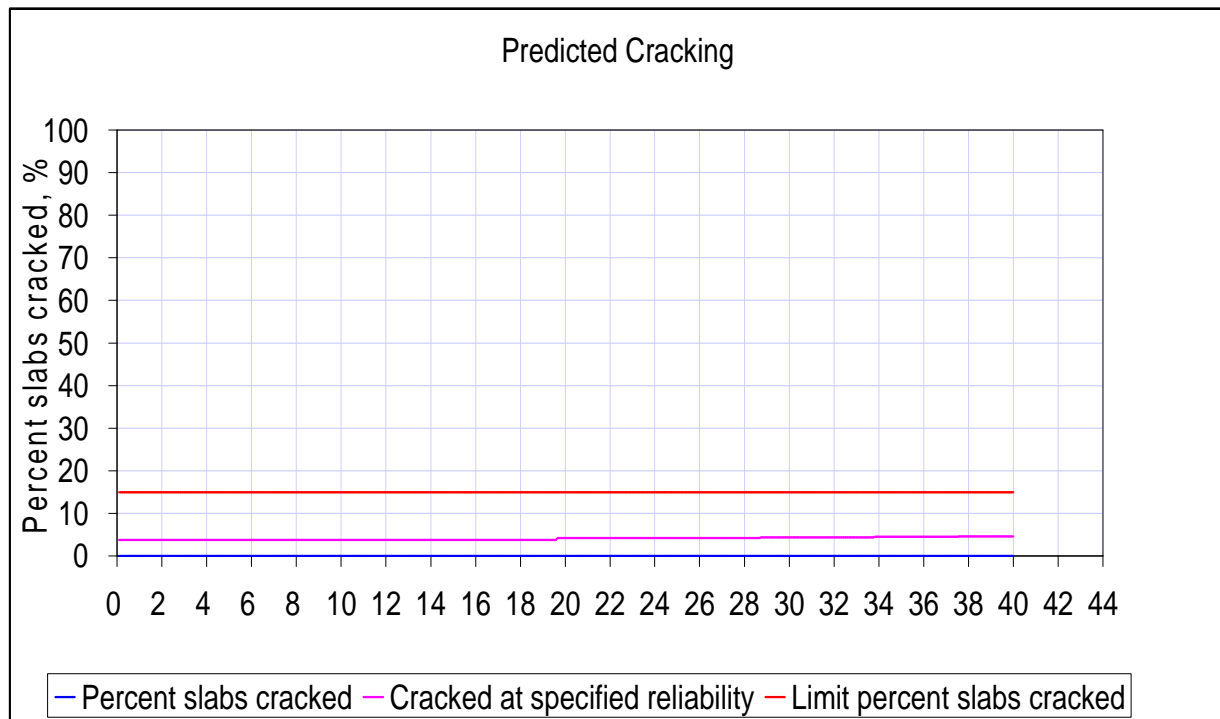


Figure B-42: % slab cracked for truck case L9

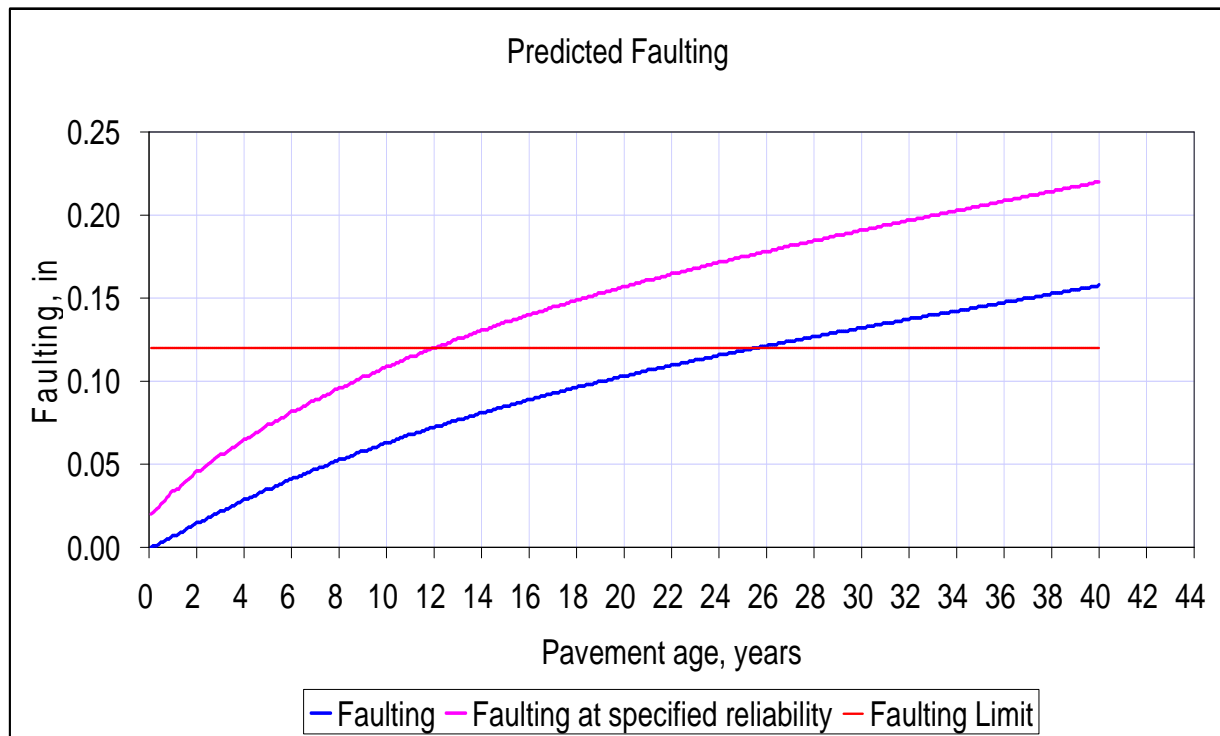


Figure B-43: Faulting for truck case L10

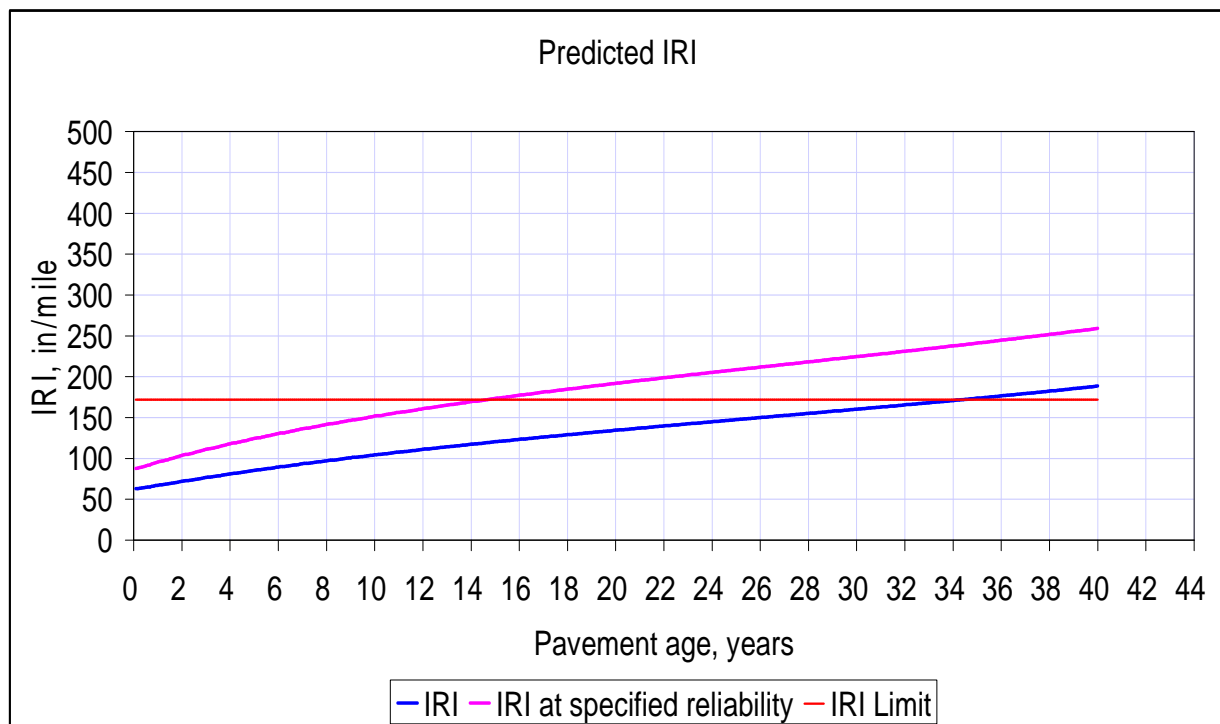


Figure B-44: IRI for truck case L10

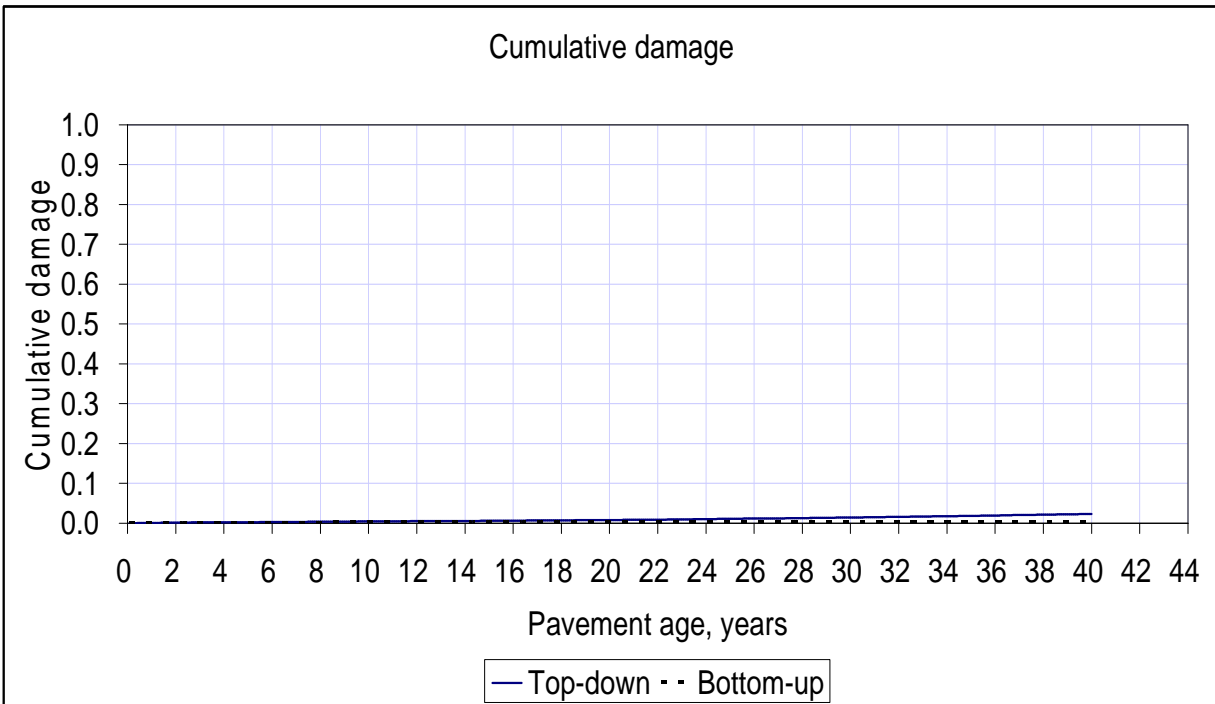


Figure B-45: Top down and bottom-up cracking for truck case L11

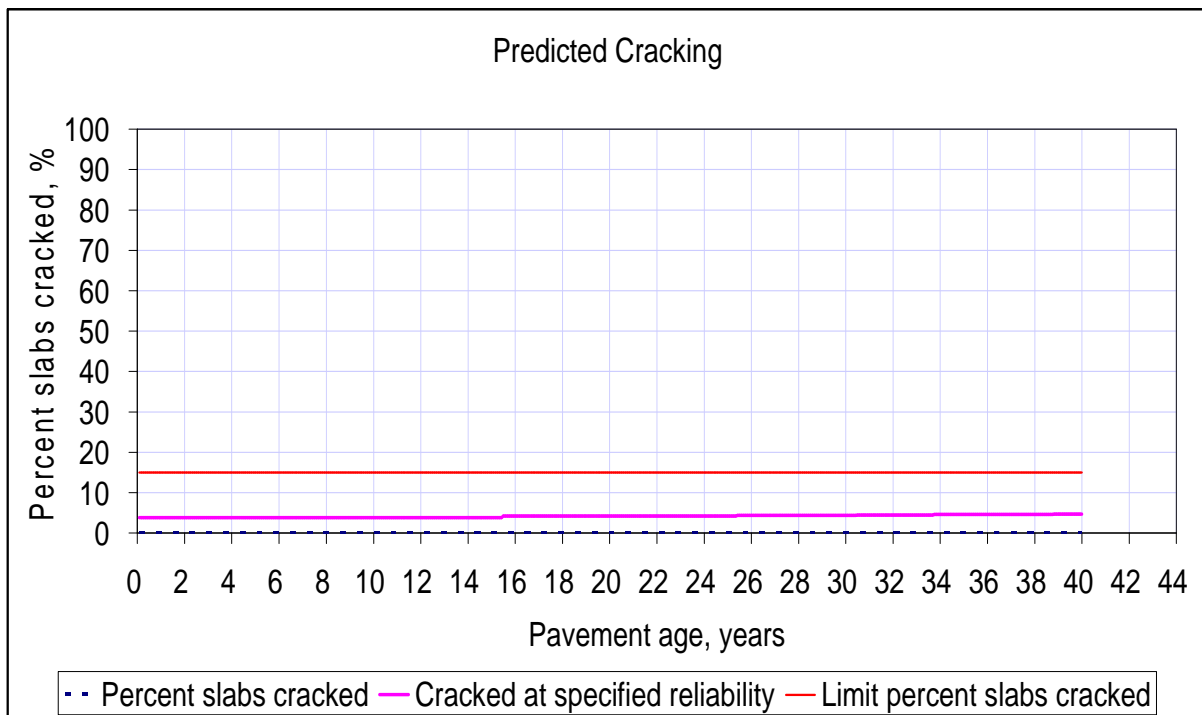


Figure B-46: % slab cracked for truck case L11

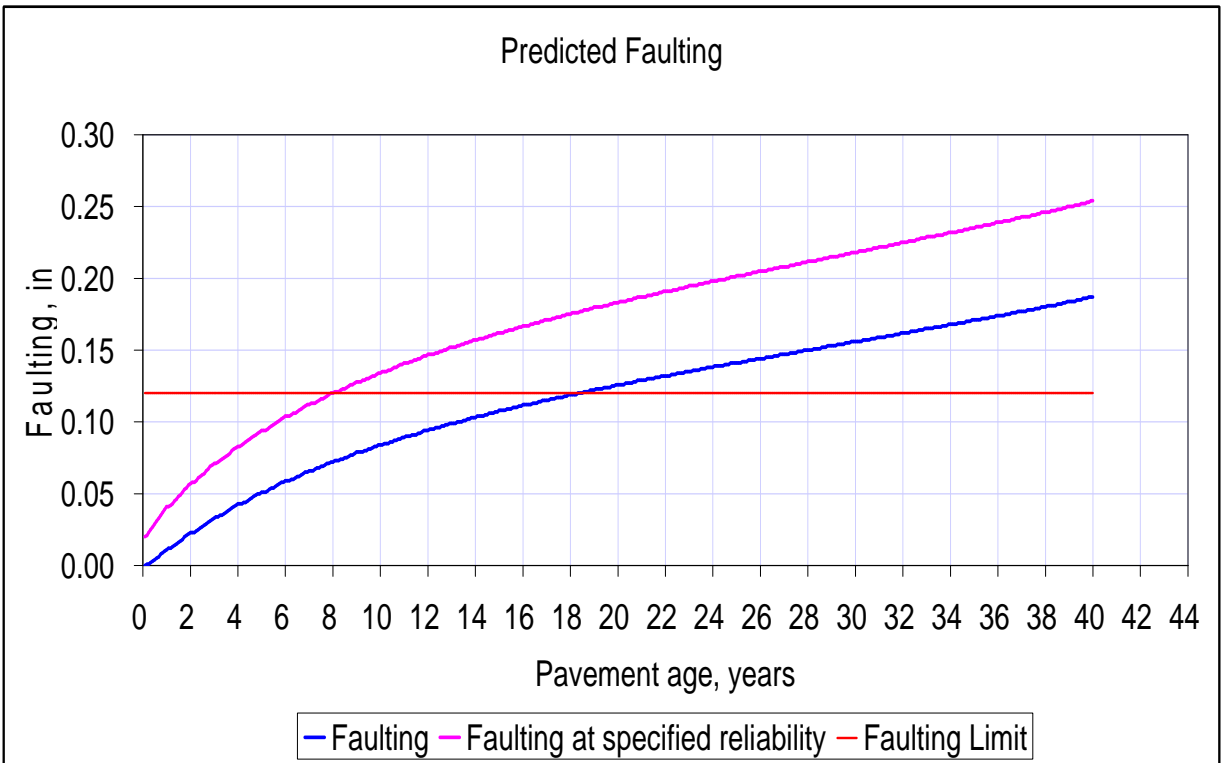


Figure B-47: Faulting for truck case L11

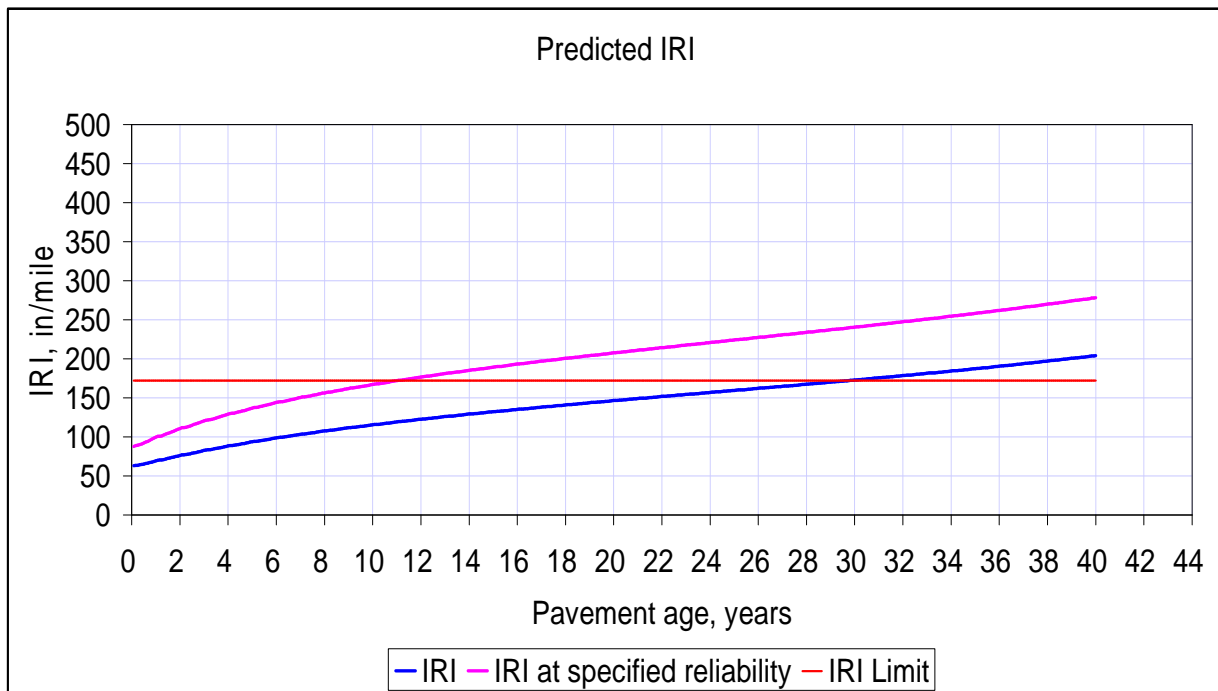


Figure B-48: IRI for truck case L11

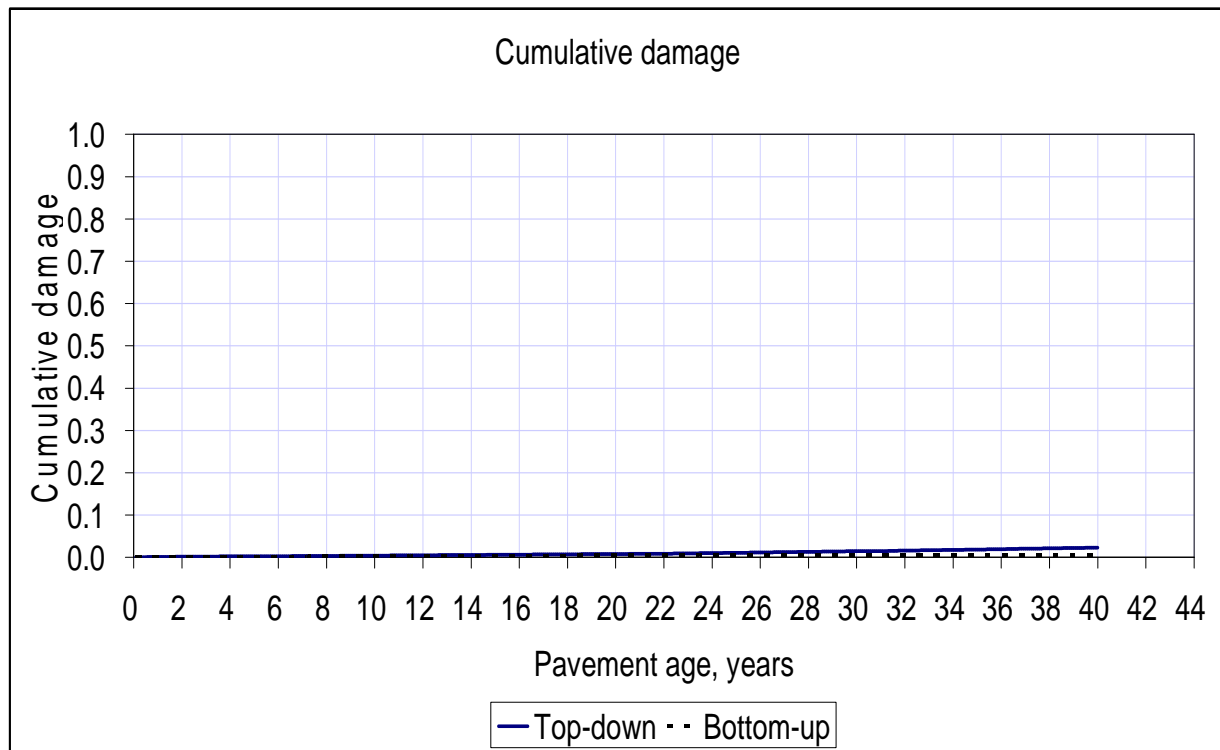


Figure B-49: Top down and bottom-up cracking for truck case L12

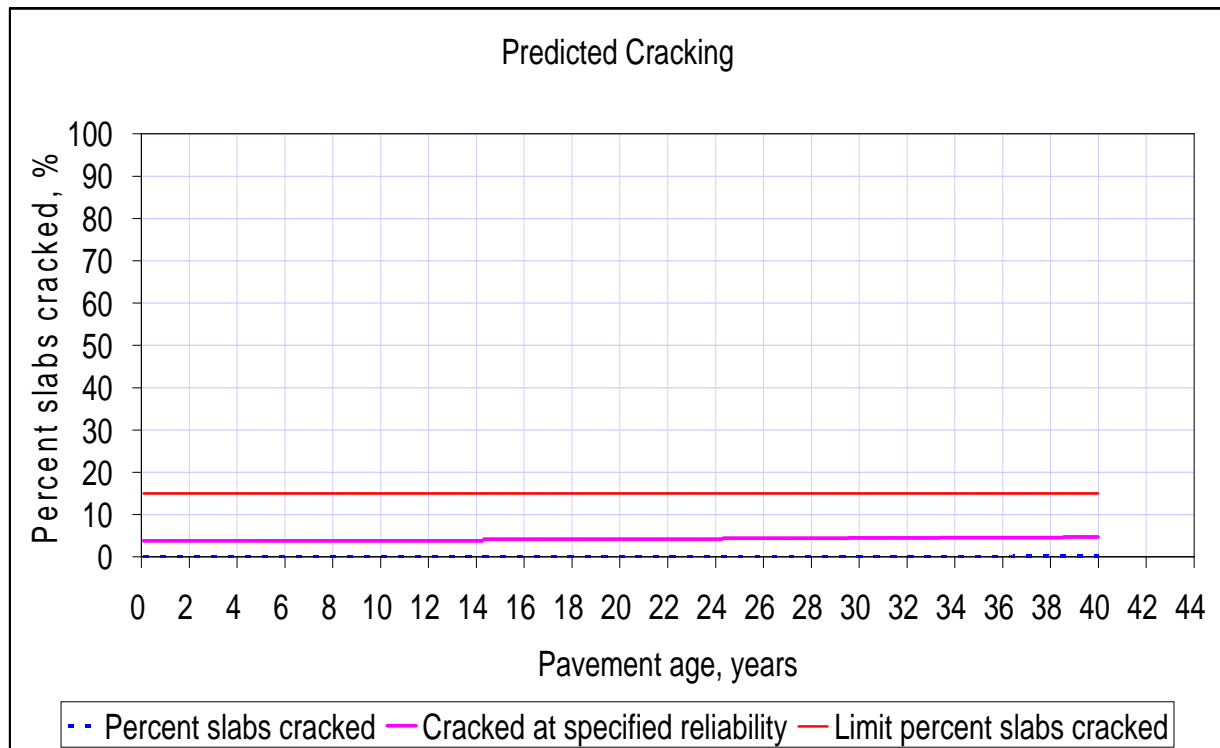


Figure B-50: % slab cracked for truck case L12

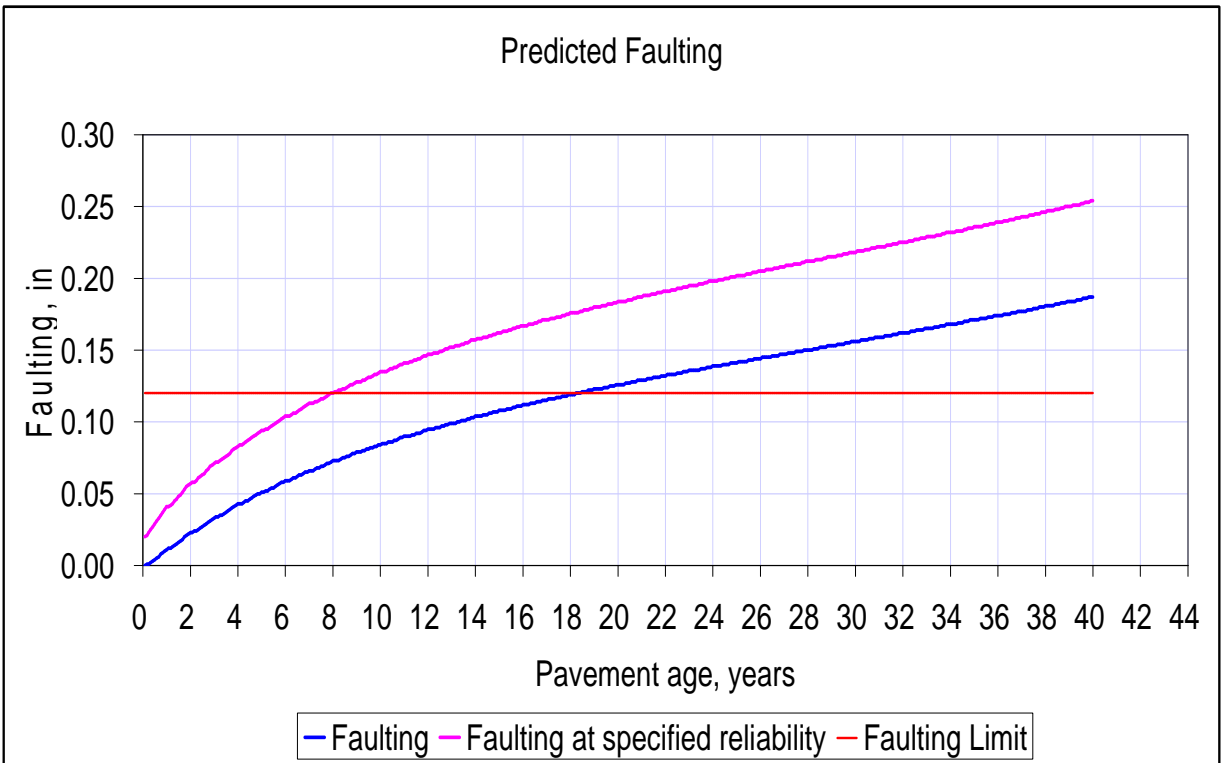


Figure B-51: Faulting for truck case L12

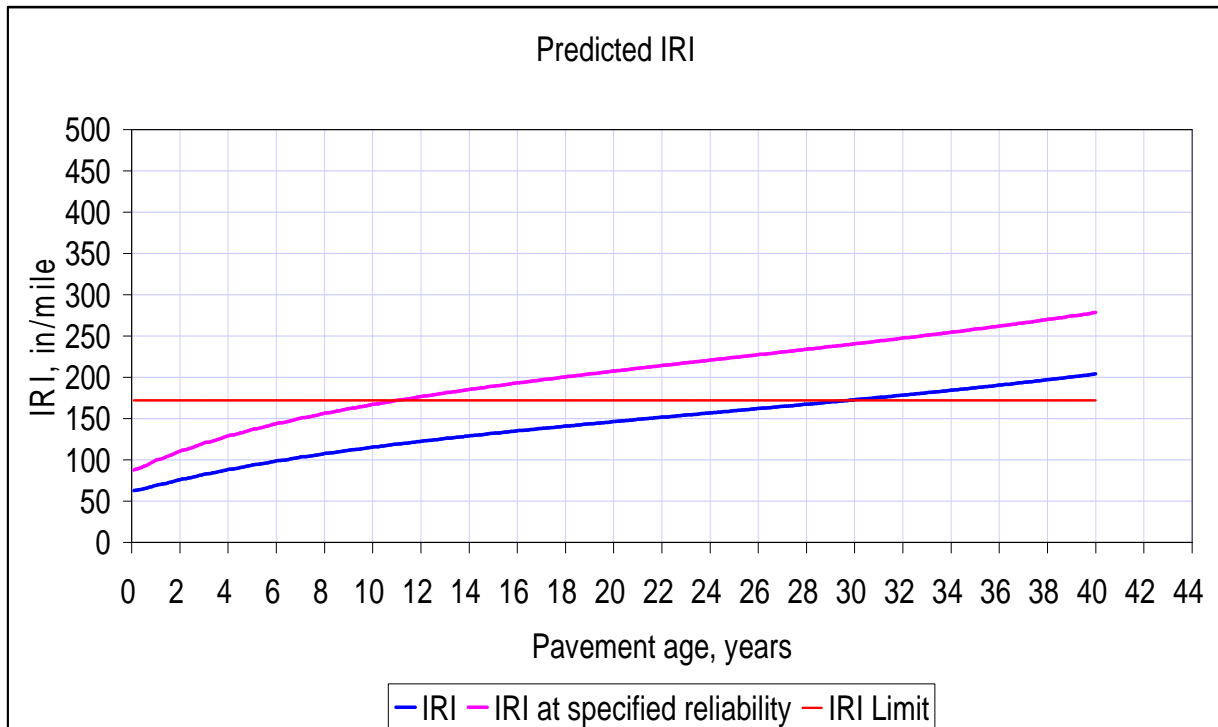


Figure B-52: IRI for truck case L12

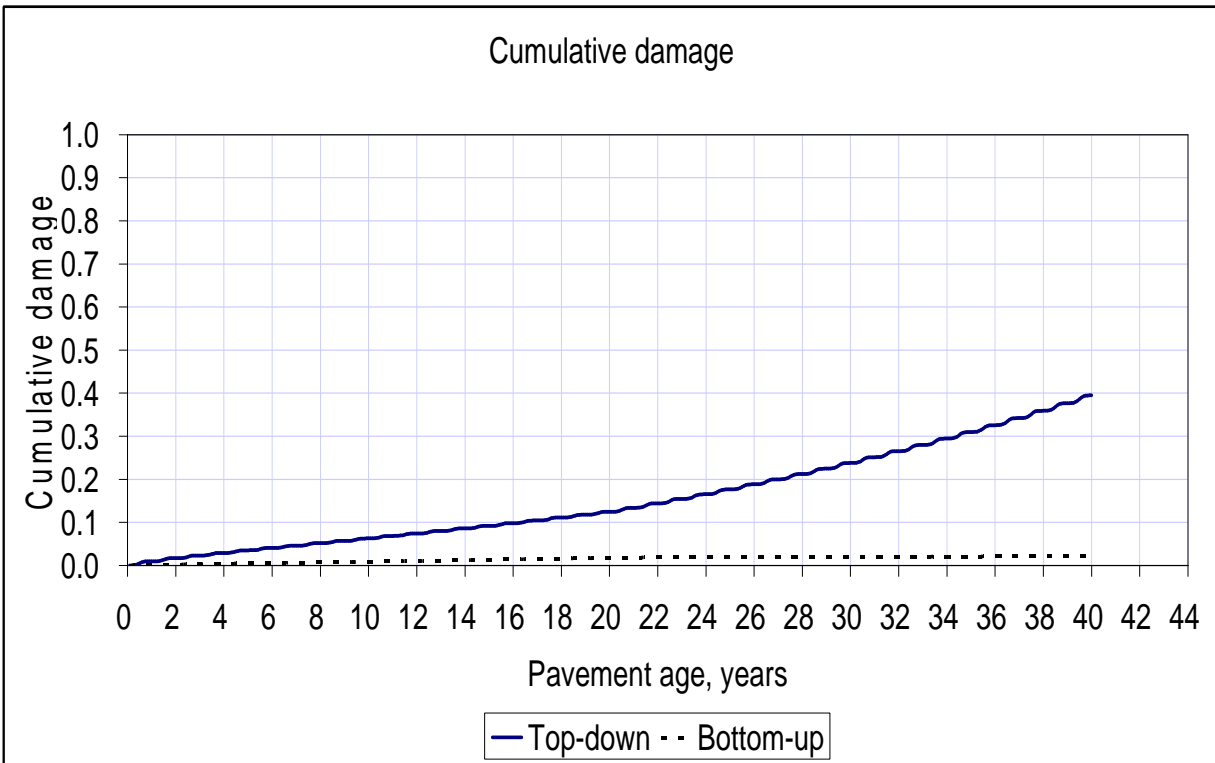


Figure B-53: Top down and bottom-up cracking for truck case L13

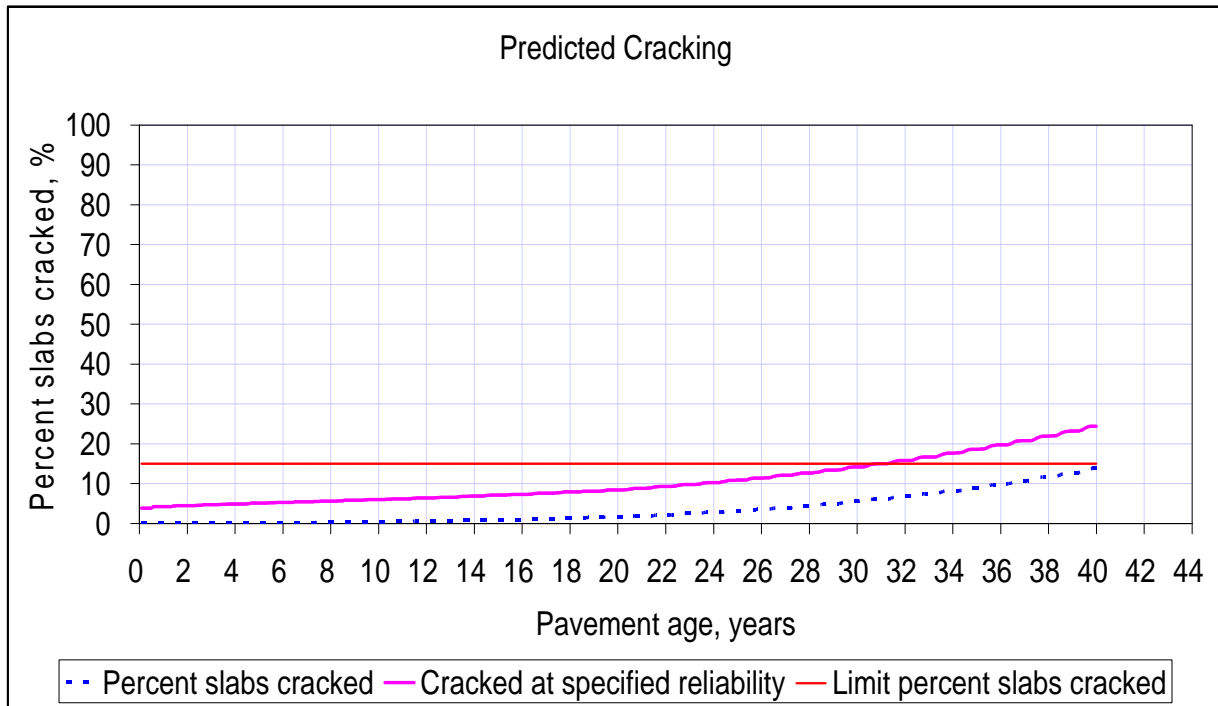


Figure B-54: % slab cracked for truck case L13

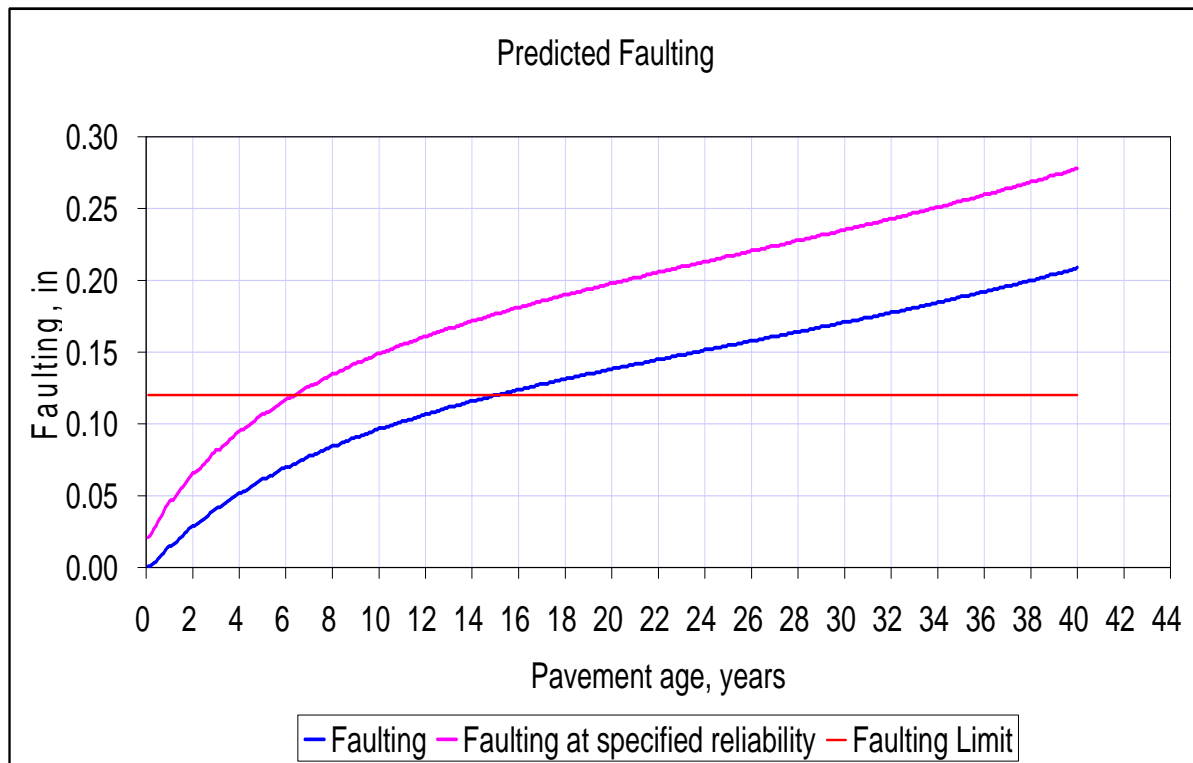


Figure B-55: Faulting for truck case L13

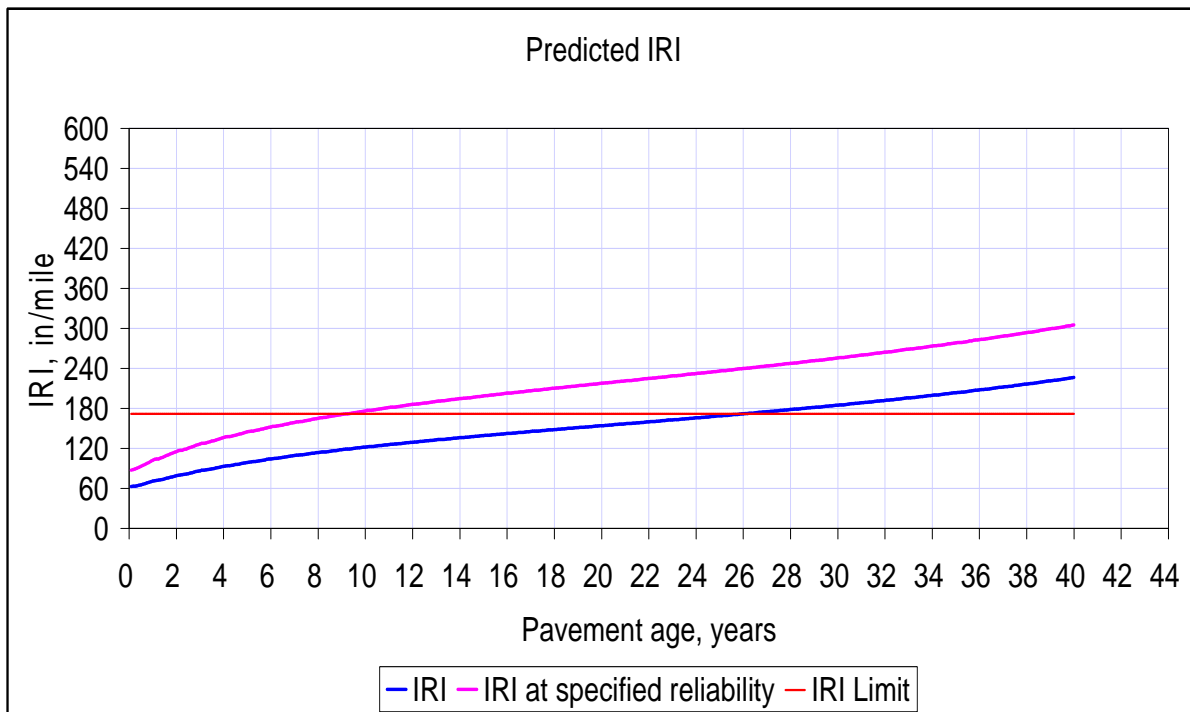


Figure B-56: IRI for truck case L13

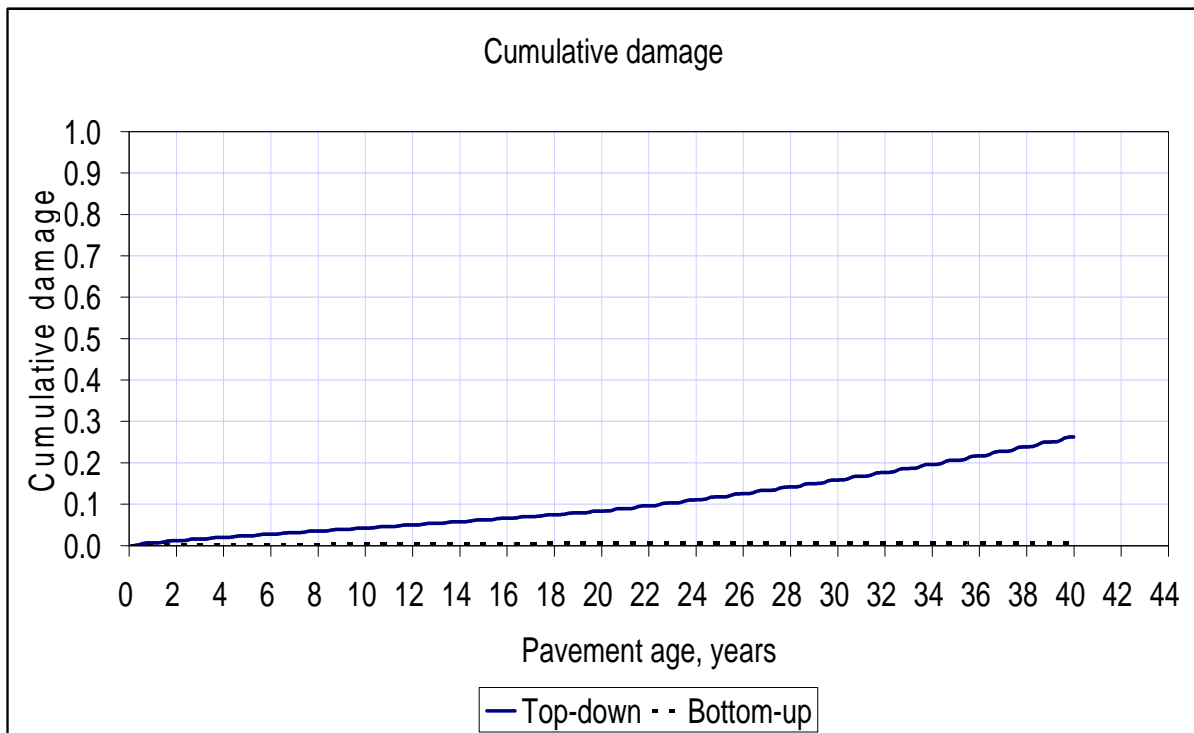


Figure B-57: Top down and bottom-up cracking for truck case L14

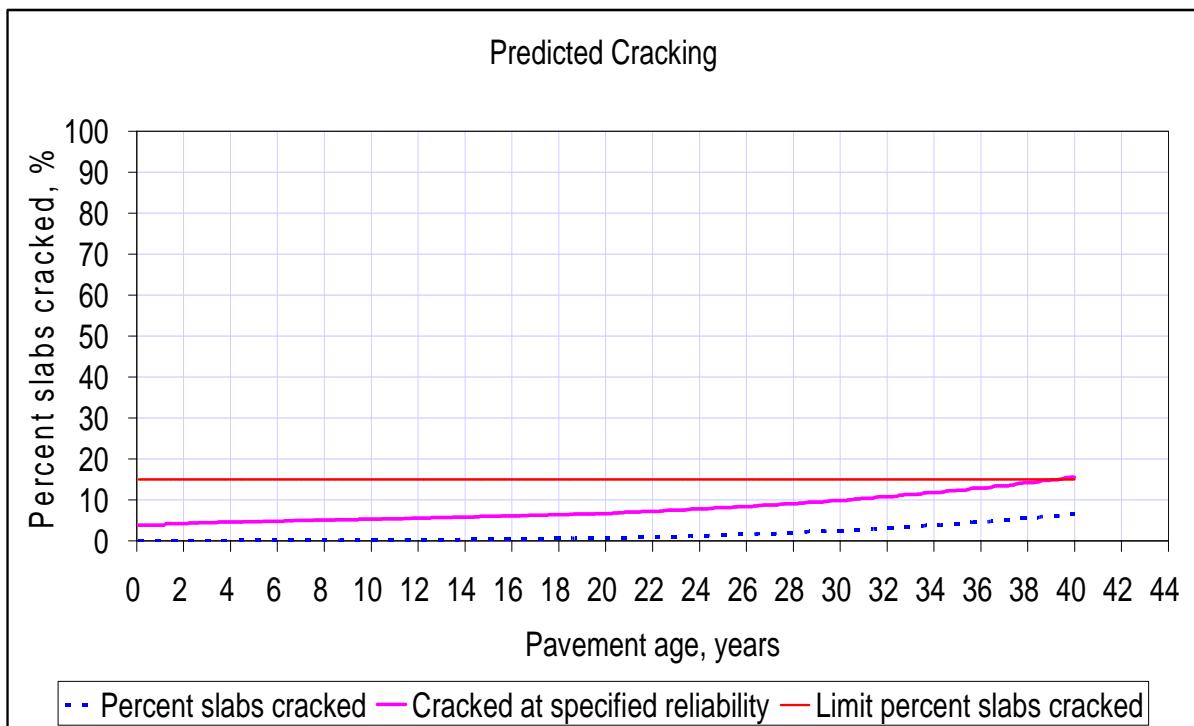


Figure B-58: % slab cracked for truck case L14

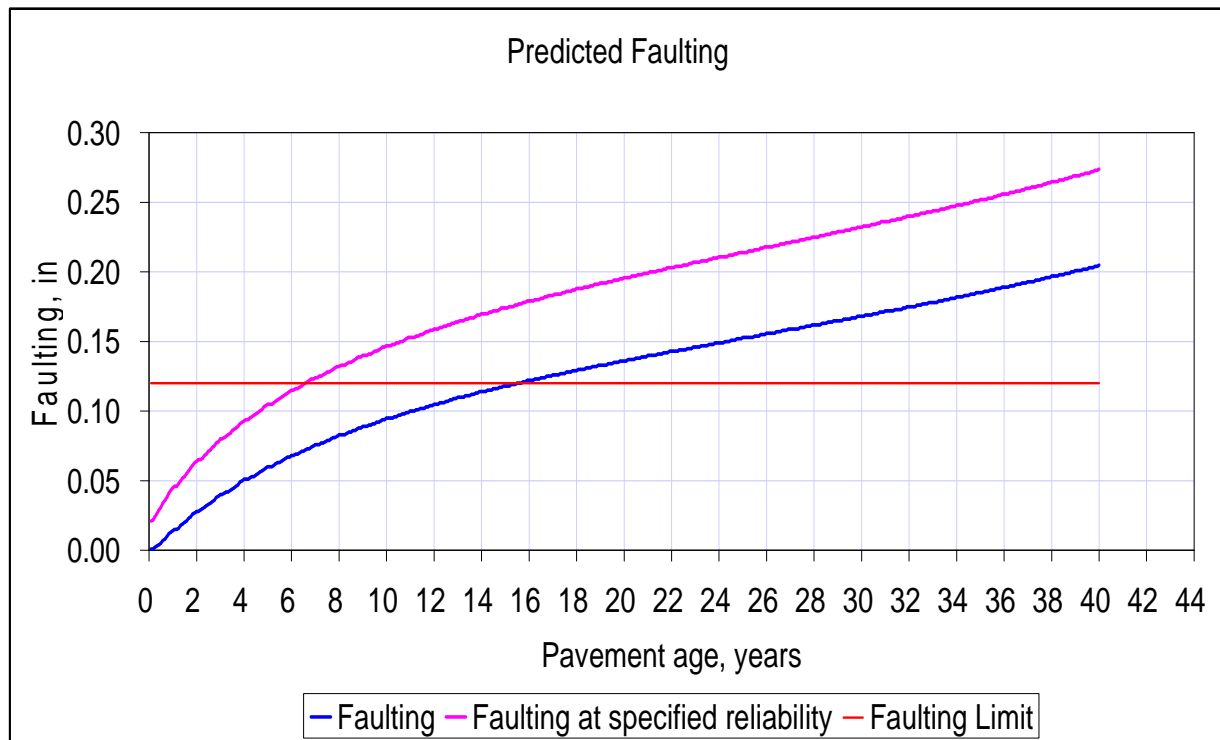


Figure B-59: Faulting for truck case L14

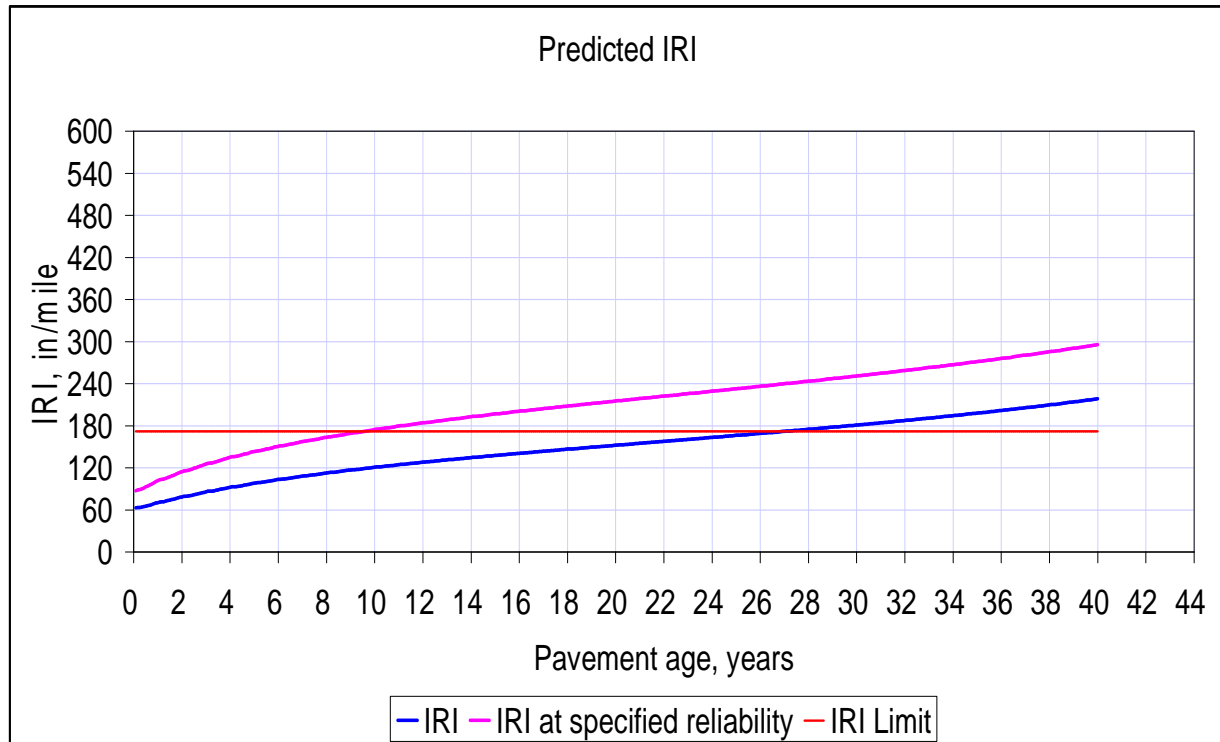


Figure B-60: IRI for truck case L14

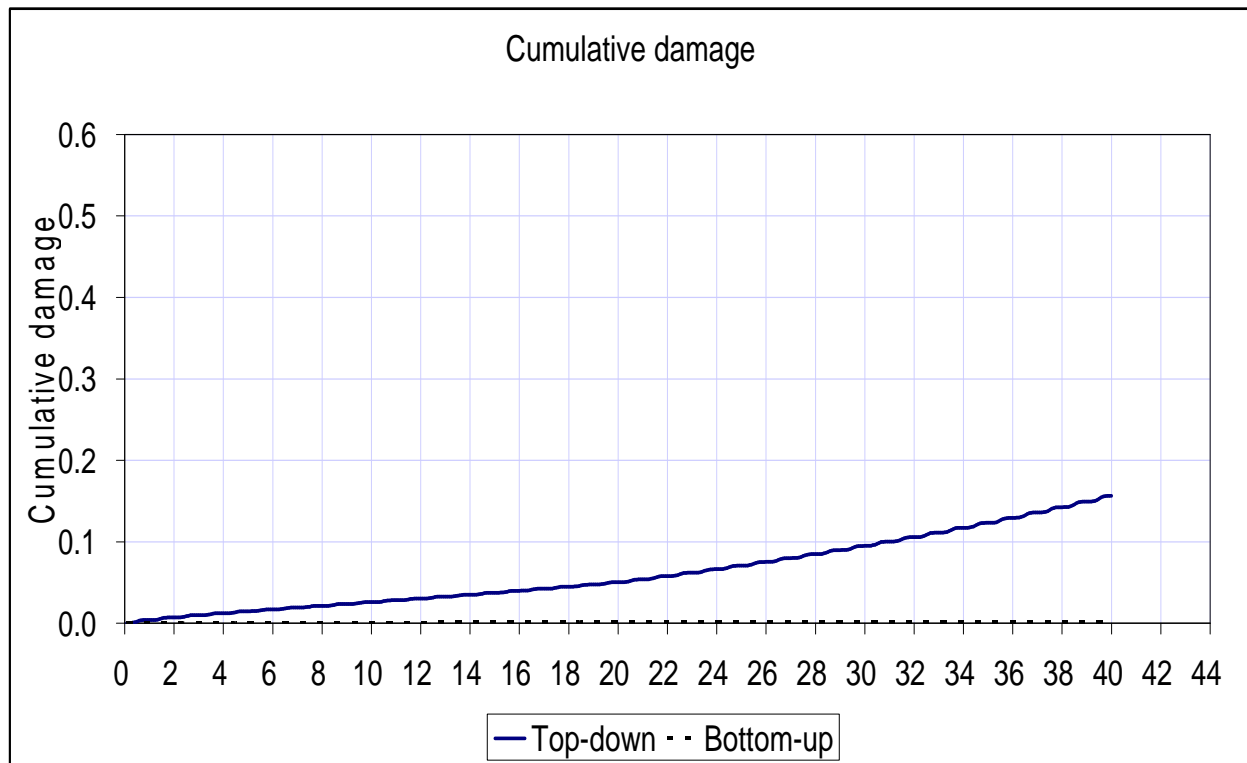


Figure B-61: Top down and bottom-up cracking for truck case L15a

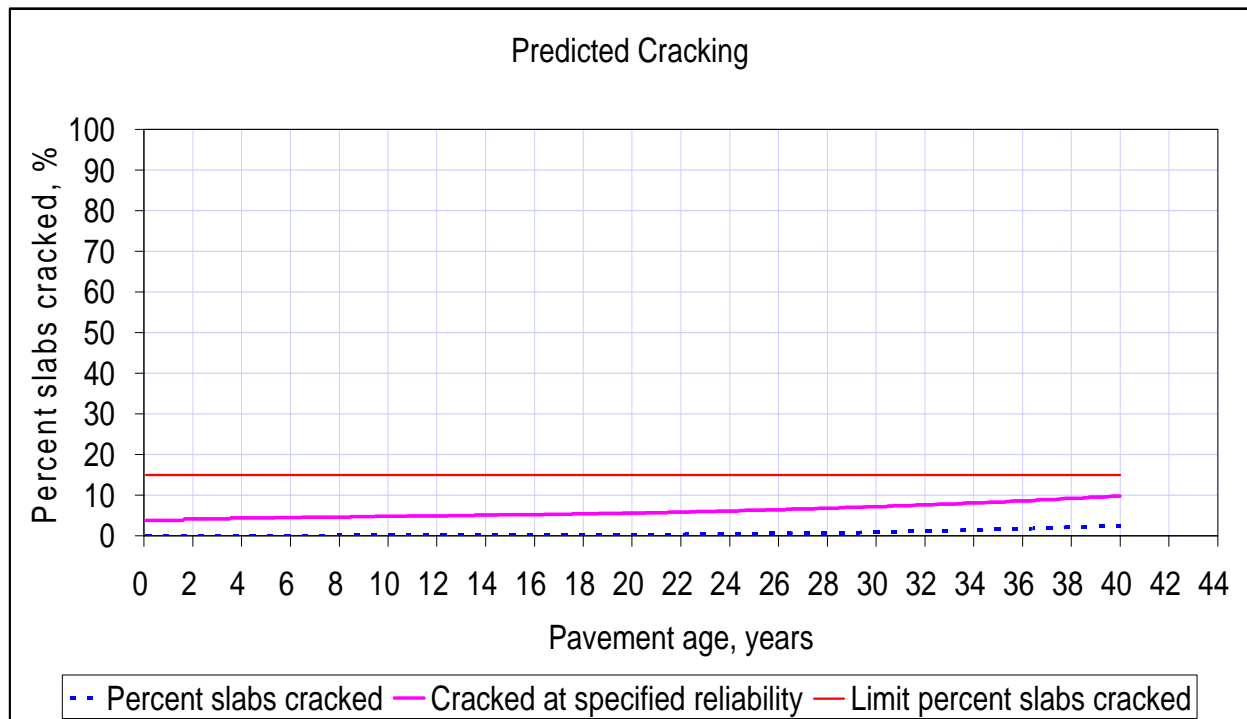


Figure B-62: % slab cracked for truck case L15a

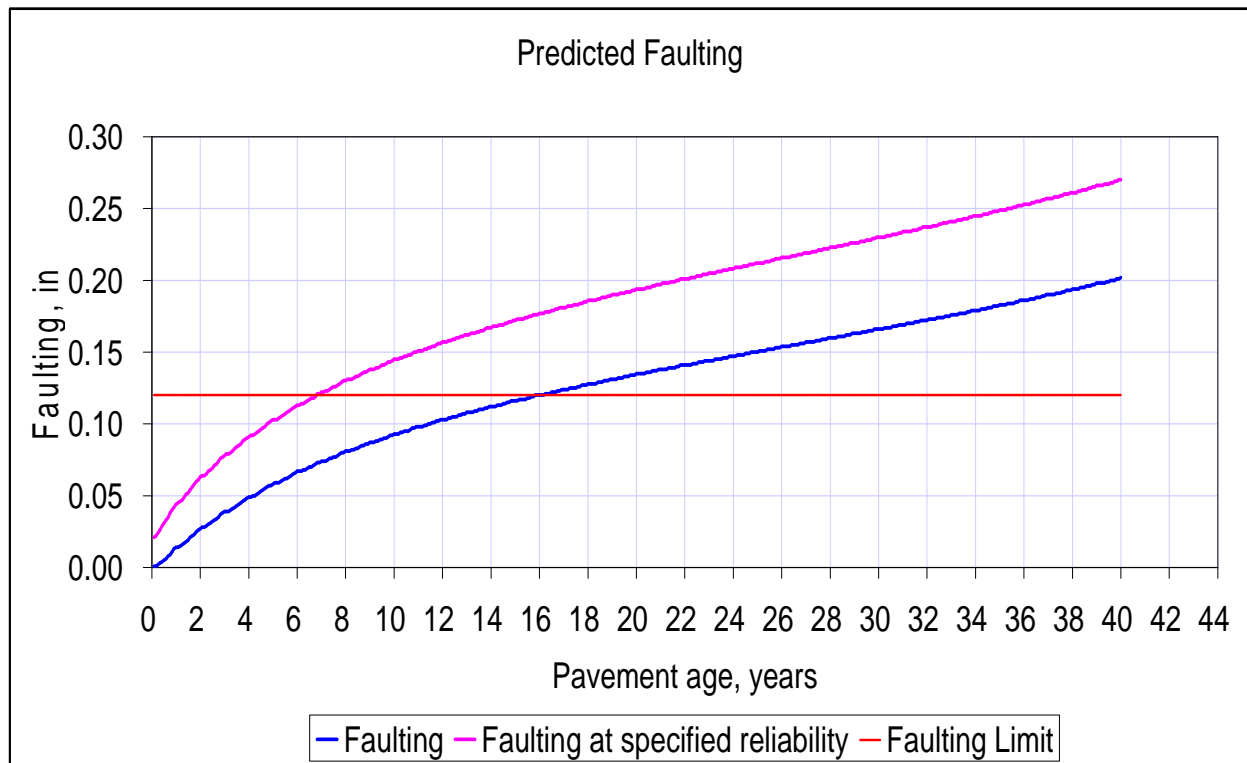


Figure B-63: Faulting for truck case L15a

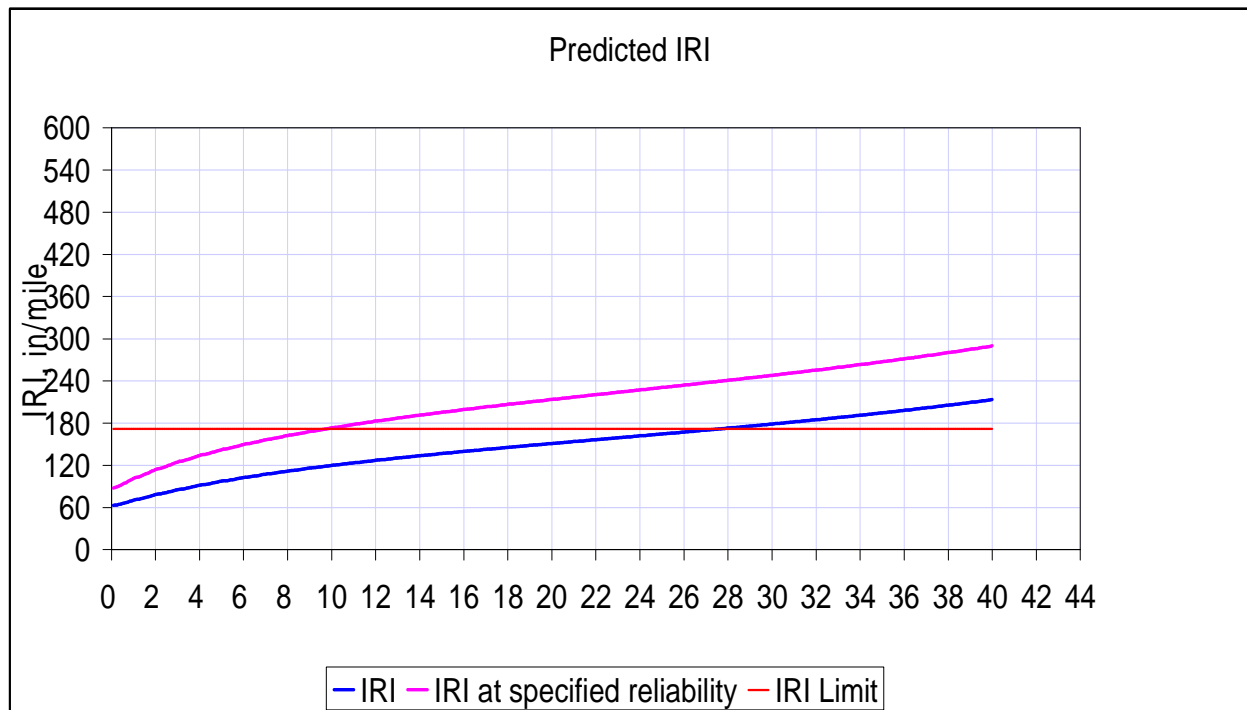


Figure B-64: IRI for truck case L15a

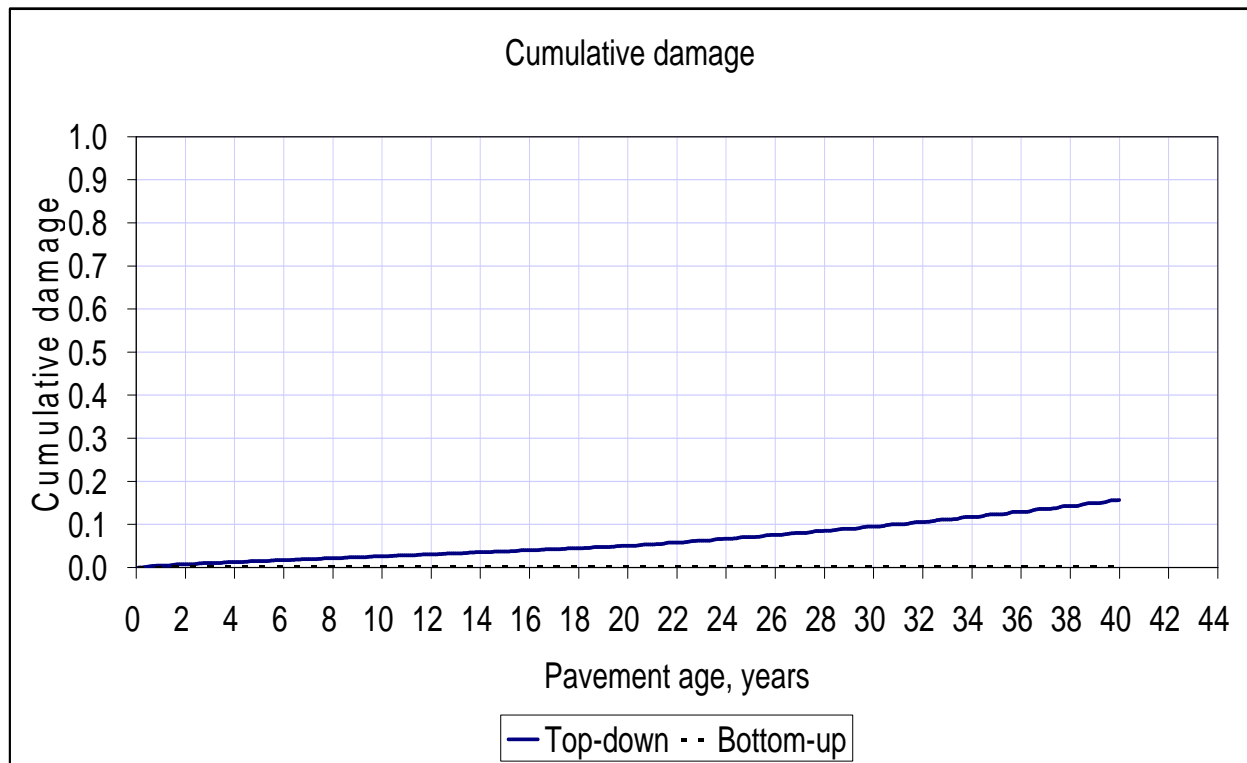


Figure B-65: Top down and bottom-up cracking for truck case L15b

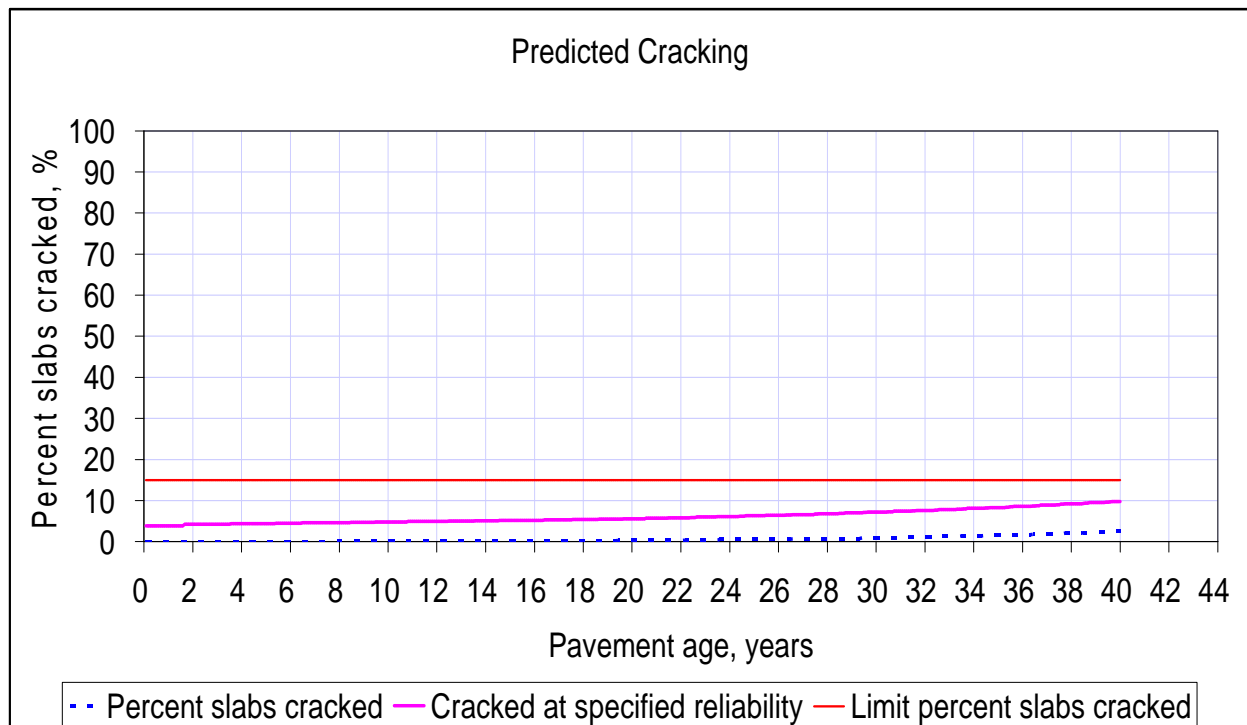


Figure B-66: % slab cracked for truck case L15b

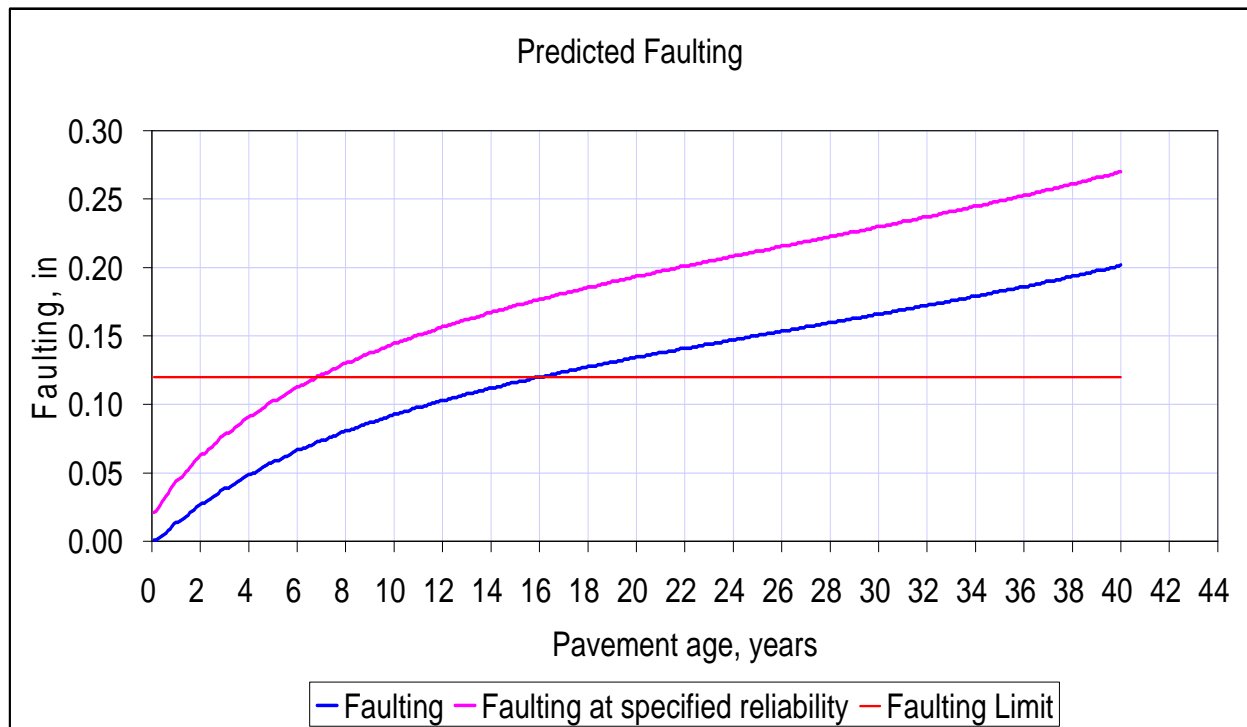


Figure B-67: Faulting for truck case L15b

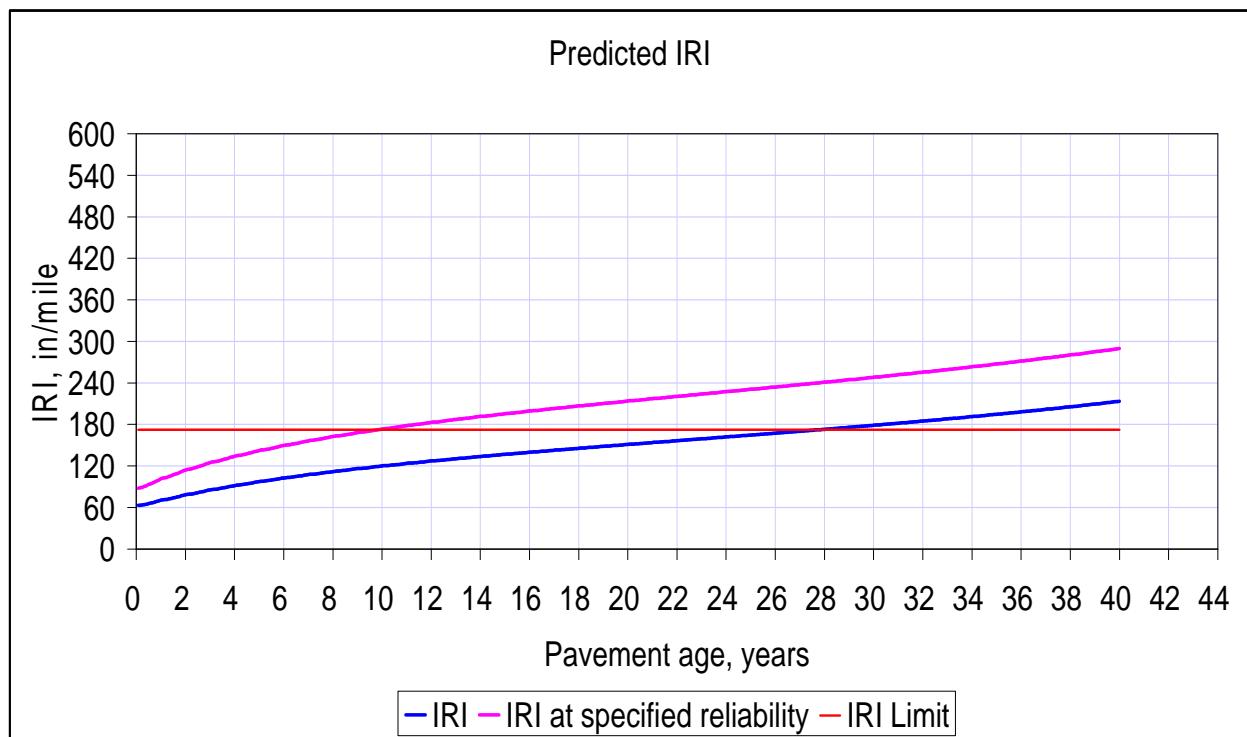


Figure B-68: IRI for truck case L15b

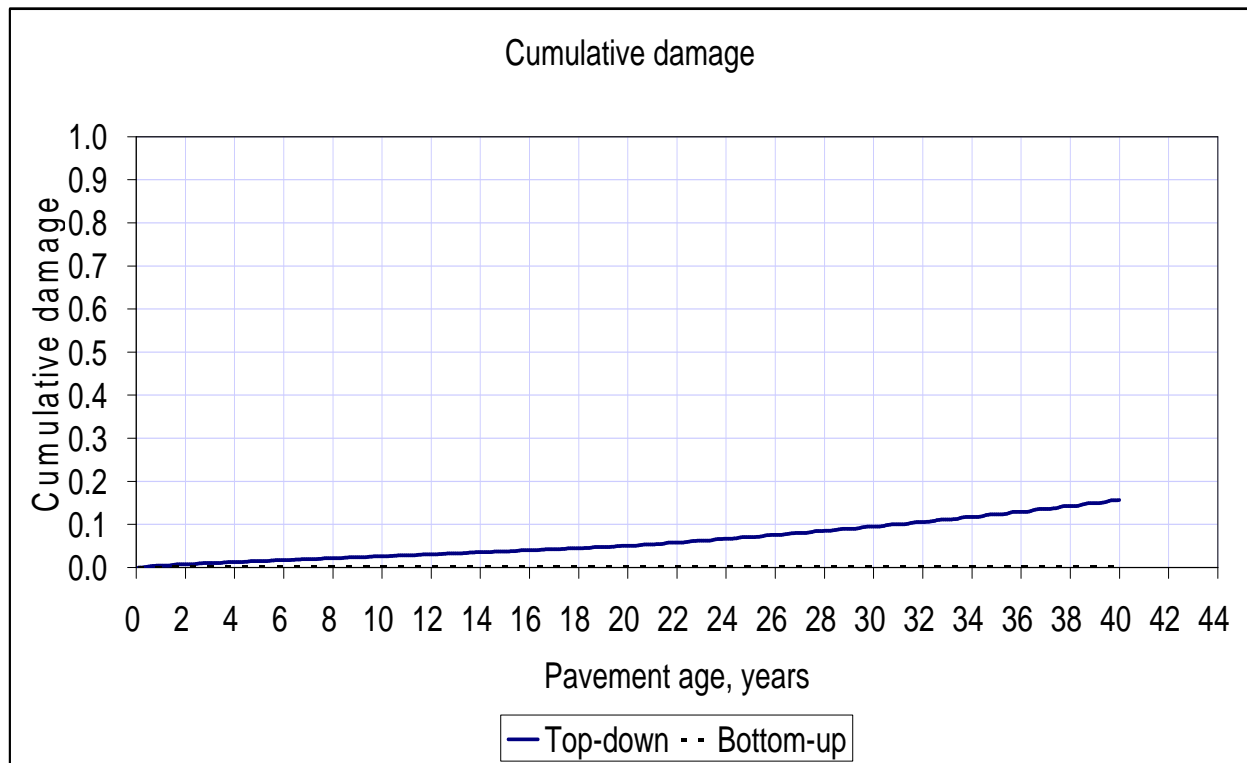


Figure B-69: Top down and bottom-up cracking for truck case L15c

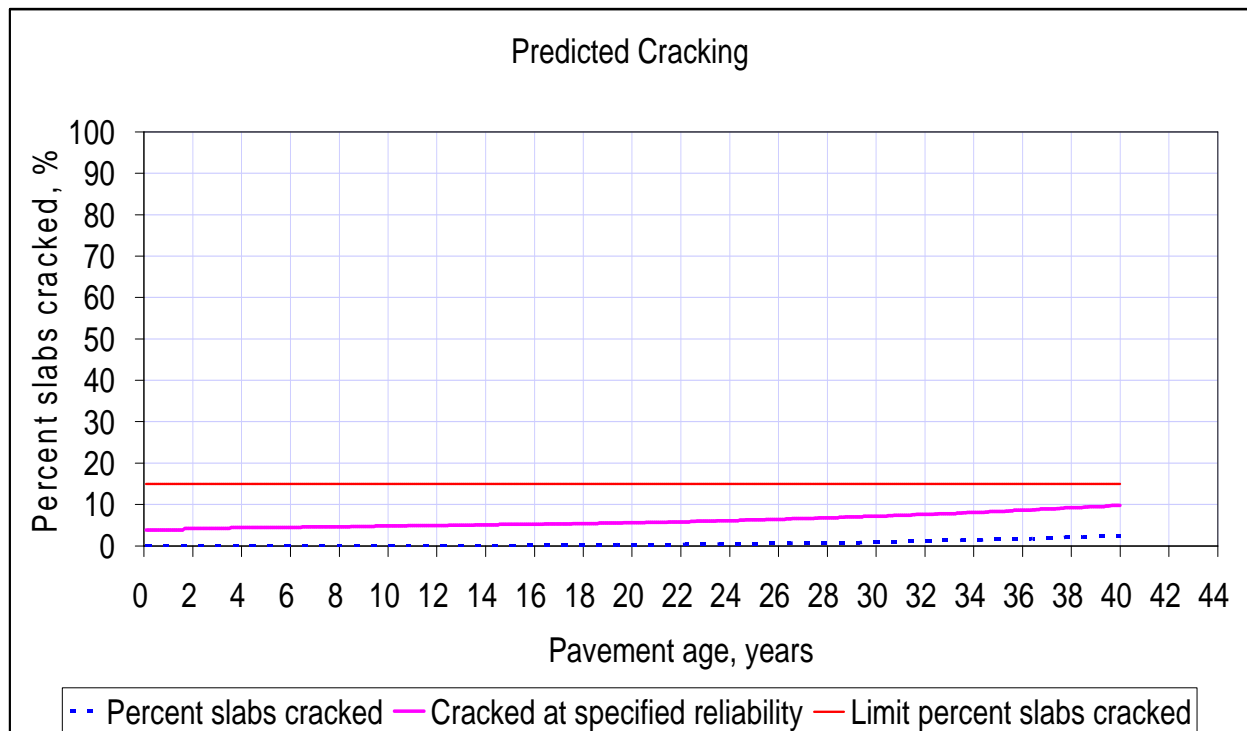


Figure B-70: % slab cracked for truck case L15c

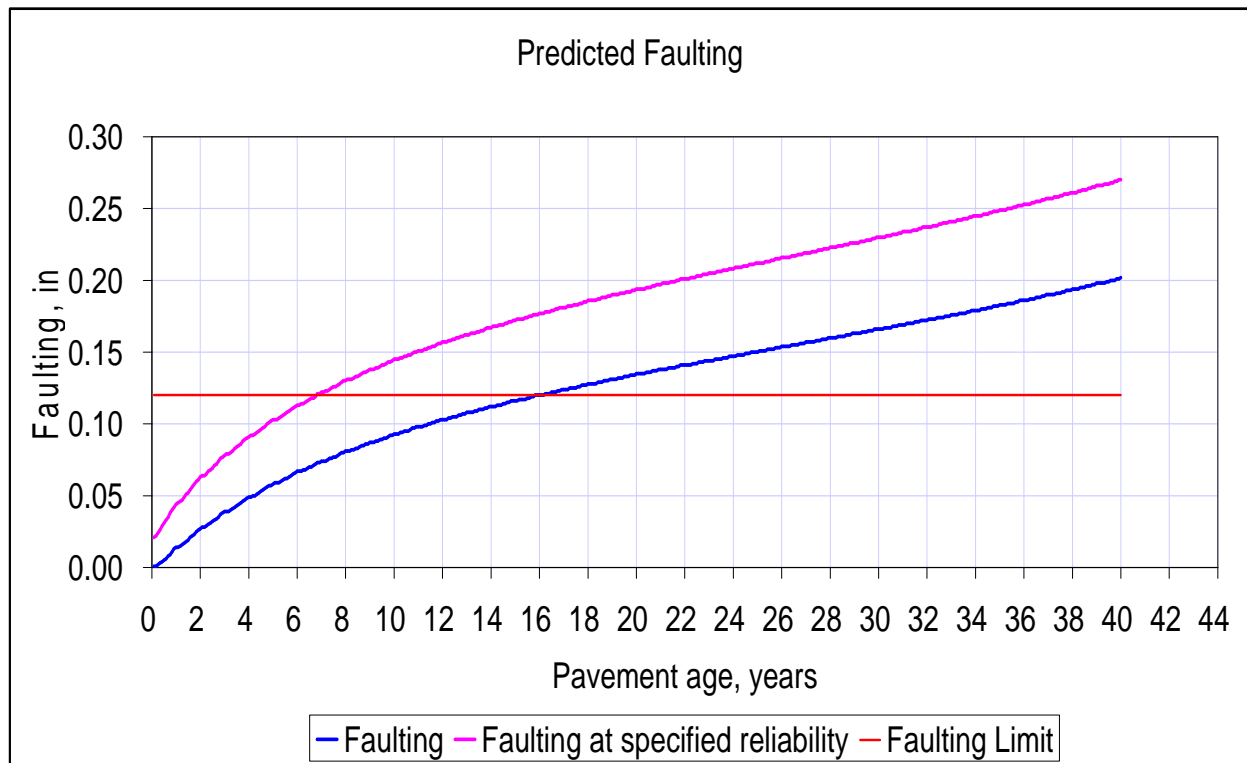


Figure B-71: Faulting for truck case L15c

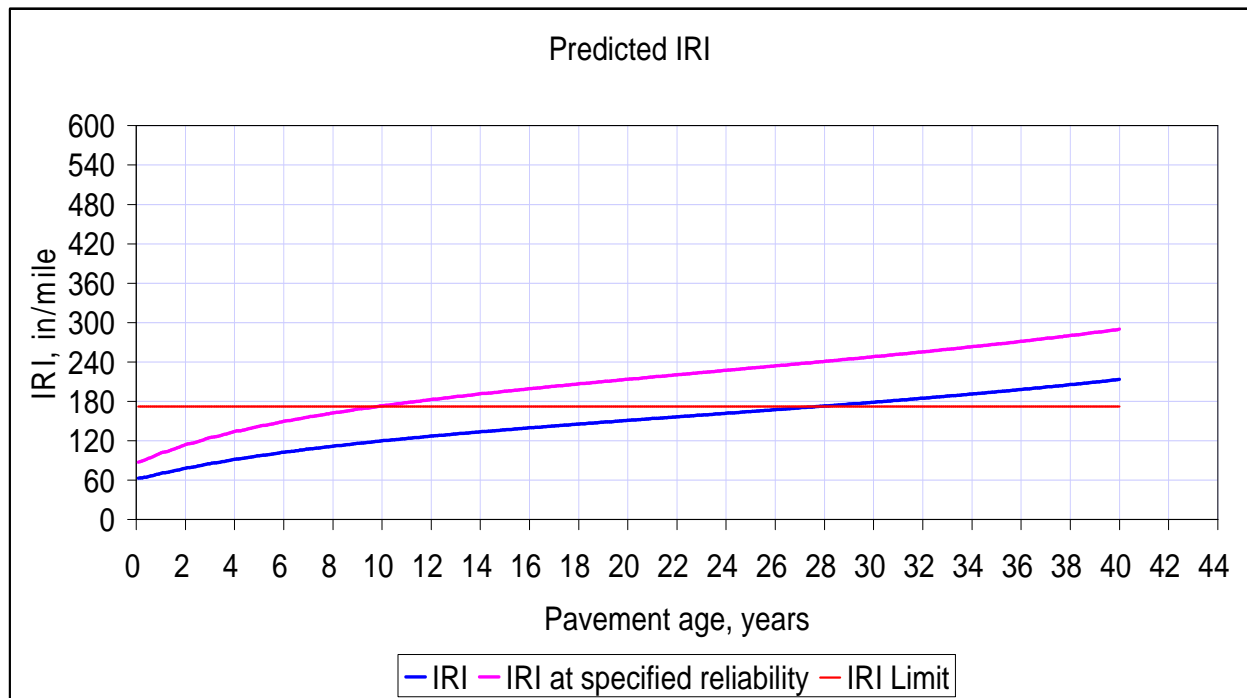


Figure B-73: IRI for truck case L15c

REFERENCES

American Association of State Highways and Transportation Officials (AASHTO), *AASHTO Guide for Design of Pavement Structures*, Washington, D.C., 1993.

American Concrete Pavement Association (ACPA). *Concrete Pavement Fundamentals*, URL: http://www.pavement.com/Concrete_Pavement/Technical/Fundamentals/index.asp, Accessed June, 2009.

Chen H., Dere Y., Sotelino E., and Archer G., *Mid-Panel Cracking of Portland Cement Concrete Pavements in Indiana*, FHWA/IN/JTRP-2001/14, Final Report 2002

Clough R. W., Wilson E. L., *Early Finite Element research at Berkeley*, University of California, Berkeley 1999.

Coree, B., Ceylan, H., and Harrington, D., *Implementing the Mechanistic-Empirical Pavement Design Guide*-Technical Report, Iowa Highway Research Board and Iowa Department of Transportation, Ames, Iowa, May 2005.

Darestani M. Y, and P. Thambiratnam, D., Nataatmadja, A. and Baweja, D. *Influence of vehicular positions and thermal effects on structural behaviour of concrete pavement*. Journal of Mechanics of Materials and Structures, 2008. pp. 567-589.

Darestani M. Y., Nataatmadja A. and David P. Thambiratnam, *A Review of 2004 Austroads Rigid Pavement Design*, 22nd ARRB Conference – Research into Practice, Canberra Australia, 2006.

Davids William. G., *Foundation Modeling for Jointed Concrete Pavement*, In Transportation Research Record, 1730, TRB, National Research Council, Washington D.C., 2000. pp 34-42.

Federal Highway Administration, *Long-Term Plan for Concrete Pavement Research and Technology - The Concrete Pavement Road Map: Volume I*, URL: <http://www.fhwa.dot.gov/pavement/pccp/pubs/05052/index.cfm>, Publication number: FHWA-HRT-05-0520, September, 2005.

Gillespie, T.D., Karamihas, S.M., Cebon, D., Sayers, M.W., Nasim, M.A., Hansen, W, and N. Ehsan. *Effects of Heavy Vehicle Characteristics on Pavement Response and Performance*, National Cooperative Highway Research Program Report 353, Transportation Research Board, National Research Council, Washington, DC, 1993.

Hiller, J.E. and Roesler, J.R., Determination of Critical Concrete Pavement Fatigue Damage Locations Using Influence Lines, *Journal of Transportation Engineering*, ASCE, Vol. 131, No. 8, July/August 2005, pp. 599-607.

Hiller, J.E. and Roesler, J.R., Transverse Joint Analysis for Use in Mechanistic-Empirical Design of Rigid Pavements, *Transportation Research Record 1809*, TRB, National Research Council, Washington, DC, 2002, pp. 42-51.

Huang, Y.H. Pavement Analysis and Design. Prentice Hall, Inc., New Jersey, 2004.

Hudson, W.R., Monismith, C.L., Dougan, C.E., and Visser, W., *Use Performance Management System Data for Monitoring Performance: Example with SuperPave*, Transportation Research Record 1853, TRB, Washington D.C., 2003.

Kim S.M., Won M.C., and Mccullough B.F., “Dynamic Stress Response of Concrete Pavements to Moving Tandem-Axle Loads”, *Transp. Res. Record*, No. 1809, 2002, pp. 32-41.

Kuo Chen-Ming, Lin Shen-Hsian, *An Analytical Study Of Axle Load Equivalency Factors Of Concrete Pavements*, Journal of the Chinese Institute of Engineers, Vol. 24, No. 2, pp. 119-130 2001.

NCHRP. *Guide for Mechanistic-Empirical Design of New and Rehabilitated Pavement Structures*. Final Report for Project 1-37A, Part 1, 2 & 3, Chapter 4. National Cooperative Highway Research Program, Transportation Research Board, National Research Council, Washington, D.C., March 2004.

WSDOT. *WSDOT Pavement Guide*, Washington State Department of Transportation, URL: <http://training.ce.washington.edu/WSDOT/>, Accessed May 2009.

Yoder, E. J. and M. W. Witczak. *Principles of Pavement Design*, John Wiley and Sons, Inc, New York, N.Y., 1975.

Yu, H. T., Khazanovich, L., Darter, M. I., and Ardani, A. Analysis of Concrete Pavement Responses to Temperature and Wheel Loads Measured from Instrumented Slabs. In Journal of Transportation Research Board No. 1639, TRB, National Research Council, Washington, D.C., 1998, pp. 94–101.

Zaghloul, S., and White, T.D., Guidelines for permitting overloads – Part 1: *Effect of overloaded vehicles on the Indiana highway network*. FHWA/IN/JHRP-93–5. Purdue University, West Lafayette, Ind., 1994.

BIOGRAPHICAL INFORMATION

Tito P. Nyamuhokya is originally from the United Republic of Tanzania. He received his Bachelors of Science degree in Civil Engineering from the University of Dar es Salaam, Tanzania in November, 2003. After graduation he worked with different civil engineering companies for a period of three years. In January of 2007 he started the Master of Science in civil engineering program at Kansas State University in the area of pavement and geotechnical engineering. In the month of August of the same year, he transferred to the University of Texas at Arlington to continue with his Master of Science in civil engineering, and graduated in August, 2009. Throughout his masters he was guided by Dr. Stefan Romanoschi, the supervising professor. His future plans include pursuing PhD and later work either in educational institutions or civil engineering companies to acquire field experience, before establishing his own company.